INSTITUTE OF TECHNOLOGY

AIR UNIVERSITY

UNITED STATES AIR FORCE

SCHOOL OF ENGINEERING

THESIS

WRIGHT-PATTERSON AIR FORCE BASE, OHIO

WING LEADING EDGE OPTIMIZATION
FOR
AERODYNAMIC HEATING
OF
GLIDE RE-ENTRY VEHICLES

THESIS

Presented to the Faculty of the School of Engineering of
the Institute of Technology
Air University
in Partial Fulfillment of the
Requirements for the Degree of
Master of Science

By

Richard [redacted] Russell, B. S.

Capt USAF

Graduate Aeronautical Engineering

August 1961

Preface

This study represents an attempt to help solve the problem of aerodynamic heating on atmospheric glide re-entry vehicles. The results of the investigation are considered to be an aid to designers which, upon the advent of improved theory or experimental evidence, may be tempered to give better predicted temperatures for re-entry vehicles. This is especially true of the heating rate distribution theory which is approximate in its present form.

My interest in the subject started with my acquaintance with Mr. Wilbur Hankey, Chief Aerodynamisist of the Dyna-Soar Project Office of Wright-Patterson Air Force Base, Ohio. When thanks are due for the completion of the study, the first and foremost should go to Mr. Hankey. The topic is one of ten which he suggested as possible thesis topics. Needless to say, without his infinite patience and wealth of technical advice the study would never have been completed. Emphatic thanks are also due to Mr. Lawrence Odell of the Computer Branch of Wright Field. Mr. Odell's technical ability, and, even more so, his personal interest and enthusiasm and his desire to do more than merely complete a job are worthy of special mention. Dr. Andrew Shine deserves thanks, as my faculty advisor, for his helpful suggestions throughout the study. Last but certainly not least, thanks are extended to my wife for her typing of the draft copies of the text.

Perhaps special mention should be made of the organization of the study, or, of two sections in particular. These are Section III and Appendix A, each with very similar titles. Section III is included to

give the reader a brief descriptive background of the computer program and its capabilities and limitations. Appendix A, then, contains the details and assumptions, and the mathematical formulation of the computer solution of the problem. Finally, the last page of Appendix A contains a fold-out diagram of the mathematical model used. It is included at this location to provide easy access and to help the reader through some of the complex descriptions of the study.

Richard E. Russell

CONTENTS

CONTENTS

LIST OF FIGURES

LIST OF FIGURES

List of Symbols

Symbols

A	interior element area (in.^{2}/unit span)
a	conductive area between elements (in.^{2}/unit span)
$\bar{a}$	numerical constant
b	conductive length between elements (in.)
C	center of major nose segment
D	denominator of heating rate distribution equation
K	conductivity of main body (BTU/sec. -in. ^oR)
K_b	conductivity of back plate (BTU/sec. -in. -^oR
F	black body view factor
^oF	degrees Fahrenheit
$\mathcal{F}$	gray body factor
G	solar radiation constant (BTU/in.^{2} -sec.)
I	integral operator
L	length (in.)
L_L	length of lower afterbody (Figure 23)
$L_{1,2,3}$	geometric lengths (Figure 23)
m	slope
N	numerator of heating rate distribution equation
P	pressure
P_o	pressure at stagnation point
$\dot{q}_i$	heating rate to general element (BTU/in.^{2} -sec.)
$\dot{q}_o$	stagnation point heating rate (BTU/in.^{2} -sec.)
$\dot{q}\sqrt{\rho_o}$	stagnation point heating rate parameter (BTU -in.$^{\frac{1}{2}}$/in.^{2}-sec.)

List of Symbols (cont.)

Symbols

R	internal radius (in.)
R_o	internal radius at stagnation point (in.)
^oR	degrees Rankine
S	arc length from stagnation point to center of exterior element (in.)
S'	length from lower junction of curved and straight elements to center of straight element, page 100
ΔS	external element area (in.^{2}/unit span)
T	temperature (^oR)
V	velocity
V_δ	velocity at the boundary layer thickness
V_∞	free stream velocity
V_{∞_n}	normal component of freestream velocity

Greek Symbols

α	vehicle angle of attack (degrees)
β	non-dimensional velocity gradient
β_o	non-dimensional velocity gradient at stagnation point
γ	ratio of specific heats c_p/c_v
δ	wing section angle of attack (degrees)
δ'	wing section angle of attack with respect to the + x axis (Figure 21)
ϵ_b	emissivity of back plate

List of Symbols (cont.)

Greek Symbols (cont.)

ε_{ext}	emmissivity of main body, external
ε_{int}	emissivity of main body, internal
θ	major body segment angle (degrees)
$\theta_u, \theta_L, \theta'_u$	(see Figure 21) (degrees)
θ_6, θ_7	(see Figure 23) (degrees)
Λ	wing sweep angle
Λ_e	effective wing sweep angle
ν	angle between stagnation tangent and + x axis
$\rho = R + \tau$	external radius of nose cap (in.)
$\rho_o = R_o + \tau$	external radius of nose cap at the stagnation point
ρ_∞	freestream density
σ	Stefan-Boltzman constant (BTU/in.^{2}-sec. -$^oR^4$)
τ	main body (wall) thickness (in.)
τ_b	back plate thickness (in.)
ϕ	angle between stagnation tangent and element tangent (radians) (see Figure 3)
ϕ'	angle between element tangent and + x axis (radians) (see Figure 3)

Subscripts

b	backplate
δ	boundary layer thickness
i	general element
∞	freestream conditions
L	lower surface

List of Symbols (cont.)

Subscripts (cont.)

n	normal component
o	stagnation point value
u	upper surface

Abstract

The object of this investigation is to reduce the high temperatures on the wing leading edge of hypersonic glide re-entry vehicles. A heat transfer analysis of an arbitrary shaped wing leading edge is made. The analysis includes convection, internal and external radiation, and conduction as mechanisms of heat transfer. The wing leading edge temperature distribution is obtained from a computer program written as part of the study.

An investigation was conducted for a typical re-entry vehicle. The basis for comparison of results obtained was the temperature distribution, on a cylindrical leading edge, obtained without conduction or internal radiation in the analysis. The variables considered were exterior shape; back plate shape and orientation; and the physical properties of conductivity, emissivity and wall thickness.

The investigation demonstrated that a reduction in peak nose temperature of about 700 ^{o}F could be obtained by optimization of the exterior shape, orientation of the back plate and by including conduction and radiation in the analysis. The investigation of material properties demonstrated that external emissivity is the only property of major consequence.

WING LEADING EDGE OPTIMIZATION FOR AERODYNAMIC HEATING OF GLIDE RE-ENTRY VEHICLES

I. Introduction

The problem under consideration in this study is aerodynamic heating on the wing leading edge of hypersonic glide re-entry vehicles. The object of the investigation is to analyze this problem and attempt to reduce the high temperatures by means of optimization of the wing leading edge geometry. Figure 1 shows a typical highly swept re-entry vehicle and the wing leading edge detail. The wing is shown, in the side view, at an angle of attack α with respect to the free stream velocity V_∞. The plan view depicts the high degree of wing sweep, denoted by the angle Λ. Section A-A is an enlarged view of the area under consideration in this study. This body, called a heating cap in this report, is considered to be a non-structural member attached to the wing, for the purpose of shielding the load carrying structure from the high temperatures of atmospheric re-entry. The heating cap is considered to be thermally insulated from the load carrying structure of the wing.

Past design methods in hypersonic heating have been conservative and, in general, not accurate. For example, the standard approach to a problem of this type has been to ignore conduction and internal radiation as modes of heat transfer. All energy entering the wing leading edge, under

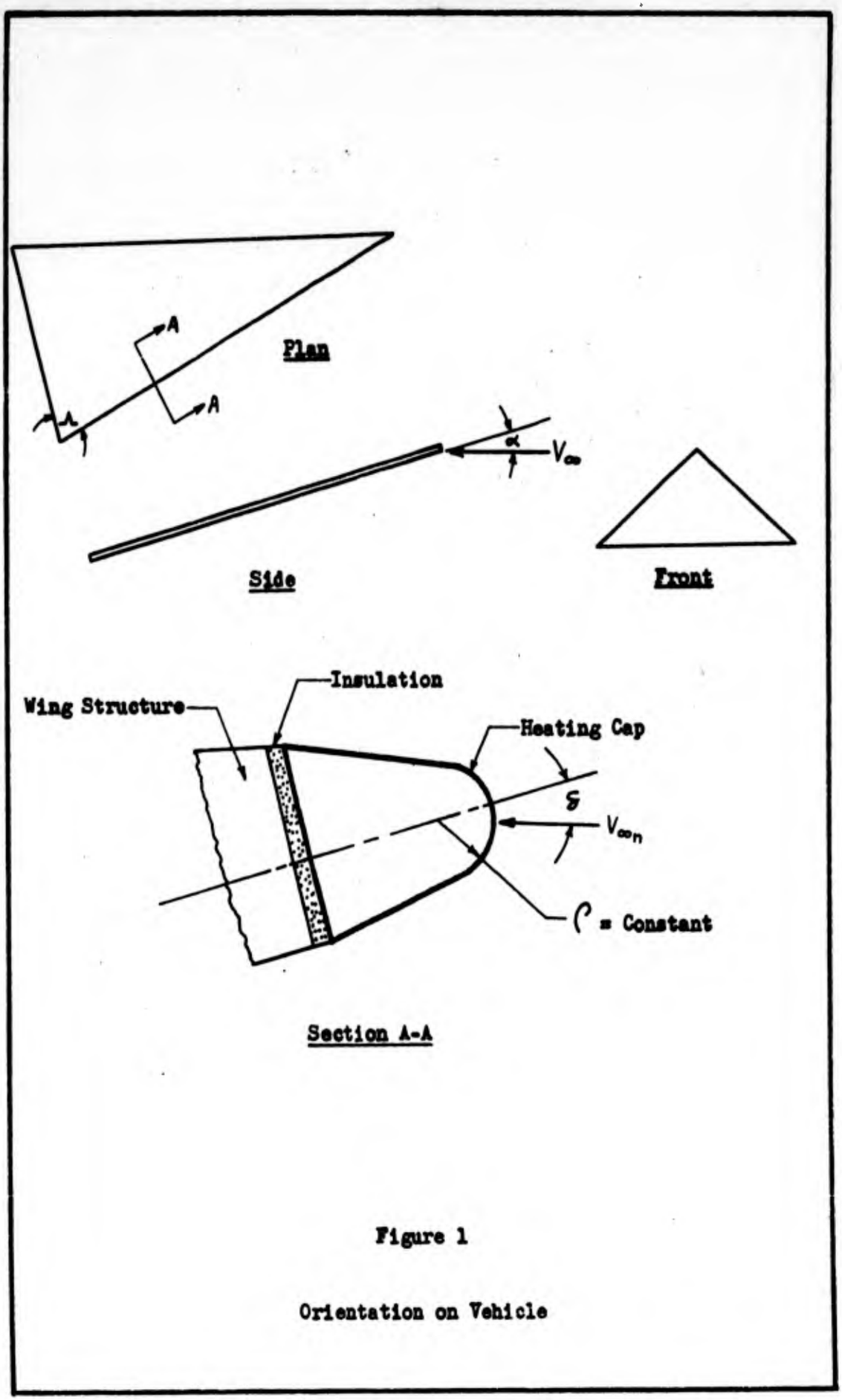

Figure 1

Orientation on Vehicle

steady-state conditions, was assumed to be radiated externally into the atmosphere. Then, knowing the convective heating rate and radiation properties of the cap, an equilibrium temperature was obtained which, in general, was conservative or too high. At the temperatures involved, around 3000 ^{o}F, conduction in the solid material, and even more important, heat transfer by radiation internal to the cap, become important modes of heat transfer.

In addition, past design procedures have been to shape the curved portion of the cap as a cylinder as shown in Figure 1. Blunt leading edge shapes are mandatory with high heating rates and, for want of a better shape, the cylinder has been used.

More recently, several investigations have been made to determine the effects of conduction and radiation on peak equilibrium temperatures. Chance Vought Aircraft Corporation and Bell Aircraft Corporation each made studies in this area. The work initiated by Bell was continued at the Wright Air Development Division (WADD), now called Aeronautical Systems Division, under Project Number 1366, Task Number 14018, in the Flight Dynamics Laboratory. Figure 2 shows the mathematical model investigated under the WADD program. This model consisted of a cylindrical cap followed by two straight and parallel after-bodies. A straight back plate, or reflector, not capable of heat conduction and insulated from the load carrying structure was included. The physical cap was approximated mathematically by sub-division into 70 small energy balance elements, each with an unknown temperature at its geometric center. These unknown temperatures were then obtained by a numerical computer solution

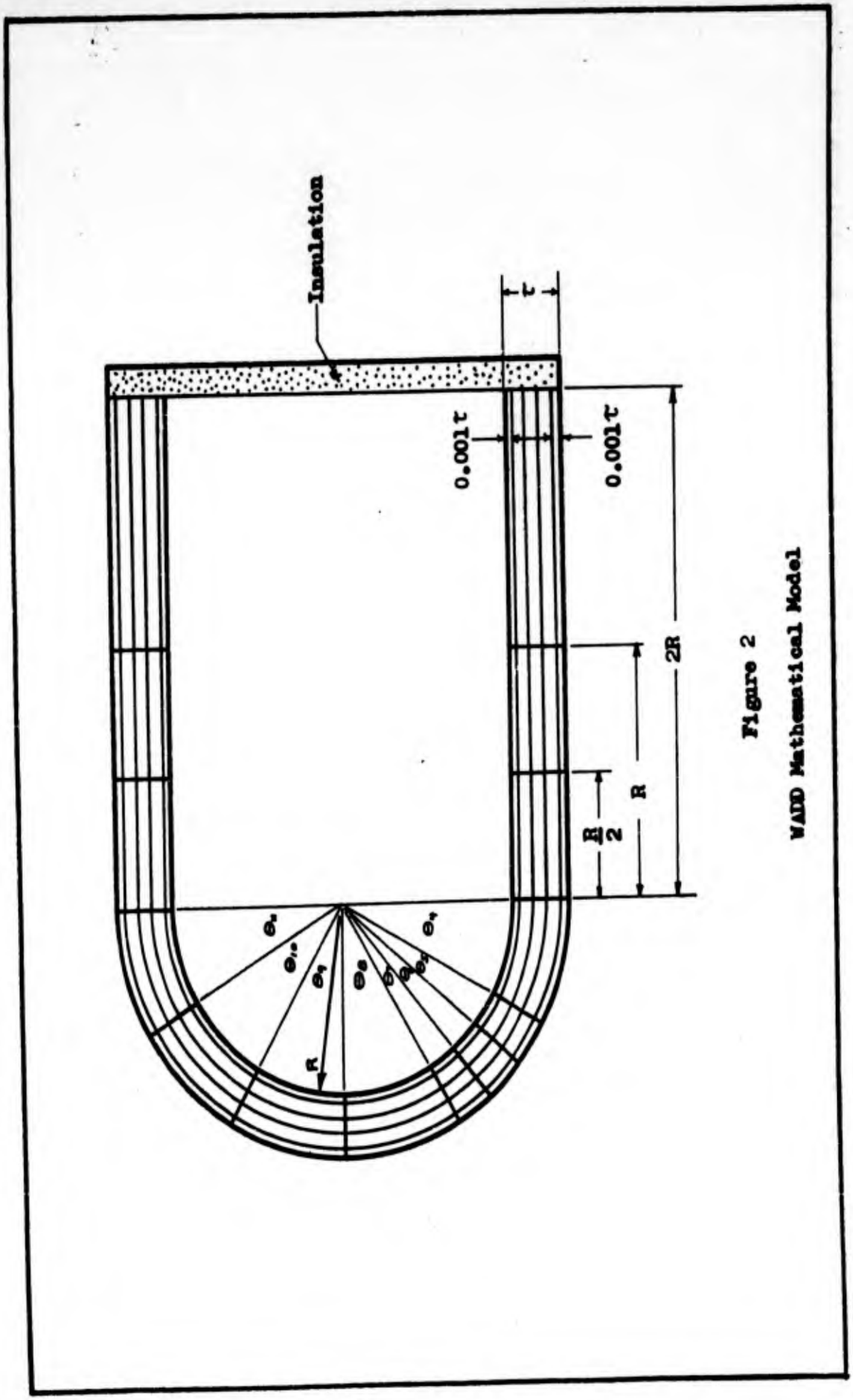

Figure 2
VADD Mathematical Model

which included internal conduction and radiation effects. Although the WADD program was a successful improvement over past investigations and did represent a rigorous analysis of the cylinder, there was still a need for further modifications and improvement.

Primary in this need is the critical state of design and safety factors in re-entry vehicles. The state of the art has developed to the point that the conservative estimates of the past are a luxury which cannot be tolerated. In addition, a program was desired at WADD which would enable an investigation of the variation of external shape and after-body angle, and, an investigation of the effect of the back plate reflector. As a consequence, a large portion of this study was the formulation of a new and improved computer program to accomplish the above tasks. The problem ultimately was programed and solved on the IBM 7090 digital computer of WADD.

The variables under consideration in this study are as follows: exterior body and back plate reflector shape; wall thickness and conductivity of the main body and back plate reflector; and emissivity, with an allowance for different internal, external and back plate reflector values. In addition, provisions have been made for variable flight conditions, convective heating rate and angle of attack. For this investigation, the latter three were held at a fixed design-point value corresponding to critical heating conditions. This was done to reduce the number of variables under consideration.

Little material was available for direct comparison of the results obtained. Where possible, results were compared with known data such as from the WADD program in operation at the beginning of this study.

Also, numerous checks were made of computed values during the program check out phase. The most conclusive check of results was an over-all energy balance of heat added to the cap against heat radiated from the cap, the latter based on the temperatures obtained from the computer solution. This comparison gave an error of between 0.10 and 0.005 pe cent based on heat added.

The problem is presented, first, from the theory involved, and then from the investigation and results obtained. Appendix A contains the detailed account of how the problem was mathematically formulated for computer solution. This is followed by Appendix B which contains sample data sheets from the computer runs and, finally, Appendix C with the complete computer program in IBM FORTRAN language.

II. Theory

A diagram of the mathematical model used in the analysis is shown in Figure 23, located in Appendix A. The body is analyzed as a two-dimensional leading edge of infinite length operating under steady-state, laminer flow conditions. The assumption of flight at maximum lift to drag ratio, and at the altitude and velocity for critical aerodynamic heating, is also made. From Figure 23, it can be seen that the model is subdivided into 71 elements for purposes of numerical solution. The method of analysis is to write a steady-state energy balance equation for each element. This results in 71 equations, which contain as unknowns, the temperature at the center of each subdivided element. These equations are then solved simultaneously by computer techniques for the unknown temperature distribution.

Energy Balance Equation

The energy balance equation for the "i"the element is

$$\Delta S_i \left(\dot{q}_i + \varepsilon_{ext} G - \varepsilon_{ext} \sigma T_i^4 \right) - \sum_{j=1}^{n} K a_{i-j} \left(\frac{T_i - T_j}{b_{i-j}} \right) - \sum_{j=1}^{N} \left(A_i \mathfrak{F}_{i-j} \right) \sigma \left(T_i^4 - T_j^4 \right) = 0 \qquad (1)$$

where ΔS_i = external area of element "i"

$\dot{q}_i$ = external convective heating rate of element "i"

ε_{ext} = emissivity , external, of element "i"

σ = Stefan-Boltzmann radiation constant = $3.3402 \times 10^{-15} \frac{\text{Btu}}{\text{in}^2\text{-}^\circ\text{R}^4\text{-sec}}$

G = solar radiation constant = $0.000854 \frac{\text{Btu}}{\text{in}^2\text{- sec}}$

K = thermal conductivity

a_{i-j} = conductive area between element "i" and an adjacent element "j"

$T_{i,j}$ = unknown temperature of element "i" or "j"

b_{i-j} = conductive length, center to center, between element "i" and element "j"

$A_i \mathfrak{F}_{i-j}$ = gray body view factor between interior elements "i" and "j"; and where n = 2, 3, or 4, and represents the number of elements adjacent to the "i"th element. N = 25, the number of interior elements engaged in mutual interior radiation when "i" is an interior element.

The equation is written in its most general form, and it should be noted that any one element will not encounter all three modes of heat transfer. For example, an external element will receive energy by virtue of the first two expressions in Eq (1) but will not be involved in internal radiation while a centrally located element will only conduct energy to its adjacent elements. The equation will now be examined in detail.

External heating

The first of the three expressions of Eq (1) applies to external elements of area ΔS_i and contains the external heating parameters examined below.

Convection. A detailed study of current procedures for estimating the aerodynamic convective heating to a blunt nosed hypersonic vehicle has been conducted by the Hypersonic Flight Section of the Flight Dynamics Laboratory,

WADD, Wright-Patterson AFB, Ohio (Ref 4). Of six different methods investigated, the method proposed by Lees (Refs 4 and 6), has been adopted as a standard. This selection was based on the relative accuracy and the relative ease of application of the Lees method.

Lees' simplified equation for the heating rate at the stagnation point of a highly swept wing at an angle of attack is

$$\dot{q}_o = 15.5\sqrt{\frac{\rho_\infty}{(R_o + \tau)}}\left(\frac{V_\infty}{1000}\right)^3 \cos^n \Lambda_e \qquad (2)$$

where ρ_∞ = free-stream density

V_∞ = free-stream velocity

$(R_o + \tau)$ = external radius at the stagnation point = ρ_o

$\Lambda_e = \cos^{-1}\left[1 - \sin^2 \Lambda \cos^2 \alpha\right]$ (effective sweep angle)

and where Λ = wing sweep angle

α = wing angle of attack.

The value of n in the above equation has been found to be 1.5 for wing sweep angles of less than sixty degrees and less than 1.5 for sweep angles of higher than sixty degrees (Ref 4:22). Two items should be noted in Eq (2). First, the stagnation point heating rate varies with the degree of wing sweep and with wing angle of attack as reflected in Λ_e; and second, for a given velocity, altitude, and wing configuration, the heating rate is inversely proportional to the square root of the stagnation radius, or

$$\dot{q}\sqrt{\rho_o} = \dot{q}\sqrt{R_o + \tau} = \text{constant}\Big|_{V_\infty,\ \rho_\infty} \qquad (3)$$

Eq (3) demonstrates the fact that for reduced heating rates in hypersonic heating, blunt nosed shapes are mandatory.

Equation (2) gives the heating rate for element "i" only if "i" is the stagnation point element. For the heating rate distribution over the surface of a blunt nosed two-dimensional body, an equation expressed by Lees is used (Ref 4:24):

$$\frac{\dot{q}_i}{\dot{q}_o} = \frac{\left(\frac{P_i}{P_o}\right)\left(\frac{V_\delta}{V_\infty}\right)_i}{\left[\frac{2\beta_o}{(R_o + \tau)}\int_o^{S_i}\left(\frac{P}{P_o}\right)\left(\frac{V_\delta}{V_\infty}\right) dS\right]^{\frac{1}{2}}} \qquad (4)$$

where $\frac{P_i}{P_o}$ = the local static to stagnation pressure ratio

$\left.\frac{V_\delta}{V_\infty}\right|_i$ = the ratio of the velocity at the boundary layer thickness to the freestream velocity

β_o = non-dimensional stagnation point velocity gradient,

thus $\beta_o = \frac{(R_o + \tau)}{V_\infty}\frac{dV_\delta}{dS}$

S = distance from stagnation point to the center of the "i"th element. (See Fig. 3)

With the value of $\dot{q}_o$ from Eq (2) in Eq (4), the value for $\dot{q}_i$ is obtained in terms of the flight conditions, body configuration, pressure and velocity ratios, and the location of the "i"th element from the

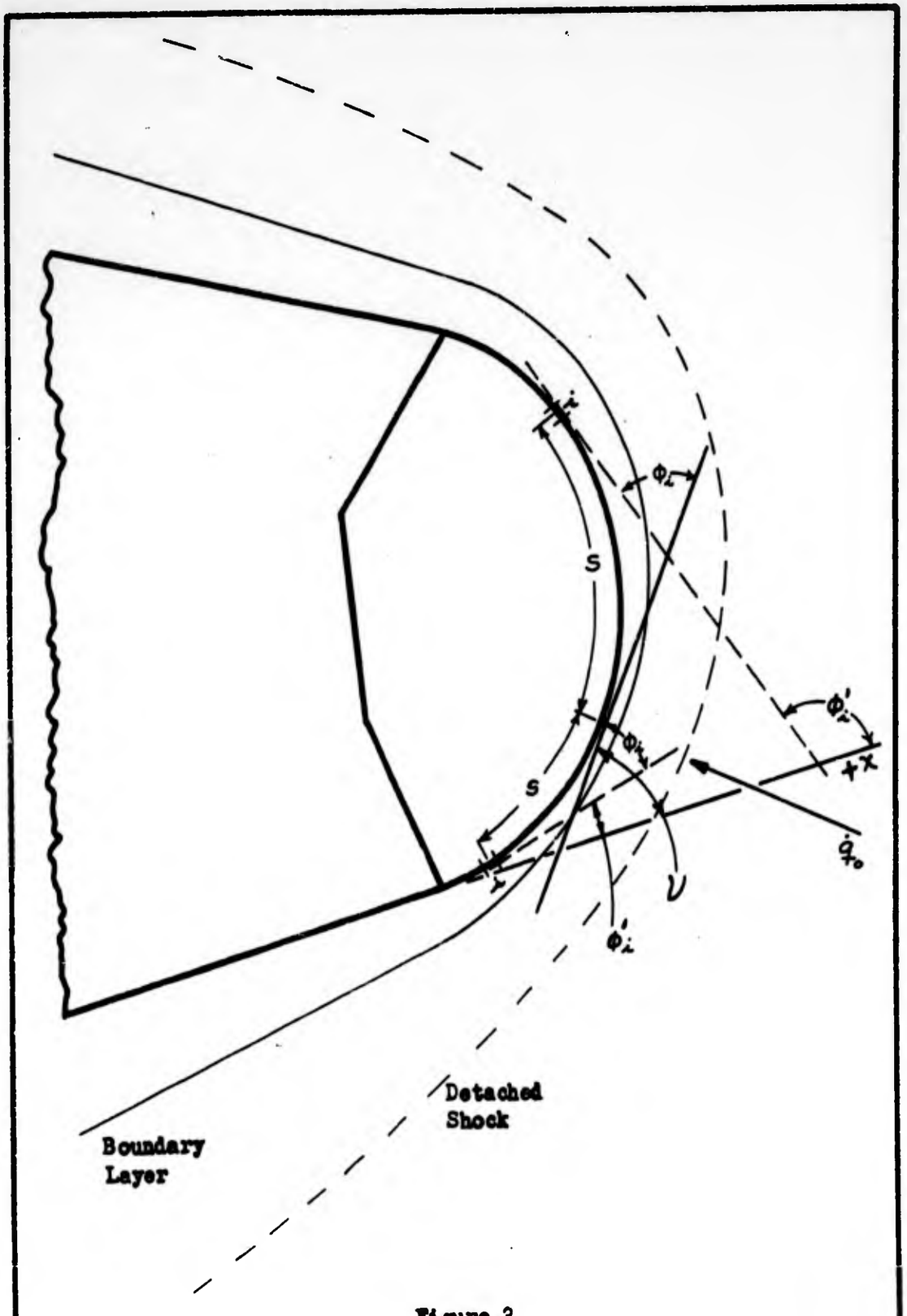

Figure 3

Element Location from the Stagnation Point

stagnation point.

Solar Radiation. A solar radiation constant G has been included for external elements in Eq (1). It is treated as a constant for all external elements which neglects shadow effects for part of the cap. For this reason, the solar radiation treatment has a conservative effect on the external heating rate.

External Radiation. Radiation of external elements to the atmosphere is treated by the standard radiation equation for a hot surface:

$$\dot{q}\ )_{\substack{\text{radiation to}\\ \text{surroundings}}} = \Delta S_i \varepsilon \sigma\, T_i^4 \tag{5}$$

The temperature of the sink has been assumed small compared to the temperature of the body surface and is therefore neglected.

Conduction Between Elements

The second of the three expressions of Eq (1) is for heat transfer between elements by conduction. This energy transfer between adjacent elements is accounted for by the Fourier heat-conduction law (Ref 3-27), or

$$\dot{q} = - K A \frac{\partial T}{\partial n} \tag{6}$$

as the heat transfer rate in the n direction through Area A. In the finite difference form and symbology of Eq (1)

$$\dot{q}_{i-j} = - K \quad (a_{i-j}) \quad \frac{(T_i - T_j)}{b_{i-j}} \tag{7}$$

It should be noted that a linear temperature gradient is assumed to exist between elements. In addition, thermal conductivity is not considered to be a function of temperature over the body surface. To include a temperature dependence of thermal conductivity would have greatly complicated the analysis. This effect is considered to be small when compared to other variables of the problem.

Internal Radiation

The last expression in the energy balance equation is for the radiation exchange among the 25 interior elements in Figure 23. The mathematical model described by Hottel (Ref 5:72) was used. The enclosure is assumed to be made of gray body elements which are diffuse reflecting with emissivity values of less than one. The net exchange of energy between any two interior elements is given by

$$\begin{aligned} \dot{q}_{1 \rightleftharpoons 2} &= A_1 \mathcal{F}_{12} \sigma \ (T_1^4 - T_2^4) \\ &= A_2 \mathcal{F}_{21} \sigma \ (T_1^4 - T_2^4) \end{aligned} \tag{8}$$

The determination of the gray body view factors $A_i \mathcal{F}_{ij}$ requires a computer subroutine before the set of Eqs (1) can be solved. This subroutine consists of an energy balance for the 25 interior elements and subsequent solution for the $A_i \mathcal{F}_{i-j}$ factors. The method used is as presented in Reference 5, and includes the simultaneous solution of 25 equations for each $A_i \mathcal{F}_{ij}$ factor, or, the solution of 625 equations.

III. Computer Program

A detailed discussion of the mathematical formulation of the problem for the computer is given in Appendix A. The purpose of the present section is to enumerate the variables involved and present the general mathematical model.

The major criteria under which the program was written were simplicity of input and the ability to solve for the temperature distribution of an arbitrary (non cylindrical) geometry. The input sheet shown in Figure 4 is used to tabulate the required computer input data. These variables are discussed below with reference to Figures 4 and 23.

The conductivity of the cap material is given by K and K_b in Figure 4. Provisions have been made for conductivity of the reflector K_b different from the main body conductivity K.

The convective heating rate for the stagnation point is introduced into the problem as the heating rate parameter $\dot{q}\sqrt{\rho_o}$. Then, as shown in Eq (3), the external radius may be varied, at a fixed altitude and flight speed, without specifying a different heating rate for each run. The heating rate distribution over the surface is automatically computed as explained in detail in Appendix A.

The effective angle of attack of the heating cap, δ', is included as a part of the computer input. This is the effective angle of attack of the cap with respect to the + x axis system as defined in Figures 21 and 23.

ARBITRARY LEADING EDGE HEAT TRANSFER PROGRAM

7090 INPUT DATA

GENERAL DATA

K			BTU/sec.-in.-^oR
K_b			BTU/sec.-in.-^oR
$\dot{q}\sqrt{\rho_o}$	BTU-in.$^{\frac{1}{2}}$/in.^{2}-sec.	δ'	^{o}
ϵ_{ext}			none
ϵ_{int}			none
ϵ_b			none
L_1	L_2	L_3	inch
θ_u	θ_6	θ_7	Deg.
τ	τ_b		inch

PROGRAM INPUT

Center	x inch	y inch	$R_i \geq R_j$
C_1			
C_2			
C_3			
C_4			
C_5			

Compute R_i, ρ_i, θ_i.

Note: x_i excludes τ_b. $\theta_1 < 90^o$. $R_i \neq R_{i+1}$. $C_i \neq C_{i+1}$

ALTERNATE PROGRAM INPUT

θ_1	^{o}	ρ_1	inch
θ_2	^{o}	ρ_2	inch
θ_3	^{o}	ρ_3	inch
θ_4	^{o}	ρ_4	inch
θ_5	^{o}	ρ_5	inch
$L_1 = x_1$			inch

Compute x and y location of $C_1 \ldots C_5$ and R_i.

Note: L_1 excludes τ_b.

Figure 4
Computer Input Data Sheet

One of the major areas to be investigated in the study was the affect of thermal radiation on the nose temperature. For this reason, three possible values of emissivity were included as computer input. ε_{ext}, external emissivity, applies to elements 1 through 24. ε_{int}, internal emissivity, is for the internal elements 47 through 68, and ε_b is for the back plate elements 69, 70, and 71.

Material thickness is introduced as τ for the main body and τ_b for the back plate reflector. It should be noted that, for investigations of the effect of wall thickness, the variation of τ is manifested in the program by a change in interior dimensions, i.e., the external size and shape remains fixed as τ is varied. In addition, from Figure 23 it may be seen that the main body is subdivided, in the τ direction, into three elements, with the outer and inner elements 0.001τ in thickness while the center elements are 0.998τ thick. The purpose of this material division is to give more accurate surface temperatures, both exterior and interior, for evaluating the radiation exchange of energy.

The above defined variables of the problem list the physical properties of the cap in question as well as the flight conditions. The last item to be specified is a geometrical description of the cap. This is accomplished in two different ways as shown in Figure 4 under Program Input and Alternate Program Input.

The computer program is capable of solving for temperatures for any shape nose cap which can be approximated by five tangent circular arcs and

two straight after-bodies. The curved nose portion is specified, in the Program Input, by giving the locations of the centers of the circular arcs in x,y-coordinates from the x,y-axis as shown in Figure 23. In addition, a statement is required as to whether $R_2 \gtrless R_1$, $R_3 \gtrless R_2$ . . . $R_5 \gtrless R_4$. From this simple input, the values of external radius ρ_i and angular segment θ_i are then calculated by the computer.

In using the Alternate Program Input, values of the angular segments θ_i of constant external radius ρ_i are given as input. In a manner similar to the calculations in the Program Input, the values of x_i, y_i for C_i and internal radius R_i are then calculated. With either input, the end result is a tabulation of R_i, ρ_i, θ_i, x_i and y_i which are needed for further calculations as described in Appendix A. The lower straight after-body is described in the alternate input and is the length as shown in Figure 23. This value need not be explicitly given in the program input as it is, in reality, the value given for x_1. The upper surface is similarly given as L_1 and is the length shown in Figure 23. The upper surface divergence angle, θ_u, from the lower surface and consequently from the + x axis, is also a part of the general data input.

Finally, the back plate reflector is described by the two angles θ_6 and θ_7 and the two lengths L_2 and L_3. Element 71 is not specified in length because it closes the cap as a straight element from the specified location of elements 70 and 1.

To summarize, the program will calculate temperatures for any body which may be approximated by five tangent circular arcs and straight upper and lower afterbodies. Provisions are made for a back plate reflector which can be approximated by three straight segments. Finally, variations in conductivity, emissivity, thickness, heating rate, and angle of attack can be included.

IV. Investigation

Introductory Remarks

With the problem formulated on the I. B. M. 7090 digital computer, the investigation of shapes other than a cylindrical curved surface was now possible. Several problems were evident at the beginning of the investigation of the variables. First, unlike many problems in heat transfer, there are no known groups of variables or dimensionless parameters such as Nusselt numbers and Prandtl numbers which may be used to simplify the investigation. Some time and effort has been spent at WADD in this direction but to date, no generalized parameters have been derived. As a consequence, any investigation will be for a specific installation on a particular vehicle in question at the time. The investigation conducted in this report is for one representative size and shape of current glide re-entry vehicles. Thus, the numerical answers obtained cannot be considered general in nature but are for the one configuration analyzed below. But, the investigation does indicate trends of the several variables considered. In addition, it does demonstrate at least one approach to the reduction of peak temperatures.

The following constraints as to size and general shape were adhered to. First, a nose cap was assumed with a zero length lower after-body. The consideration here is toward a saving of weight and space as might be attempted in a practical design approach. Next, it was decided that the upper after-body would be at an angle θ_u of

45°, oriented at a distance from the x,y-axis coordinate system as shown in Figure 5. This constraint represents a typical cambered upper surface as might be dictated from sub-sonic aerodynamic considerations. With these constraints so established, the investigation becomes one of choosing optimum exterior and back plate shape and, in addition, an investigation of the physical property variables involved, all for minimum nose temperature.

An additional problem involved is that of the many variables of the configuration. Including shape, physical properties and flight conditions, there are a total of 26 variables (Figure 4) which may be investigated. The major problem then becomes one of attempting to derive the optimum nose cap with a large number of variables. The method followed was to fix certain variables while others are investigated to obtain minimum nose temperatures. The constraints of Figure 5 eliminate the lower after-body length L_L and upper body divergence angle θ_u, thus eliminating two of the 26. Next, consideration was given to the physical variables of conductivity, emissivity, and material thickness. From previous knowledge gained in the WADD program, indications were that conductivity K and K_b would have a small effect on temperature over the possible range of K and K_b values. Similarly, a variation of the thickness τ and τ_b was thought to have a small effect. Here, practical considerations of weight also dictate as thin a structure as possible that will still sustain given air loads. Conversely, emissivity

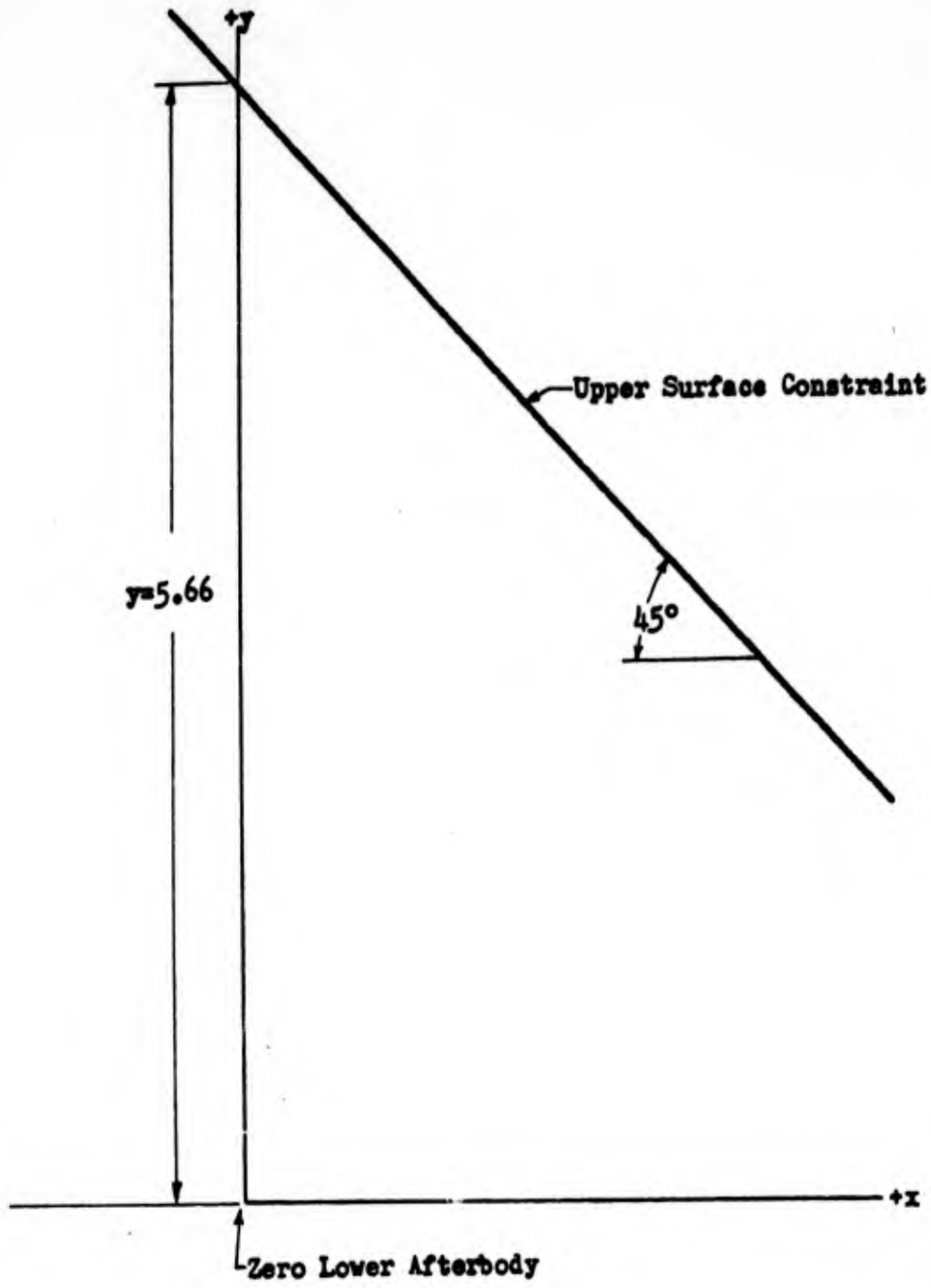

Figure 5

Problem Constraints

values can be varied for different materials, surface conditions and coatings, and it was known that external emissivity does have a large influence on peak temperatures. From the above considerations the decision was made to fix the physical variables at practical values during the investigation of the exterior shape and the back plate reflector.

Two design points for the physical variables were ultimately used as shown below.

Table I

Design Point Values

Design Point 1	Design Point 2
$K = K_b = 0.00083333$	$K = K_b = 0.00083333$
$\varepsilon_{ext} = 0.6$	$\varepsilon_{ext} = 0.9$
$\varepsilon_{int} = 0.8$	$\varepsilon_{int} = 0.9$
$\varepsilon_b = 0.1$	$\varepsilon_b = 0.05$
$\tau = 0.040$	$\tau = 0.040$
$\tau_b = 0.015$	$\tau_b = 0.015$
$\theta_u = 45^\circ$	$\theta_u = 45^\circ$
$L_L = 0.001$	$L_L = 0.001$
$\dot{q}\sqrt{\rho_o} = 0.6944$	$\dot{q}\sqrt{\rho_o} = 0.6944$
$\delta' = 45^\circ$	$\delta' = 45^\circ$

The effective angle of attack δ' is chosen for the maximum lift to drag ratio which represents the critical leading edge flight attitude. Also, the heating rate parameter $\dot{q}\sqrt{\rho_o}$ was selected to give temperatures near the critical values for present materials. δ' and $\dot{q}\sqrt{\rho_o}$ are held constant throughout the investigation. The conductivity values chosen represent a general average for high strength metals of 0.00083333 BTU/sec-in-^oR (Ref 3:496). The number of significant figures retained is a result of converting the normal units for the average conductivity to the units of the computer program. The emissivity values used in design point 1 represent average values thought practical at the beginning of the investigation. Design point 2 emissivities are values later found to be possible through coating developed for skin surfaces. The only difference, then, between design points 1 and 2 are the emissivity values which represent a high and low limit to be expected. Finally, the thickness values τ and τ_b are considered practical from a weight and strength standpoint.

With the variables fixed at the practical design point values shown in Table 1, the investigation was then conducted to determine the effects of the nose shape and the back plate reflector on the temperature distribution. The plan, then, was to first investigate the exterior nose shape at each design point. With the optimized shape so obtained, design points 1 and 2 were then extended to include this optimum. Next, the reflector was investigated and an attempt to optimize was made with all other variables at the design points. Finally, with the optimum nose and

reflector configuration, the properties ε_{ext}, ε_{int}, ε_b, K, K_b, τ and τ_b were varied through approximately one order of magnitude either side of the design point values to establish their effect on the peak temperature. The final optimum shape is thus derived in a step-wise procedure for each of the major areas: nose shape, reflector, and physical properties -- while the other areas are held fixed at the design point values.

Exterior Shape

Past Methods. To show the past design procedures and an estimate of the magnitude of the error inherent therein, the constraints of the problem were met with a simple cylindrical shape tangent at the origin and tangent to the 45^o upper surface. The conductivity and the internal radiation were made extremely small or zero to duplicate the past design assumptions. In addition, a straight back plate reflector was assumed which closed from the origin to the point of tangency of the cylinder and the upper surface. Figure 6 A and B shows a sketch of the configurations while the computer solution for these runs are shown in Appendix B. The results of these analyses are shown in Figure 6 A and B as the maximum nose temperature on the cap.

Next, the same configuration was run at design points 1 and 2 but with ε and $\varepsilon_b = 0$. These results are shown in Figure 6 C and D, and runs 6 C and D, Appendix B. Note the relatively small effect that internal conduction has on maximum temperatures in this thickness range. Conductivity variation, for material thicknesses around an order of

Design Point 1	Design Point 2
A  $\epsilon_{int} = \epsilon_b = 0$ $K = K_b \neq 0$ $T_{max} = 3411\ ^{o}F$	B  $\epsilon_{int} = \epsilon_b = 0$ $K = K_b \neq 0$ $T_{max} = 3039\ ^{o}F$
C  $\epsilon_{int} = \epsilon_b = 0$ $T_{max} = 3392\ ^{o}F$	D  $\epsilon_{int} = \epsilon_b = 0$ $T_{max} = 3023\ ^{o}F$
E  $T_{max} = 3209\ ^{o}F$	F  $T_{max} = 2881\ ^{o}F$
G 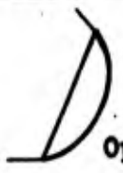 $T_{max} = 3026\ ^{o}F$	H  $T_{max} = 2710\ ^{o}F$
$\Delta T = -385\ ^{o}F$	$\Delta T = -329\ ^{o}F$

Figure 6

Past Design Methods

magnitude greater than the design point thickness, does have a substantial effect on the peak nose temperature, as will be shown later in the investigation. Finally, runs 6 E and F were made to include both internal conduction and internal radiation. A comparison of Figure 6 A with 6 E and 6 B with 6 F shows the overall effect of conduction and internal radiation for this cylindrical shape.

Optimum Exterior Shape. Recently, an investigation was conducted using Lees' equation in the Hypersonic Flight Section of WADD to attempt to establish an optimum exterior shape for minimum convective heating. Lees' equation for the convective heating rate distribution (Eq (4)), as shown in Appendix A, can be reduced to a function of the angular position of the "i"th element on the body and of the external body radius ρ_i. Expressed mathematically

$$\frac{\dot{q}_i}{\dot{q}_o} = f(\rho_i, \phi_i) \tag{9}$$

where ϕ_i is the angle between the tangents of the stagnation point and the "i"th element as defined in Figure 3. Considering a given quantity of heat flux to a body of variable shape, the optimum configuration is one which will result, insofar as possible, in a constant energy distribution over the nose. Thus $f(\rho_i, \phi_i)$ in Eq (9) was set equal to unity and the coordinates ρ_i and ϕ_i of the optimum shape were obtained. It should be noted that this constant heating rate can be maintained up to

but not past about ± 38° on either side of the stagnation point depending upon the value of γ used. Figure 7 shows the derived optimum shape and the mathematical approximation of the optimum shape as used for the computer solution.

This shape was then used, rather than the cylinder, to meet the constraints of the investigation. Figure 6 G and H and runs 6 G and H, Appendix B, show this surface. A comparison of Figure 6 A with G and 6 B with H show the effect of internal radiation, internal conduction, and the optimum exterior shape. In addition, a comparison of Figure 6 E with G and 6 F with H show the effect of exterior change of shape only, for this configuration.

It may be recalled from Eq (3) that large radii are desirable to minimize convective heating rates. Figure 7 shows how this fact is reflected in the optimum shape with a large radius at the stagnation point and then smaller radii on either side of the stagnation point for approximately constant heating. Figure 8 shows the effect of this constant heating rate on temperature distribution over the nose. The exterior surface skin temperature distribution for the cylinder and optimum shape are plotted for design points 1 and 2.

Also, from Figure 8, it may be seen that the variation of temperature on either side of the stagnation point for the optimum is small, i.e., within about one percent of the peak temperature between points. Because of the finite difference method of solution and because the

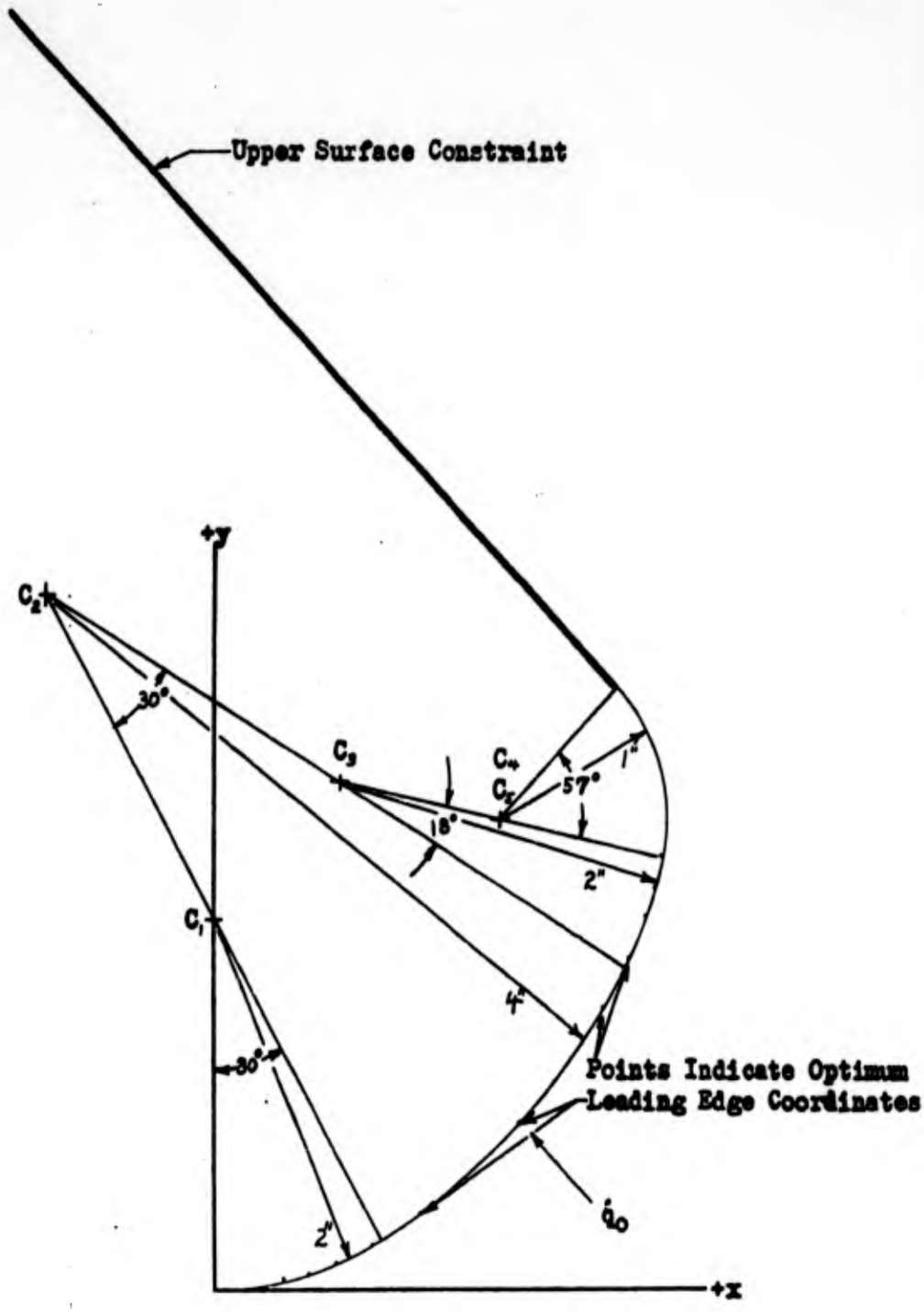

Figure 7

Mathematical Approximation of Optimum Leading Edge

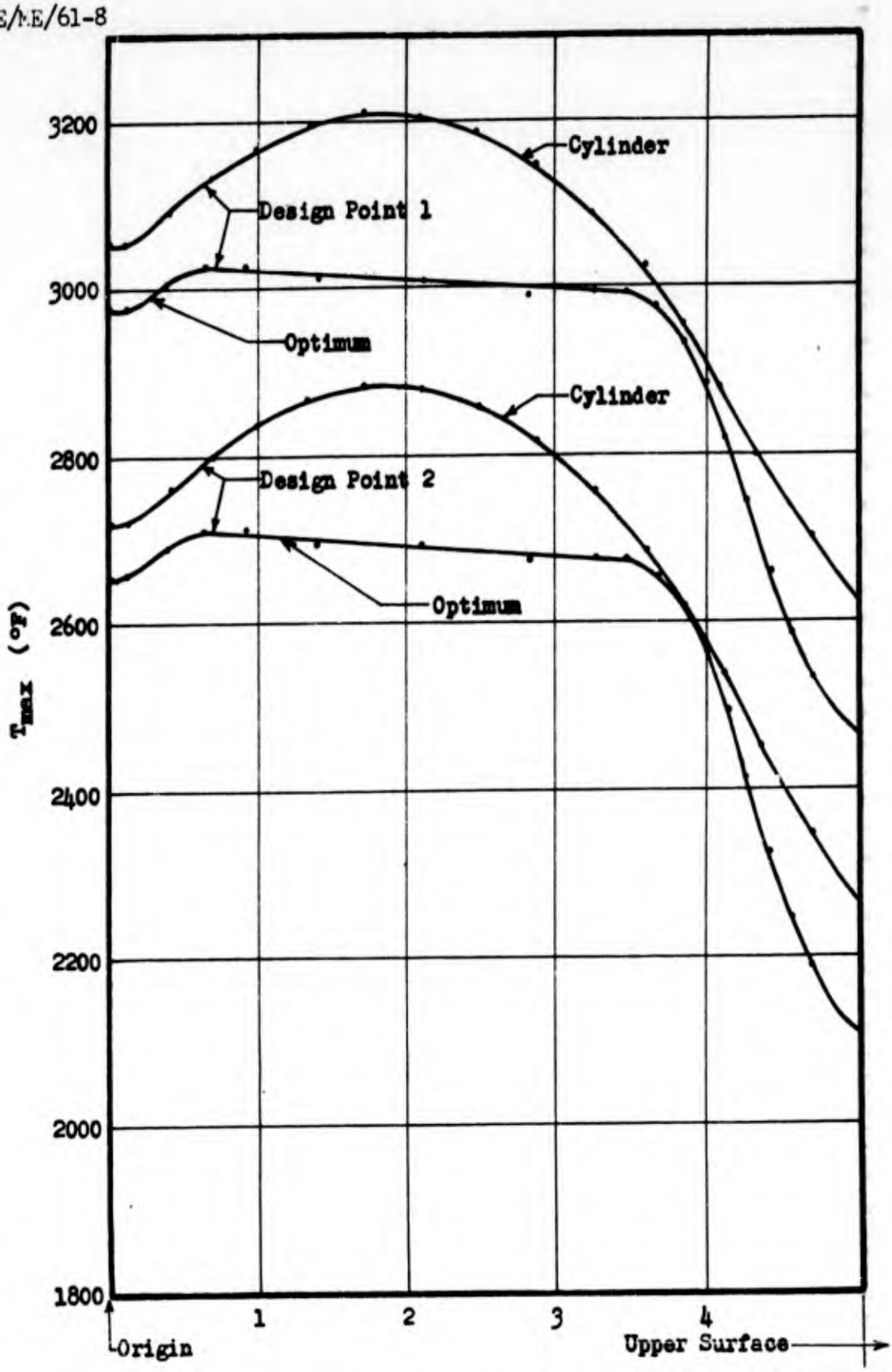

Figure 8

Comparison of Optimum and Cylinder Nose Temperature Profile

optimum shape must be described by only five radii and five angles in the computer program, this small variation in temperature was accepted as negligible and no attempt was made to further refine the optimum shape to a more constant temperature distribution. In addition, Lees' equation is thought to be reliable only so long as sharp corners are avoided. Any attempt to extend the region of relatively constant temperature distribution was thought to be beyond the capability and the theory of the problem solution. Thus, the shape as derived by the Hypersonic Flight Section is considered to be a practical optimum from the results of this investigation. This shape is then adapted at this point as the design point exterior nose configuration and is added to the design points 1 and 2 given in Table I.

Back Plate Reflector

Straight Reflector. A design proposal for a recent glide re-entry vehicle was to include a nose shape similar to the optimum thus far investigated but with a straight reflector across the two tangent points as shown in Figures 9 A and B. The question was raised as to what effect rotation of the reflector, about the origin, would have on the peak temperature. Several runs were made to investigate this effect. The first run made was for the reflector arbitrarily set in a vertical position with respect to the x,y-axis system. The results are shown in Figure 9 C and D. Using the added length of the upper after-body between the two different configurations in Figure 9 A and C (or 9 B and D) as a unit of change in top area, several additional runs were made to further investigate the apparent effect of

Design Point 1	Design Point 2
A  T_{max} = 3115 °F	B  T_{max} = 2779 °F
C  T_{max} = 2889 °F	D 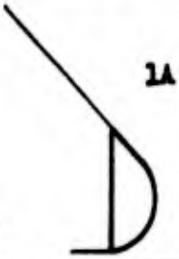 T_{max} = 2601 °F
E  T_{max} = 2786 °F	F  T_{max} = 2523 °F
G  T_{max} = 2736 °F	H  T_{max} = 2486 °F
I  T_{max} = 2705 °F	J  T_{max} = 2464 °F
ΔT = -410 °F	ΔT = -315 °F

Figure 9

Effect of Orientation of Reflector-Top Area

this top area addition. The results of adding successively 1xA top area are shown in the remainder of Figure 9. As can be seen, the combination of the addition of this area and the rotation of the reflector can cause a substantial change in the peak temperature on the heating cap nose. A plot of the change in maximum temperature, ΔT max., per unit of top area added, is shown in Figure 10 for the two design point runs. It should be noted that the change in maximum temperature per unit top area is non-linear and seems to be approaching a zero value after the 4xA point. From practical consideration of size, shape, and weight, rotation of the reflector to about the 1xA point seems feasible and shows a significant reduction in peak temperature. Rotation past about 1xA remains beneficial in lowering of peak temperature but the exact optimum point, for any specific installation, will be a compromise study between temperature reduction, weight, and allowable space.

Figures 11 and 12 are graphs of the maximum temperatures versus added top area. Figure 13 shows the nose temperature profiles for the basic zero top area and the four addition runs previously discussed for design point 1. Similar curves may be obtained for design point 2.

The final phase of the straight reflector investigation was a series of runs, similar to those above, but with equal increments of reflector rotation as the parameter.

Figure 14 A and B show again the basic optimum shape and the

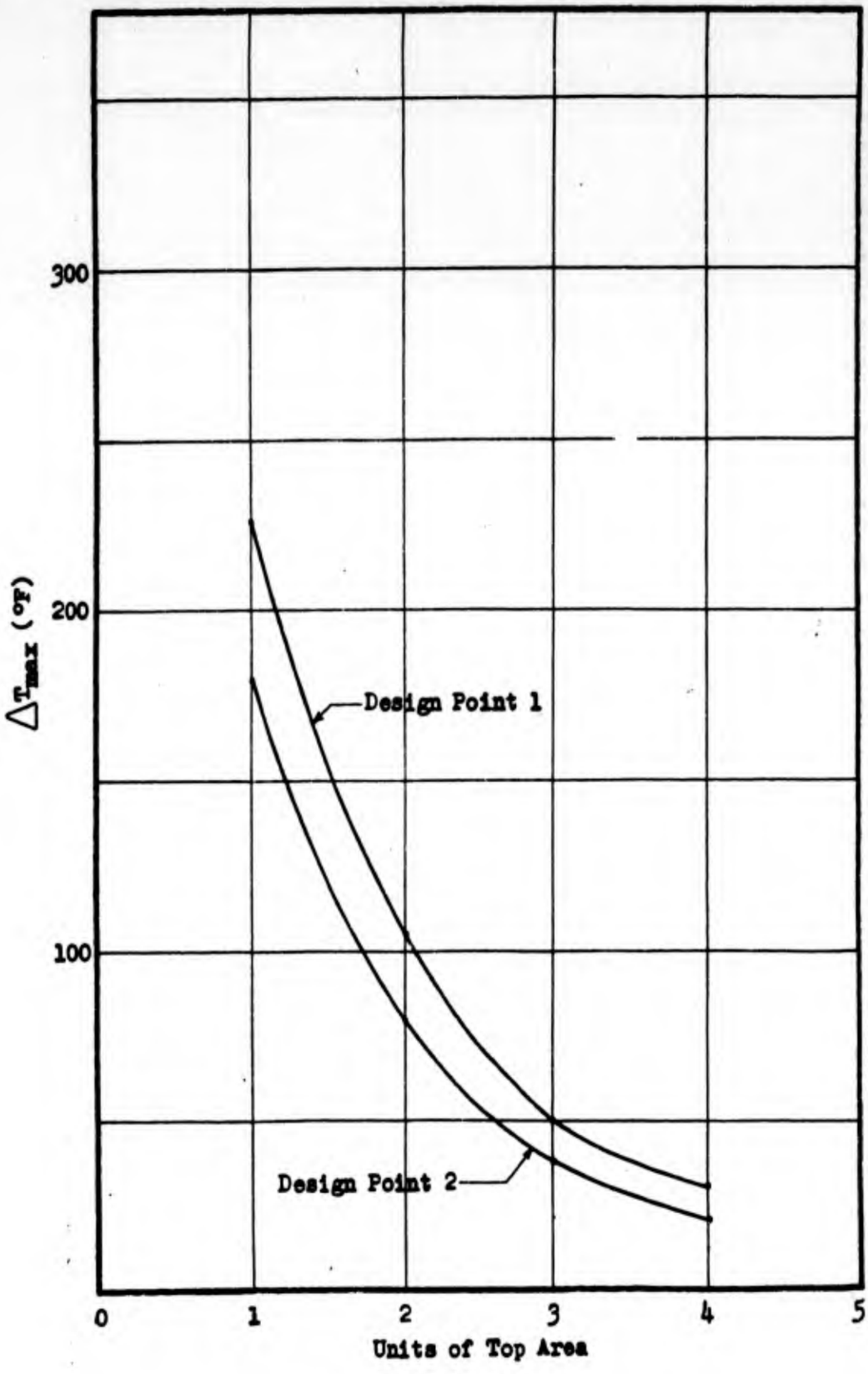

Figure 10

Variation of Temperature Reduction with Top Area

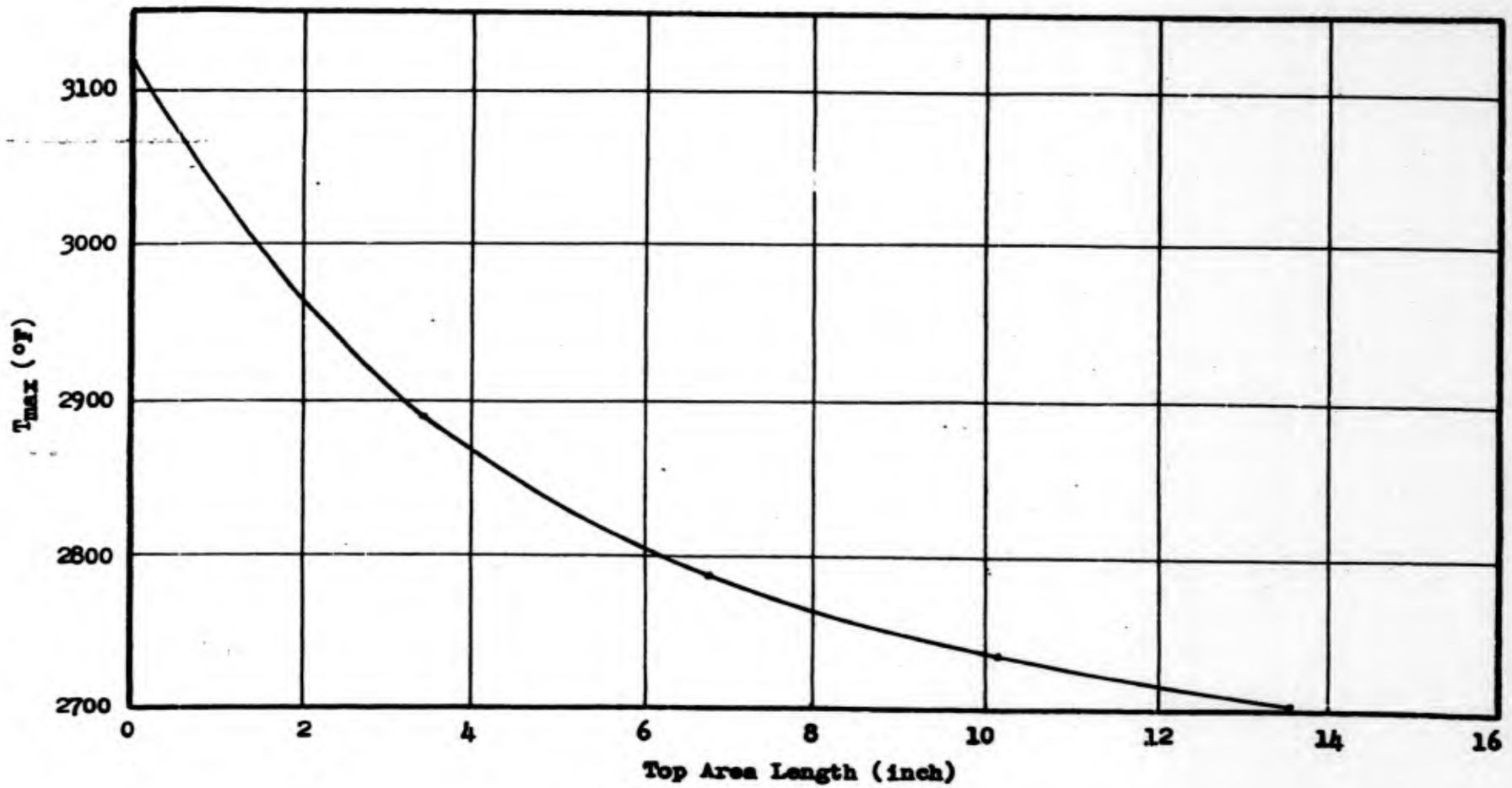

Figure 11

Variation of Temperature with Top Area-Design Point 1

GAE/ME/61-8

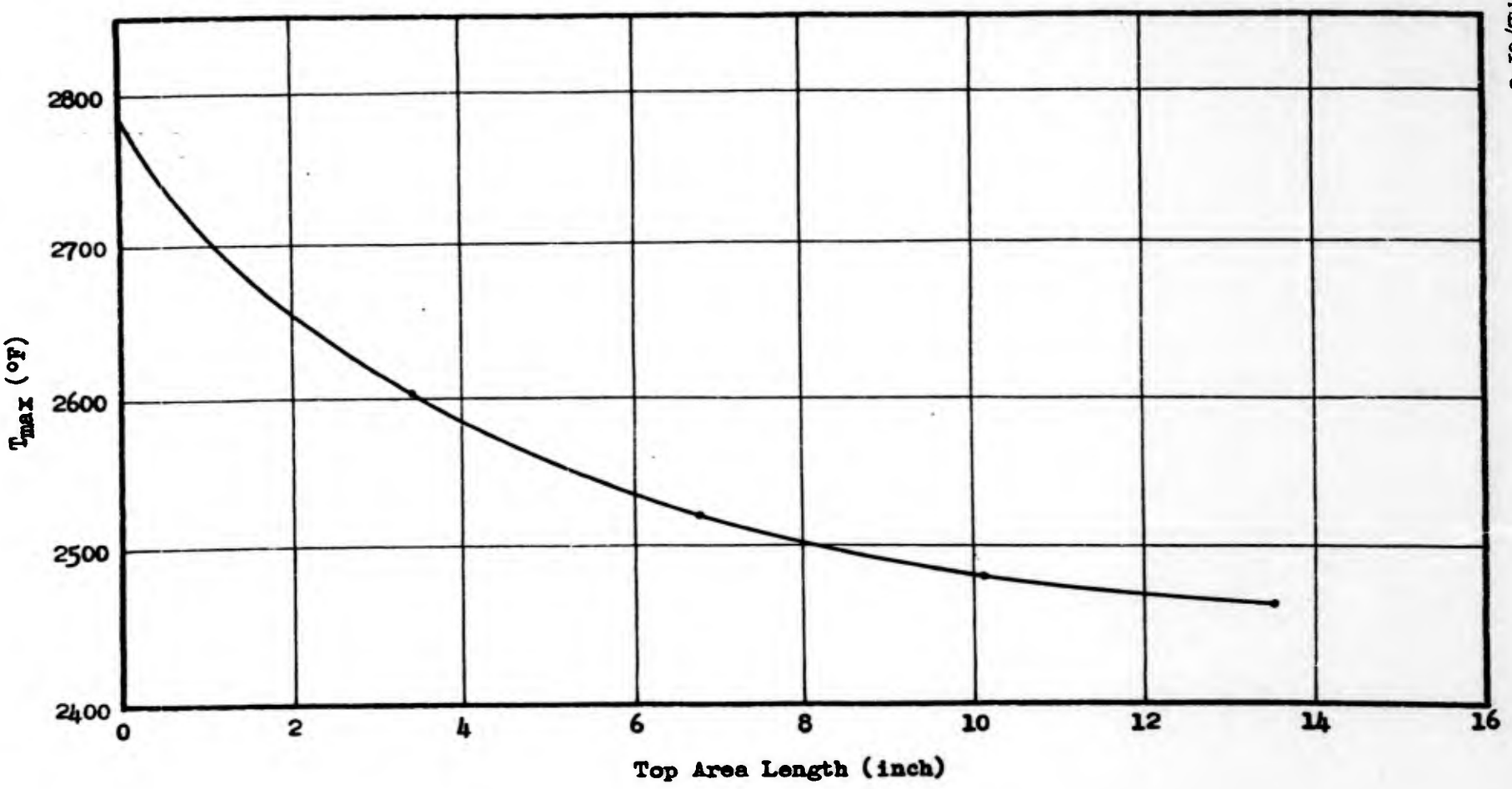

Figure 12

Variation of Temperature with Top Area-Design Point 2

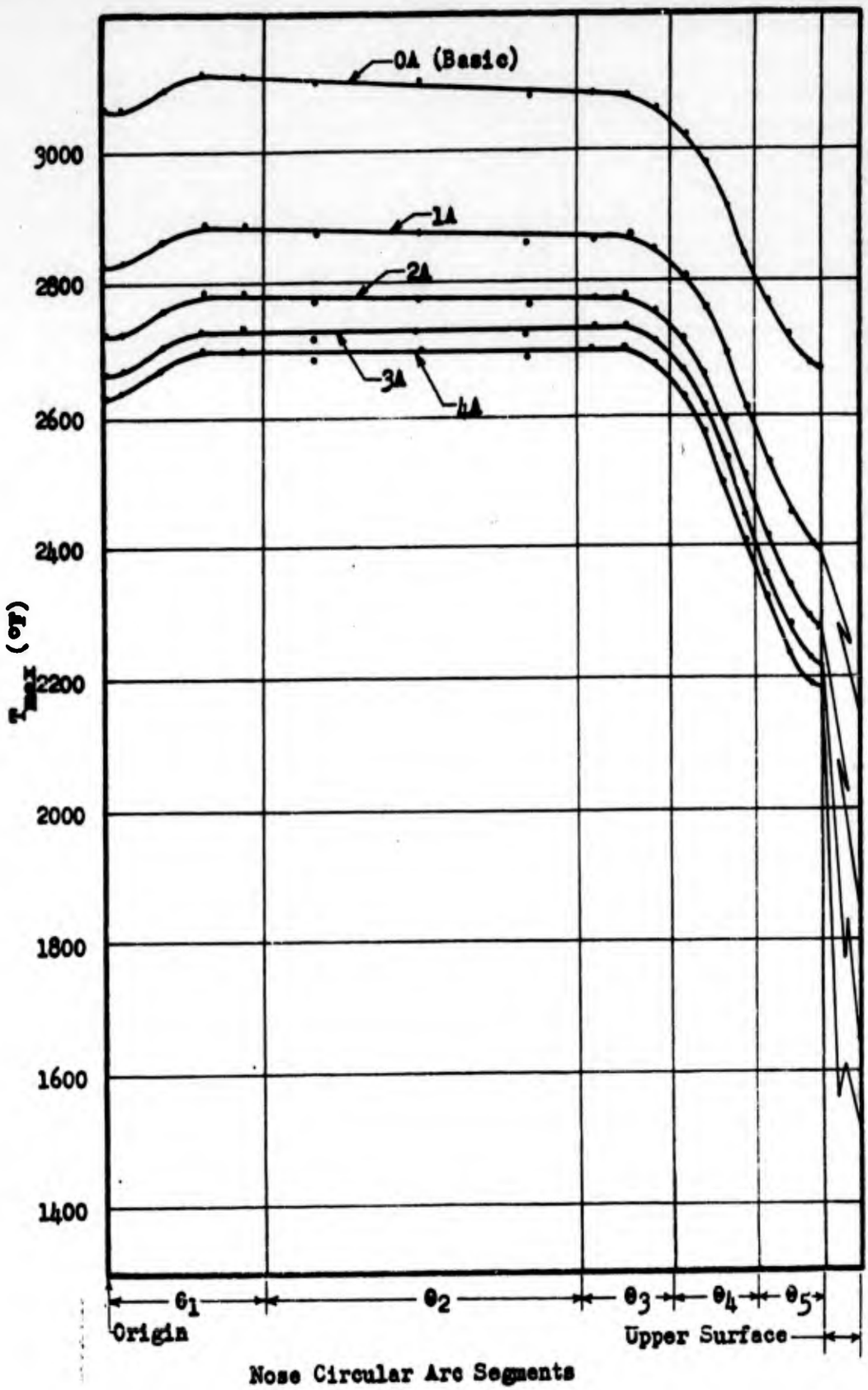

Figure 13

Nose Temperature Profile for Several Top Area Configurations

Design Point 1	Design Point 2
A  T_{max} = 3115 °F	B  T_{max} = 2779 °F
C 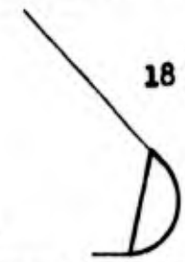 18 1/2° T_{max} = 3002 °F	D  18 1/2° T_{max} = 2691 °F
E 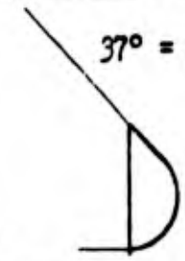 37° = 1A T_{max} = 2889 °F	F 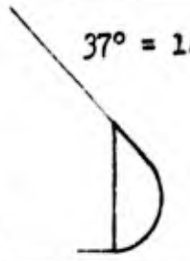 37° = 1A T_{max} = 2601 °F
G  55 1/2° T_{max} = 2785 °F	H 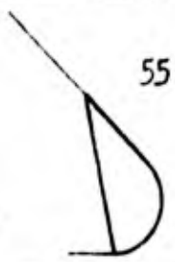 55 1/2° T_{max} = 2523 °F
I  66.2° T_{max} = 2708 °F	J  66.2° T_{max} = 2466 °F
ΔT = -407 °F	ΔT = -313 °F

Figure 14

Effect of Orientation of Reflector-Rotation

closed reflector. Figure 14 C and D show the reflector rotated through an angle of 18½ degrees and the corresponding reduction in temperature. Figure 14 E and F show the next 18½ degree increment which is equivalent to the 1xA run of Figure 9 C and D. Figure 14 G and H show the next 18½ degree increment, and finally I and J show the total angular displacement of the back plate at an angle of 66.2 degrees. The total reduction in maximum temperature is shown below Figure 14 I and J. It can be seen that the possible reduction in temperature is less for design point 2 than design point 1. This is due to higher external radiation cooling for design point 2 and therefore potentially less energy available for the mechanism of interior radiation to dissipate out through the upper surface.

A plot of the peak temperature against angular rotation of the back plate is shown in Figure 15. The change in temperature as a function of angular rotation is seen to be very nearly a straight line function. For design point 1, a temperature reduction of 6.11° F per degree of rotation may be taken as a constant within one percent accuracy of computer values. For design point 2, 4.81° F per degree rotation is constant within one percent accuracy of computer values. In conclusion, for rotation of the back plate from the closed position, the angle through which the reflector is rotated becomes a convenient parameter, for this configuration, to predict maximum temperatures.

A similar investigation made recently by the Dyna-Soar Aerodynamics Group, on a different shaped nose cap but using the computer program

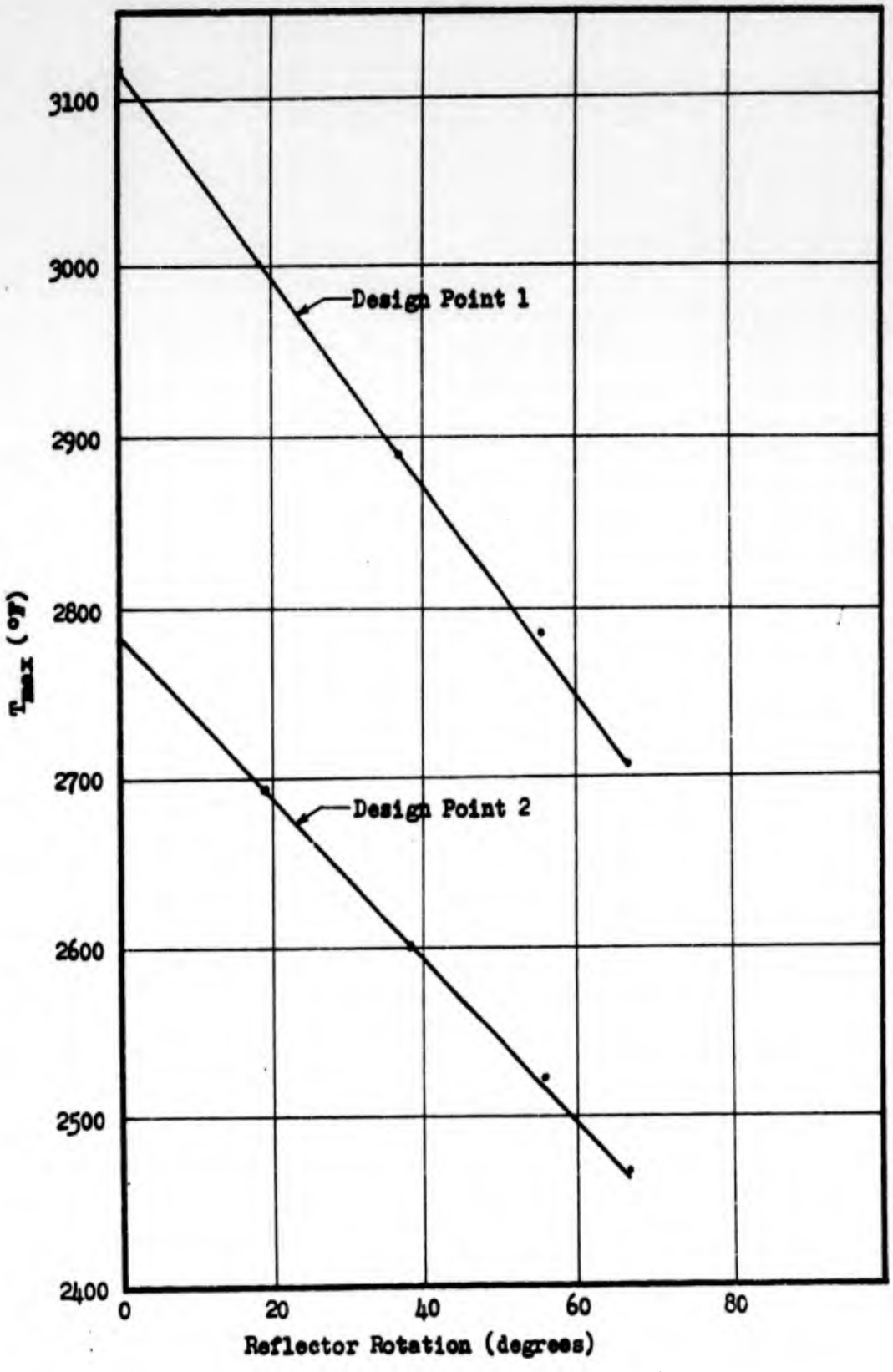

Figure 15

Variation of Temperature with Angular Rotation

developed in this study, gave a temperature reduction-constant close to the value obtained in this investigation for design point number 2.

During the investigation, the question was raised as to whether the addition of the top area or the rotation of the reflector, or both, contributed to the reduction of the peak nose temperatures. In Figure 17 C-4 and D-4 are shown the same configurations as Figure 9 E and F with the exception that the second top area is insulated from radiating externally into the atmosphere. This was accomplished by extending the reflector, which is mathematically insulated from the structure or the atmosphere, over the second top area as shown in Figure 17 C-4 and D-4. Comparison of Figures 9 C, E and 17 C-4 (or 9 D, F and 17 D-4) show that about 20 and 25 percent of the temperature reduction is from the rotation of the reflector or the improved "view" which the cooler radiating areas have of the reflector, for the two design points.

Curved Reflector. With the knowledge thus gained of the effect of rotation of a straight reflector, an investigation of the effects of a curved reflector was made. Several restrictive features of the mathematical solution with respect to internal radiation should be mentioned. First, a requirement exists that all internal elements must be able to "see" all other internal elements. That is to say that no internal element can be hidden from any other internal element or that the back plate reflector must be shaped concave outward as shown, generally, in Figure 23. It should be noted that two reflector

elements oriented in a straight line do not violate the above restriction.

Secondly, in the determination of the $A_i \mathcal{F}_{ij}$ grey body view factors for Eq (1), the assumption is made that the internal elements are diffuse reflecting. Had this restriction not been imposed, an investigation of specular or regular reflection of internally radiated energy would have been possible. To clarify, the possibility exists that "mirror" type reflection could be used to advantage to increase the transport of energy from the hot lower elements out through the upper elements by mirror reflection from a suitably curved back plate reflector. But, because of the diffuse reflection assumption, effects of improved element orientation from the view standpoint are the only effects which may be investigated in this mathematical solution.

As mentioned before, the choice of the angular orientation of the straight reflector of Figures 9 and 14 will be a compromise of allowable weight, size and temperature for the cap on any one vehicle. For the purposes of this study, the vertical reflector of Figure 9 C and D is arbitrarily chosen as a practical optimum. This reflector configuration, together with the optimum nose shape, is added to Table I for the design points. The purpose, then, of the present investigation is to curve the reflector concave outward, maintaining the constraints of one top area as in Figure 9 C and D.

First, for all configurations of Figure 9 C through J, an arbitrarily shaped concave reflector was tested. The maximum decrease in

T max was around 35° F for the 4xA run while for the more practical configuration of 1xA the reduction was around 20° F. Figure 16 shows these concave shapes for a direct comparison with the runs of Figure 9. In addition to the runs shown in Figure 16, several more radical departures from the straight reflector were made. In all cases the temperature reduction was around one percent or less of the peak temperature. Finally, a series of runs were made to ascertain gross effects, if any, from the reflector shape. Figure 17 shows the results of these runs.

The reflector was assumed in two pieces. First, the upper part was assumed at a 90° angle to the upper straight after-body. Then, the lower part was rotated from the vertical position through increments of 15 degrees. From the figure, it can be seen that the major reduction in temperature occurs in the first 15 degree increment and that the reduction finally becomes zero. Also, the magnitude of the temperature reduction is small when compared to the larger reductions in temperature shown by other means.

Adopting momentarily, the first 15 degree rotation point as an optimum, another series of runs was made to investigate reflector rotation about the upper corner as shown in Figure 17 C and D. For this series, the reflector was rotated and three runs were made as shown in the figure. Again the reduction in peak temperature occurs mainly in the initial movement but, in this case, an increase in

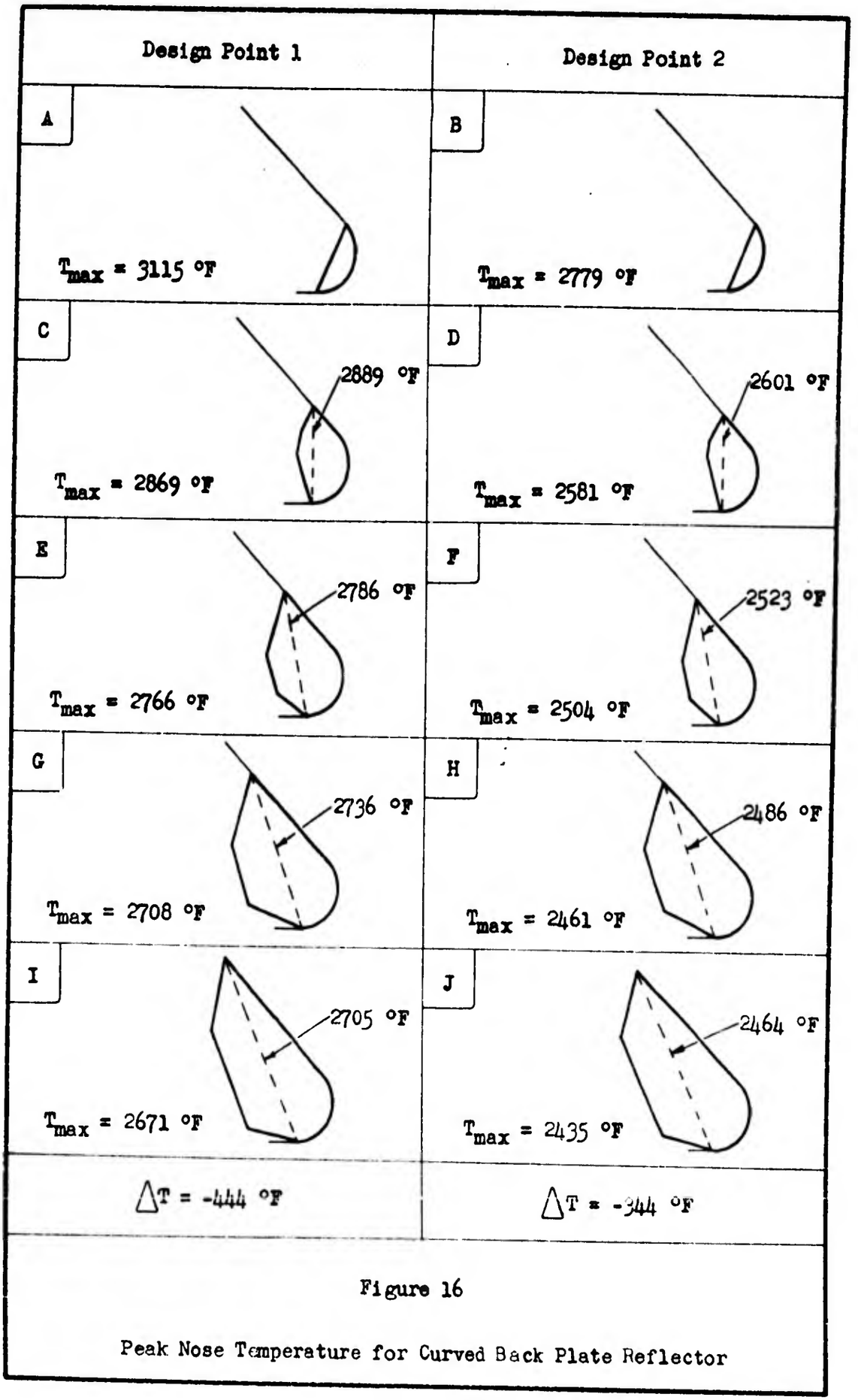

Figure 16

Peak Nose Temperature for Curved Back Plate Reflector

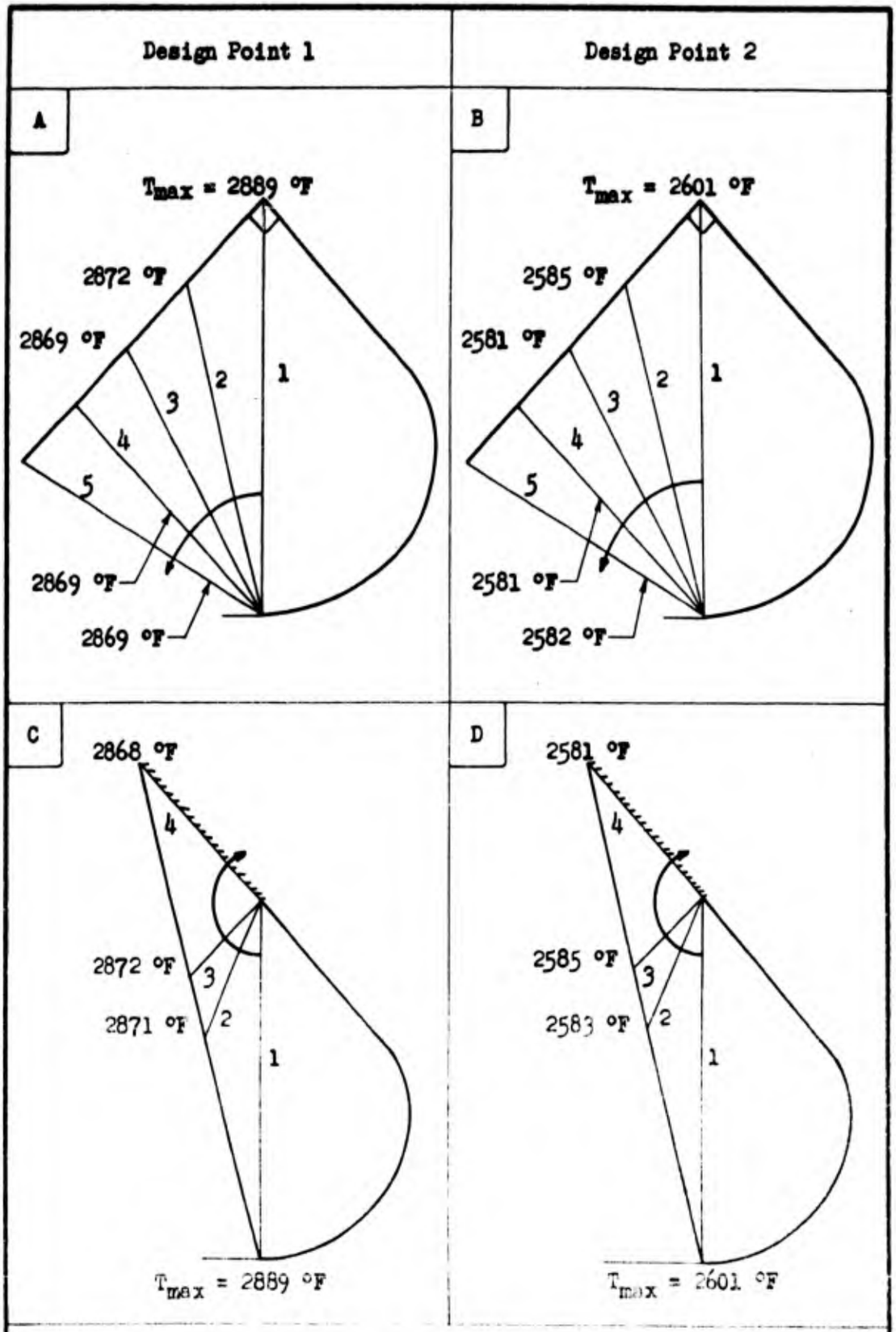

Figure 17

Gross Effects of Curved Back Plate Reflector

temperature is noted with a further reflector rotation.

From the results of the two series of runs shown in Figure 17, it is concluded that there is an optimum reflector shape for a given top area constraint. The order of magnitude of the temperature reduction is small (less than one percent) and for this reason, the curved reflector is abandoned in this investigation. It is believed that more fruitful results might be obtained in an investigation which would include specular reflection from a back plate reflector shaped for this purpose.

Physical Variables

Adapting the vertical straight reflector as the optimum, the constraints of the problem have now been met. The remainder of the investigation is devoted to substantiating the assumption that variation in K, τ and ε values would have little effect on the peak temperature. The investigation of the physical variables was made on the now optimum exterior shape and reflector for design point 2. The method used for the investigation was to vary one variable through its practical range about its design point while all other variables are held fixed at their design points. For example, in Figure 18 A, the design point for external emissivity is 0.9. At this point, a peak nose temperature, called the design point temperature ($T_{D.P.}$) is obtained. Then, a plot of the ratio of peak nose temperatures ($T_{max.}$) off design point to the design point value is made against the variable in question. Figure 18 A shows the large variation in maximum temperature with external emissivity.

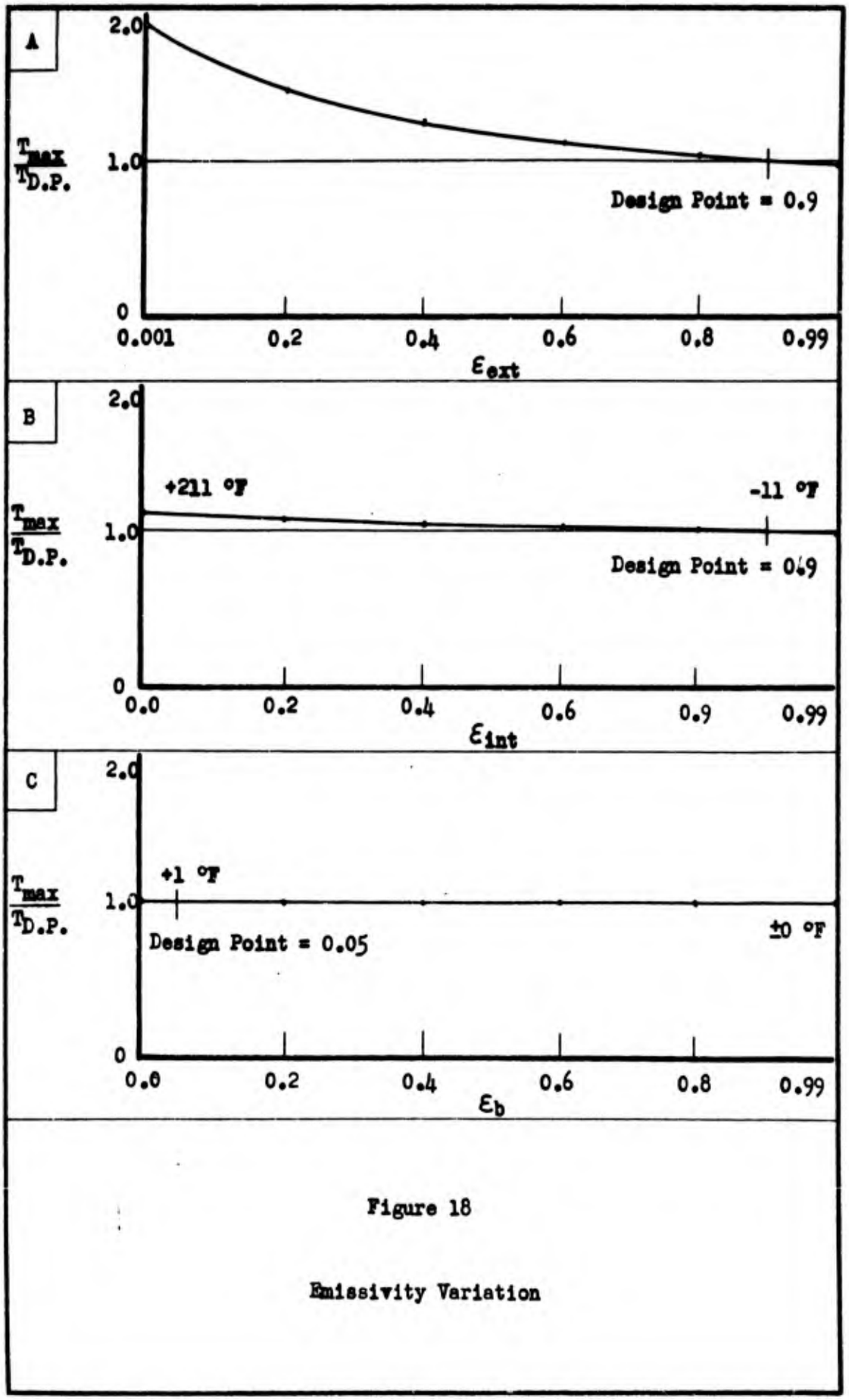

Figure 18

Emissivity Variation

Figure 18 B shows the relatively small effect that internal emissivity has on maximum temperature. The ± printed temperatures indicate the degrees temperature variation from the design point temperature when the ratio is small. Figure 18 C shows the negligible effect of the reflector emissivity ϵ_b.

For investigation of thermal conductivity, two ranges of thickness were included. First, in Figure 19 A, the design thickness of $\tau = 0.040$ and $\tau_b = 0.015$ inch was used while the conductivity of the main body K was varied. The low value of conductivity was 0.0001 BTU/in-sec-^{o}R which was the lowest value that could be used due to computer limitations. It should be noted that in Ref 3:497, the lowest listed value for conductivity is 0.0001388 BTU/in-sec-^{o}R for nickel steel while the design point average in this report is 0.0008333 BTU/in-sec-^{o}R. The high value for K is ten times the design value. The negligible effect of K variation, in this thickness range, is apparent.

Next, the variation of K for a material of ten times the design τ and τ_b was made. Figure 19 B shows the results of these runs and the larger effect that variation of K can have <u>in this thickness range</u>. Figure 19 C and D show similar results for the variation of K_b at design τ and τ_b and 10x design τ and τ_b.

Finally, the variation of material thickness for three values of K and K_b is shown in Figure 20. A and B show the negligible effect of thickness in the design point range of conductivity. C and D show

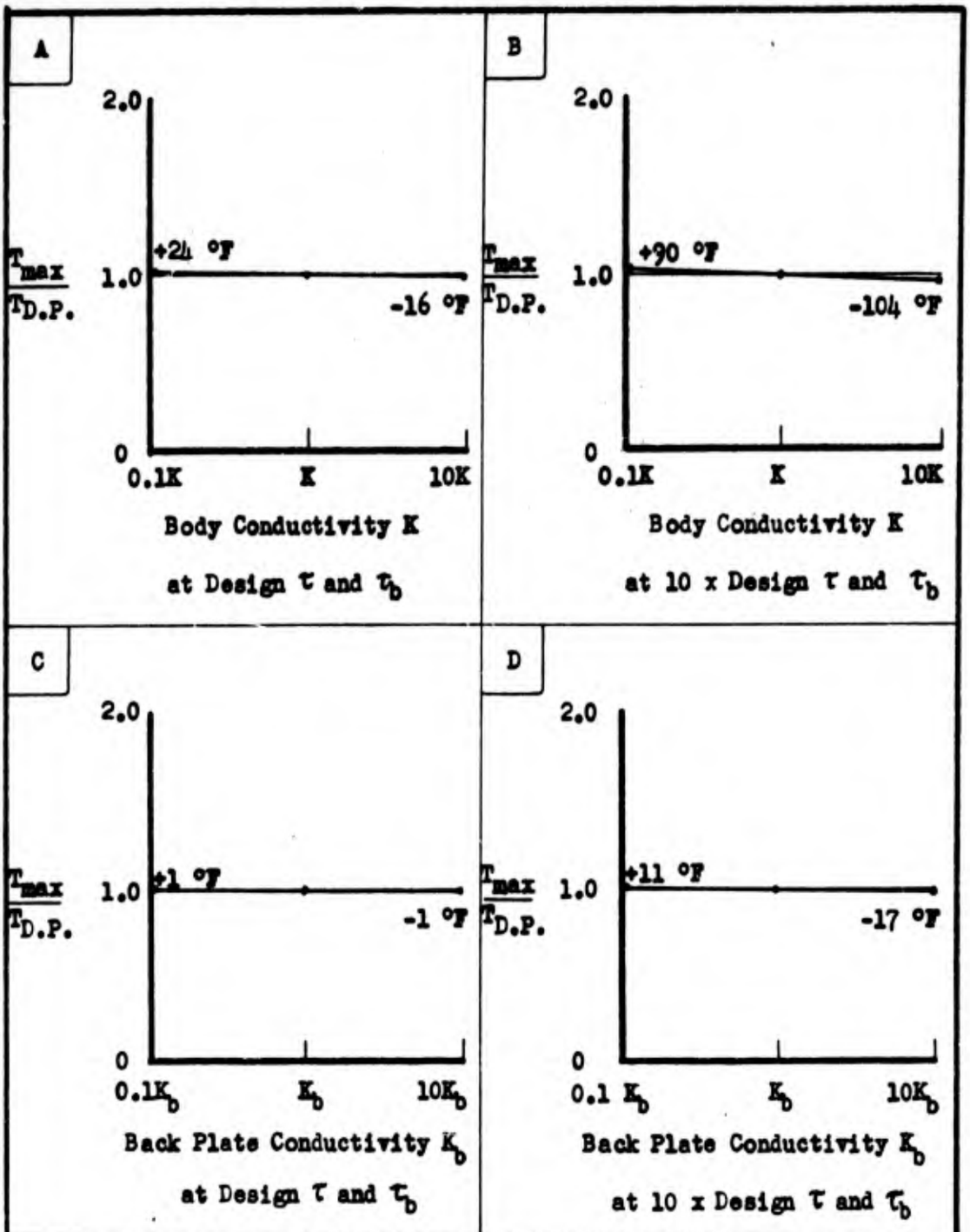

Note: K and K_b above are the design point values of 36 BTU/ft-hr-°R
Design τ = 0.040 inch
Design τ_b = 0.015 inch
36 BTU/ft-hr-°R = 0.0008333 BTU/in-sec-°R

Figure 19

Conductivity Variation

the effect for conductivity values of approximately two orders of magnitude smaller than design point. Finally, E and F show the effect of thickness variation for an order of magnitude increase in conductivity over the design point value. A strange effect of the increase in thickness of the main body material is noted.

Figure 20 A shows a decrease in peak nose temperature with increase in material thickness out to a thickness of 0.3 inch where the temperature trend reverses and increases with material thickness. This behavior is explained as follows: the normal result from an increase in the conductive path for heat transfer, would be a decrease in nose temperature. This increase in wall thickness has two detrimental effects on the radiation exchange of energy. First, the interior surface temperatures are reduced which lessens the potential for cross radiation. Second, the addition of wall thickness reduces the internal radiation area of the cap.

If the conductivity of the added wall thickness is such that the increased conduction exceeds the decrease in radiation, the net effect is a reduction of the nose temperature. This is evident in the first part of Figure 20 A. But, the internal cap area and the internal surface temperatures are being reduced with this increase in material thickness. Thus a body thickness of around 0.3 inch seems to define the crossover point where the effect of the decrease in the radiative exchange exceeds the effect of an increase in the conductive path, and the temperature starts to increase. In the limit and for this conduc -

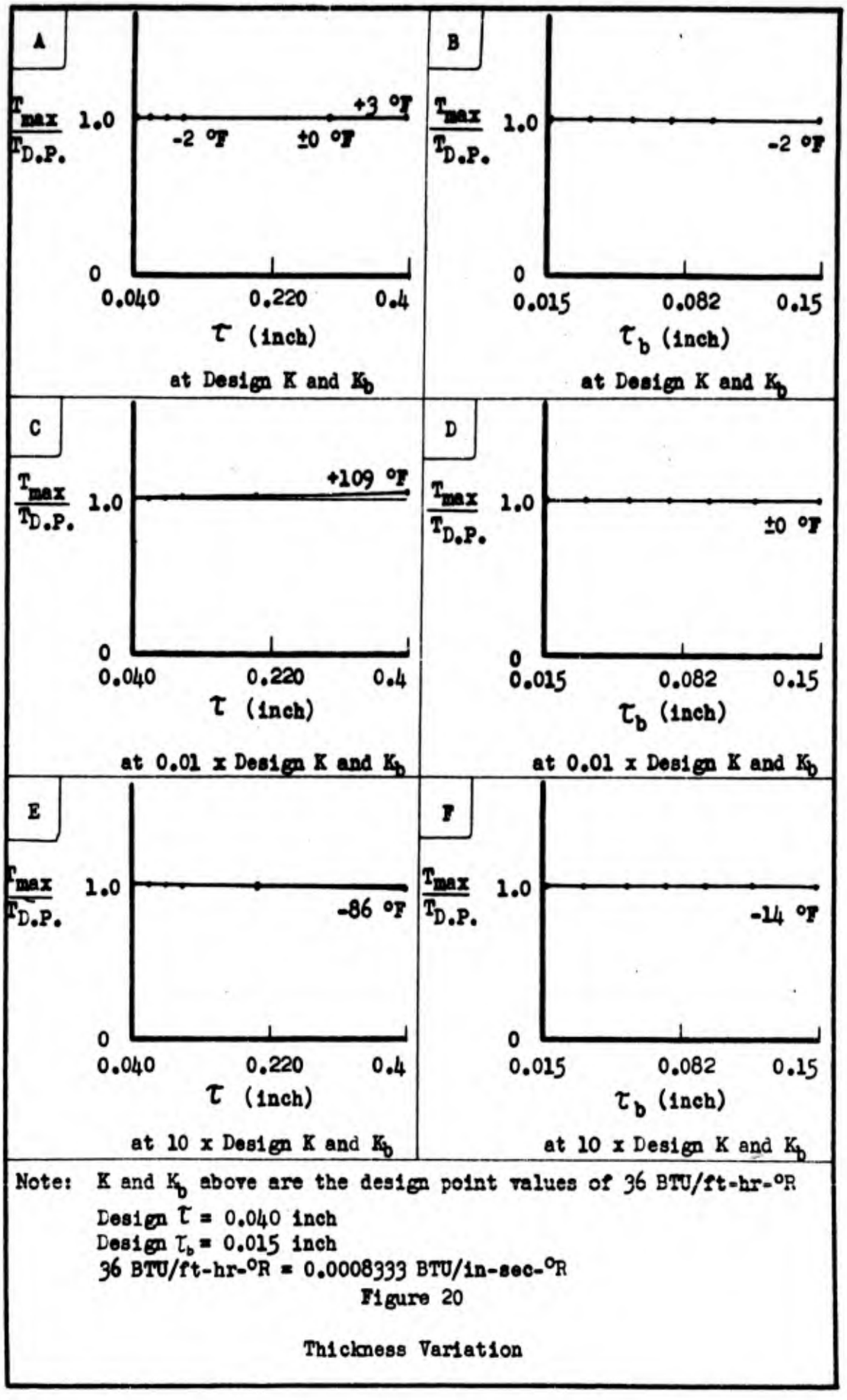

Note: K and K_b above are the design point values of 36 BTU/ft-hr-°R
Design τ = 0.040 inch
Design τ_b = 0.015 inch
36 BTU/ft-hr-°R = 0.0008333 BTU/in-sec-°R

Figure 20

Thickness Variation

tivity value, there would be no internal radiation, all heat transfer would be by conduction, and the resultant nose temperature would be higher than that for a thin shell cap. For the near zero conductivity value of Figure 20 C and D, the increase in material thickness shows a steady increase of nose temperature. This indicates that the detrimental radiation effect exceeds the increased conductive path for the complete thickness range. In contrast, for the high conductivity value of E and F, the increase in nose thickness shows a steady decrease in nose temperature, indicating here that the conductive heat transfer effects are predominate.

A series of computer runs were made to substantiate the above reasoning. These runs were made with ε_{int} and ε_{b} equal to zero thus eliminating the radiation effects. For all three conductivity values, the nose temperature decreased with an increase of material thickness as would normally be expected. Thus an analysis of the effects of material thickness variation, neglecting internal radiation, would give erroneous results.

V. Conclusions and Recommendations

The conclusions reached below are a result of the investigation conducted in this study on a representative glide re-entry vehicle configuration.

1.) An analysis for the peak temperature on a leading edge nose cap neglecting internal radiation and conduction can be in error by about six percent when compared to an analysis which does include these mechanisms of heat transfer.

2.) A substantial decrease in nose temperature may be obtained by variation of the external shape. A reduction of 183 ^{o}F in peak temperature was obtained by replacing a cylindrical cap with an optimum exterior shape.

3.) The orientation of the nose cap back plate will have a large influence on the nose temperature. For example, rotation of the reflector for 60.2 degrees caused a temperature reduction of 407 ^{o}F. This temperature decrease was a result of improved radiation area "view" and the addition of top area for radiative cooling.

4.) A curved reflector will, based on the diffuse reflection assumption, have a minor influence (less than one percent) on the magnitude of the nose temperature.

5.) Of the three emissivity material properties involved, external emissivity is the main variable of importance. Internal emissivity is the next most important variable while variation of back plate emissivity has no effect on the peak nose temperature. High values of internal and external emissivities are desired.

6.) High conductivity values are desirable, but the effects of conductivity are negligible for the thin material thickness values which are dictated by weight considerations. Conversely, for a chosen material with average or low conductivity, a large material thickness can result in increased nose temperatures. It can be thus seen that conductivity and material thickness are closely interrelated, and that one cannot be varied without having an influence on the effects of the other.

7.) For any variation of conductivity and material thickness, the effect on nose temperature is small when compared to other means of temperature reduction demonstrated in this report. For example, a ten-fold thickness increase (and thus a ten-fold weight increase) for a highly conductive material results in an 86 ^{o}F temperature reduction for design point 2 of this study. The same reduction in temperature can be obtained by the addition of one inch of top

area, at a small fraction of the previous weight increase.

The following items are listed as possible recommended areas of further study.

1.) A computer program addition should be prepared which will permit the stagnation point to be located on the major angular segments θ_1 and θ_3.

2.) An investigation could be made to determine the effects of specular reflection from a suitably shaped reflector. The author has devised a method, not included in this report, for defining an optimum reflector based on specular reflection.

3.) The possibility of using a one-way radiation heat filter similar to the one-way mirror in Optics could be investigated. Such a filter could be placed between the hot and cool regions of the cap and, if the one-way exchange of energy could be affected, could be used to advantage in reducing the nose temperature.

4.) The optimum nose shape very closely approximates an ellipse. For this reason, a mathematical model approximated by an elipse in the stagnation region and circular arcs on either side of the ellipse might give better results than that obtained with circular arcs only.

5.) An investigation to attempt to find a non-dimensional combination of conductivity, thickness, and heating rate is recommended.

Bibliography

1. Baylor, R. N. and Conney, C. L. The Calculation of the Effects of Internal Cross -- Radiation on Transient Temperature Distributions in Hypersonic Vehicles. Report No. E9R-12456. Dallas, Texas: Chance Vaught Aircraft, Incorporated, 26 November 1959.

2. Creager, M. O. Effects of Leading-Edge Blunting on the Local Heat Transfer and Pressure Distributions over Flat Plates in Supersonic Flow. NACA TN 4142. Washington, D.C.: NACA, December, 1957.

3. Eckert, E. R. G., and Drake, Robert M., Jr. Heat and Mass Transfer (Second Edition). New York: McGraw-Hill Book Company, Inc., 1959.

4. Hankey, Wilbur L., et al. Design Procedures for Computing Aerodynamics Heating at Hypersonic Speeds. WADC Technical Report 59-610. Armed Services Technical Information Agency, (ASTIA), Arlington Hall Station, Arlington 12, Virginia. June, 1960

5. Hottel, Hoyt C. "Radiant-Heat Transmissions" in Heat Transmission (Third Edition), by William H. McAdams. New York: McGraw-Hill Book Company, Inc., 1954, pp. 55-125.

6. Hottel, Hoyt C. "Notes on Radiant Heat Transmission," in Modern Developments in Heat Transfer, Massachusetts Institute of Technology Special Summer Session 2.52s, June 27 through July 8, 1960

7. Kells, Lyman M. and Stotz, Herman C. Analytic Geometry. New York: Prentice-Hall, Inc., 1949.

8. Lees, Lester. "Laminer Heat Transfer Over Blunt-Nosed Bodies at Hypersonic Flight Speeds," Jet Propulsion, Vol. 26: Nr4: 259-269, 274 (April, 1956).

9. Wagner, Richard D., et al. Laminar Heat -- Transfer and Pressure -- Distribution Studies on a Series of Re-entry Nose Shapes at a Mach Number of 19.4 in Helium. NASA TN D--891. Washington, D.C.: NASA, June, 1961.

APPENDIX A

DETAILS OF COMPUTER PROGRAM

The solution of the 71 fourth order equations requires the use of a digital computer. The criteria used in establishing the new program were:

1. The program must have an arbitrary shape capability. This was to include any nose shape which could be approximated by five radii and five angles. In addition, nonparallel upper and lower surfaces aft of the curved nose section were to be investigated. The internal reflector or back plate was to be flexible to investigate the effects of curvature of this surface.

2. Because of the finite-difference solution required, the mathematical model should be subdivided to the maximum capacity of the available computer and to optimize the distribution of elements to minimize error.

3. The computer input for each desired run must be as simple as possible. This criterion complicates the initial program but is necessary for ease in making large numbers of runs in investigative work. The general physical properties such as conductivity, emissivity, and material thickness, and the flight conditions including convective heating rate, will be required as input for each run.

This leaves the geometric description of the elements to be simplified as much as possible to meet criterion three.

Geometry of Mathematical Model

Orientation on Vehicle. Figure 21 A shows the general hypersonic wing with the general heating cap attached. The wing chord, or any major vehicle reference line, is at an effective angle of attack δ with respect to the normal component $V_{\infty n}$ of the freestream velocity V_∞. The upper and lower surfaces of the heating cap need not be parallel to the wing chord line. The divergence of the upper and lower surfaces from this reference line is given by θ_u' and θ_L respectively.

Figure 21 B shows an x,y-axis attached to the heating cap. This axis is always taken parallel to the lower surface. In so orienting the axis system, the two descriptive angles θ_u' and θ_L are replaced by a single computer input θ_u. Thus, θ_u becomes the total divergence angle of the upper surface with respect to the x axis. Or,

$$\theta_u = \theta_L + \theta_u' \tag{10}$$

The effective angle of attack of the heating cap with respect to the x axis and $V_{\infty n}$ becomes (Figure 21 C)

$$\delta' = \delta + \theta_L \tag{11}$$

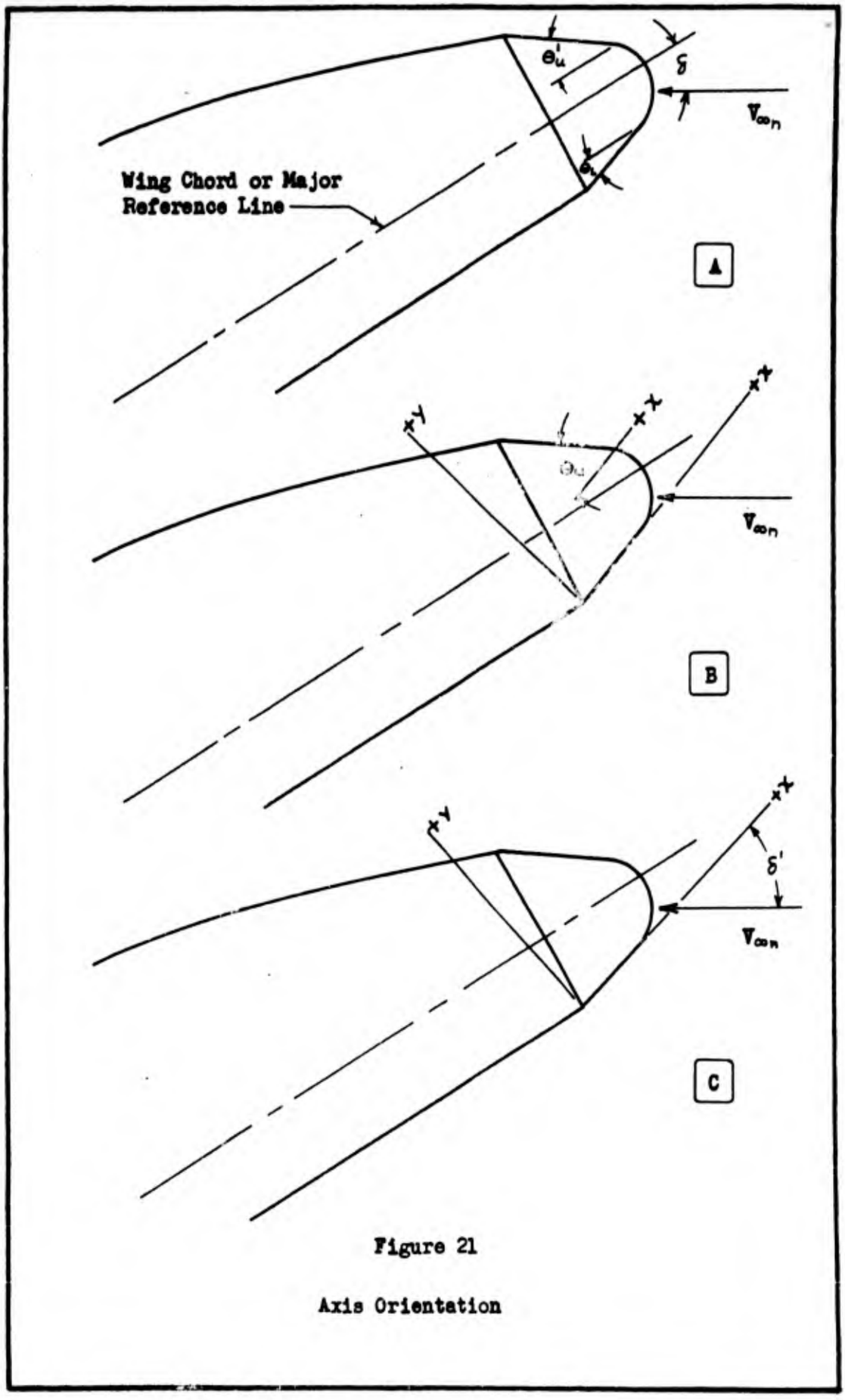

Figure 21

Axis Orientation

Element Division. From results of runs made by the author on the WADD program, several conclusions were reached in relation to the best element distribution throughout the body. First, the WADD program was intended to analyze material thicknesses of around one-half inch. For this reason, the body was divided into three equally thick elements, in the transverse or τ direction. In addition, an infinitesimally thin element was added to the exterior and interior major elements to obtain more accurate values of the skin surface temperatures for radiation purposes (Figure 2). Investigation with the WADD program indicated that, for materials under investigation at this time, around 0.050 inch, the temperature difference between the inner and outer skin elements would be of the order of three or four degrees. For this reason, the transverse element distribution of the new program is as shown in Figure 23. In essence, the body is divided into one element thickness in the transverse or τ direction, but the infinitesimally thin surface elements are again provided for more accurate radiation temperatures and in the event analyses of greater thicknesses are desired.

Additional information from the WADD program indicated that, around the circumference, high temperature differences between elements existed at locations of maximum change in heating rate. For example, in regions near the upper extreme of the curved nose, gradients as high as 450 $^{\circ}$ F were observed between element centers while near the stagnation point, gradients as low as 20 $^{\circ}$ F between element centers were noted. High gradients were also noted at the lower junction of the curved nose and

straight after-body. These observations were used in determining the best element distribution for minimizing the high gradients, and therefore obtaining a more accurate computer solution.

From computer limitations and the information mentioned above, it was decided that seventy-one elements would be a practical maximum number. From Figure 23, the element division was completed as follows: the lower after-body, length $L_L = X_1$, would be a computer input to provide for variation of this surface. It would always be divided into three segments, as shown, to provide for ahigher concentration of elements near the junction of the lower and curved surfaces. θ_1, the first major segment of the curved surface of constant internal radius R_1, would always be sub-divided into four equal angular segments. Again, this is to insure a higher concentration of elements near the critical gradients. The next two circular major segments, θ_2 and θ_3, are subdivided into three equal segments each. θ_4, again in the region of critical gradients, will be divided into four equal segments and, finally, θ_5 into three.

The upper surface, denoted by L_1 in Figure 23, is divided into two equal lengths $\frac{L_1}{2}$, and, finally, the back plate reflector is approximated by three elements as shown. Provisions are made for curving the back plate with the angles θ_6 and θ_7, each a computer input. One caution is required here. For the solution to the internal radiation problem, one assumption which is made is that <u>all</u> internal elements must "see" each other. It should be observed that two elements in a straight line are <u>not</u> hidden from each other in the definition above. For this reason, the shape of

the back plate must be restricted to either straight or concave outward as shown but can never convex inward or shaped in such a manner that an internal element cannot be "seen" by all other internal elements.

Provisions are made for a thickness of the main body τ different from the thickness of the back plate τ_b. External elements and internal elements, for example, 2, 3, 4 . . . . 23 and 47, 48, 49 . . . . 68 are the infinitesimally thin surface elements provided for obtaining accurate radiation temperatures. They are entered into the program at a thickness of 0.001 τ as shown on the figure. It should be noted that these elements are capable of radiating and conducting, the same as other elements.

Choice of Input. As mentioned previously, one of the major criteria for the program was a simple input. This might require some amplification. For example, the worst possible input would be to write the basic energy balance equation, Eq (1), seventy-one times for seventy-one elements, including measured or computed values of all conductive areas and lengths, and including calculated values of view factors and heating rate values to exterior elements. This worst possible input would be required for each desired solution or computer run and would be complex to the point that it would be prohibitive. Conversely, a better input would be a simple description of the physical shape as well as the required physical characteristics of the problem. Then, with the program written in such a manner that all parameters of the energy balance equation are calculated by the computer, the values are placed in the seventy-one equations and the final solution is made. This latter input is the one which has been successfully written in this study.

One of the major problems which had to be solved was that of geometric view factors for internal radiation. As a part of the solution for the grey body view factor $A_i \mathfrak{F}_{ij}$, the black body geometric view factor $A_i F_{ij}$ is required. As defined in (Ref 5:68) the geometric view factor $A_i F_{ij}$ between two elements is

$$A_i F_{ij} = \frac{\sum \text{crossed strings} - \sum \text{uncrossed strings}}{2} \qquad (12)$$

As an example of this equation, consider the geometric view factor between elements 47 and 67 in Figure 23. Per unit length normal to the page, $A_{47}F_{47-67}$ would be the sum of the distances, (left edge of 47 to right edge of 67 and right edge of 47 to left edge of 67, minus the uncrossed distances or left edge of 47 to left edge of 67 and right edge of 47 to right edge of 67, all divided by two). This computation, to be completed by the computer if possible, levied the requirement on any input system that the x,y-coordinate of the corner of each interior element could be mathematically formulated as a function of the input. This was the most stringent requirement and, as such, was the first area investigated for any suggested set of input values.

In the pages that follow, the detailed method of formulating the problem to a computer solution is given. Although over 1000 equations were required in the computer program, only examples of these equations are written here to describe the method used. It should be noted that there are many variations of input and subsequent calculations that could be used to accomplish the overall computer solution. The final combination

depends upon the simplicity of input, complexity of program calculations, and the degree of flexibility desired in the program. After several attempts at variation of these items, it was discovered that, for the input and degree of flexibility of the solution of this study, five items would ultimately be required to build the final solution for all areas, lengths, and view factors and the heating rate distribution. These items are θ_i, R_i, ρ_i, and x_i, y_i, the x,y-coordinates of the circular arc centers $C_1 \ldots . C_5$ of the nose. From the simple input given, these items must be computed (or partially given as input) and only then can sufficient equations be written to compute the parameters required by Eq (1).

Program Input. The standard input for the program includes the following physical properties.

K = conductivity of main body material -- BTU/sec-in-^{o}R

K_b = conductivity of back plate reflector -- BTU/sec-in-^{o}R

$\dot{q}\sqrt{\rho_o}$ = stagnation point heating rate parameter -- $\frac{\text{BTU-in}^{\frac{1}{2}}}{\text{in}^2\text{-sec}}$

δ' = effective angle of attack with respect to the x-axis-degrees

ε_{ext} = external emissivity -- dimensionless

ε_{int} = internal emissivity -- dimensionless

ε_b = back plate emissivity -- dimensionless

τ = main body thickness -- inch

τ_b = back plate thickness -- inch

In addition, the respective lengths of lower, upper, and back plate straight surfaces and the back plate angles must be given.

$L_L = X_1$ = length of lower surface, excluding back plate thickness τ_b -- inch

L_1 = length of upper surface, excluding back plate thickness τ_b -- inch

L_2 = length of No. 69 back plate element -- inch

L_3 = length of No. 70 back plate element -- inch

θ_6 = angle from upper surface to first element of back plate -- degrees (measured from the interior surface of element 68 to the interior surface of element 69)

θ_7 = angle from element 69 to element 70 -- degrees (measured <u>from</u> the direction of element 69 <u>to</u> the direction of element 70.)

The remaining required input is the description of the curved nose section. Two separate methods of describing the nose geometry have been used. The first, described below, consists of specifying the center locations C_1 . . . . C_5 of each circular segment θ_1 . . . . θ_5.

With the x,y-locations of centers C_1 . . . . C_5 given as the input, the angles θ_1 . . . . θ_5, internal radii R_1 . . . . R_5, and external radii ρ_1 . . . . ρ_5 are calculated, thus completing the required set. The calculation of R_i, θ_i from given x,y-center locations is as follows: with the x,y-axis located as shown, specifically, in front of τ_b and below τ,

$$
\begin{aligned}
R_1 &= Y_1 - \tau \\
R_2 &= R_1 \pm \sqrt{(X_2 - X_1)^2 + (Y_2 - Y_1)^2} && R_2 \gtrless R_1 \\
R_3 &= R_2 \pm \sqrt{(X_3 - X_2)^2 + (Y_3 - Y_2)^2} && R_3 \gtrless R_2 \\
R_4 &= R_3 \pm \sqrt{(X_4 - X_3)^2 + (Y_4 - Y_3)^2} && R_4 \gtrless R_3 \\
R_5 &= R_4 \pm \sqrt{(X_5 - X_4)^2 + (Y_5 - Y_4)^2} && R_5 \gtrless R_4
\end{aligned}
\qquad (13)
$$

when the ± sign is taken as $R_i \gtrless R_j$. It should be noted here that this method of calculation has the internal radii R_i as a function of body thickness τ. This is a desirable feature of the input in that as τ changes, the external radius and therefore the external heating rate, does not change. This was a noted weakness in the WADD program when comparative runs where desired for variable body thickness.

To determine the angles $\theta_1 \ldots . \theta_5$, note that, because the arc of θ_1 is always tangent to the lower straight surface, center c_1 will always lie on a line normal to the + x axis. Therefore

$$\theta_1 = \tan^{-1} \frac{X_2 - X_1}{Y_2 - Y_1} \tag{14}$$

To find θ_2, note that the centers for two adjacent radii R_i and R_j, will always lie on R_j or its extension. This requirement is due to the fact that the adjacent circular arcs must be tangent at their common meeting points. Thus, θ_2 will always be bounded by R_2 and R_3, and if the slopes of R_2 and R_3 are known, θ_2 may be found by (Ref 7:43)

$$\theta_i = \tan^{-1} \frac{m_i - m_j}{1 + m_i m_j} \tag{15}$$

where m_i and m_j are the slopes of the bounding radii of θ_i with respect to the + x axis. For the slopes of radii $R_2 \ldots . R_5$,

$$
\begin{aligned}
m_{R_2} &= \frac{Y_2 - Y_1}{X_2 - X_1} \\
m_{R_3} &= \frac{Y_3 - Y_2}{X_3 - X_2} \\
m_{R_4} &= \frac{Y_4 - Y_3}{X_4 - X_3} \\
m_{R_5} &= \frac{Y_5 - Y_4}{X_5 - X_4}
\end{aligned}
\tag{16}
$$

With these values,

$$
\begin{aligned}
\theta_2 &= \tan^{-1} \frac{m_{R_3} - m_{R_2}}{1 + m_{R_3} m_{R_2}} \\
\theta_3 &= \tan^{-1} \frac{m_{R_4} - m_{R_3}}{1 + m_{R_4} m_{R_3}} \\
\theta_4 &= \tan^{-1} \frac{m_{R_5} - m_{R_4}}{1 + m_{R_5} m_{R_4}}
\end{aligned}
\tag{17}
$$

$$
\theta_5 = 180^\circ - (\theta_1 + \theta_2 + \theta_3 + \theta_4) - \theta_u
$$

It should be noted that Eqs (14), (15), (16), and (17) are valid regardless of the relative locations of centers $C_1 \ldots . C_5$, i.e., C_i above, below, left, or right of C_j.

In addition to the above equations describing R_i and θ_i, the external radii ρ_i of the curved nose section are needed in later calculations. The

radius ρ_i is expressed as

$$\rho_i = R_i + \tau \tag{18}$$

where ρ_i remains constant, by virtue of the above routine, for all values of τ. Thus from the general physical input, the simple input of center coordinates, and the above calculated values, the set of parameters θ_i, R_i, ρ_i, x_i, and y_i is now available for the calculation of the required lengths, areas, view factors, and the heating rate distribution for the energy balance Eq (1).

Alternate Program Input. The second scheme successfully employed to describe the nose geometry is to give as input, the external radii ρ_i and the major segment angles θ_i which are used to approximate the arbitrary shape. With these values as input, it becomes necessary to calculate, from the computer routine written below, the internal radii R_i and the x,y-locations of the segment centers C_1 through C_5. For the internal radii

$$R_i = \rho_i - \tau. \tag{19}$$

It can be seen from Figure 23 that with L_L given as a part of this alternate routine, the center coordinates may be calculated as follows:

$$\begin{aligned} X_1 &= L_L \\ Y_1 &= R_1 + \tau \end{aligned} \tag{20}$$

$$X_2 = L_L - (R_2 - R_1) \sin \theta_1$$
$$Y_2 = R_1 + \tau + (R_2 - R_1) \cos \theta_1 \tag{21}$$

$$X_3 = X_2 - (R_3 - R_2) \sin (\theta_1 + \theta_2)$$
$$Y_3 = Y_2 + (R_3 - R_2) \cos (\theta_1 + \theta_2) \tag{22}$$

$$X_4 = X_3 - (R_4 - R_3) \sin (\theta_1 + \theta_2 + \theta_3)$$
$$Y_4 = Y_3 + (R_4 - R_3) \cos (\theta_1 + \theta_2 + \theta_3) \tag{23}$$

$$X_5 = X_4 - (R_5 - R_4) \sin (\theta_1 + \theta_2 + \theta_3 + \theta_4)$$
$$Y_5 = Y_4 + (R_5 - R_4) \cos (\theta_1 + \theta_2 + \theta_3 + \theta_4) \tag{24}$$

Thus, with the simple input of the alternate routine and the above calculated values the parameters θ_i, R_i, ρ_i, x_i, and y_i are again available for the computation of the required parameters in the energy balance equation. It was discovered that, in practice, the alternate program input is probably the most versatile and the easier of the two inputs to use.

The general data input as well as the two geometry inputs are summarized in Figure 4. The first block is a listing, as described before, of the physical characteristics of the body, as well as the general description of the upper surface, back plate, and thickness. The second block is used when the center locations are given as the means to describe the nose

geometry. Note that a statement in the third column is required which depicts R_i less than or greater than R_j. The computer then calculates the required values of R_i, ρ_i, and θ_i. If the alternate input is used, the third block is then completed and calculations of the centers C_1 through C_5 and R_i are then made as indicated above.

To conclude, from either input, the set of necessary calculation parameters is now available. The description to follow shows the way in which this basic set of variables is used to build the complete solution for the unknown temperatures at each element center.

Calculation Procedures

Grey Body View Factor Coordinates. Referring again to Figure 23, equations can be written to describe the x,y-location of the end-point of each interior element as a function of the standard simple input. For example, the right inside corner of element 47 is located by X_{47}, Y_{47} as

$$X_{47} = \frac{2}{3} X_1 \qquad (25)$$

$$Y_{47} = \tau$$

where both X_1 and τ are computer inputs. Continuing,

$$X_{48} = \frac{5}{6} X_1 \qquad (26)$$

$$Y_{48} = \tau$$

$$X_{49} = X_1$$
$$Y_{49} = \tau \tag{27}$$

In a similar manner, the x,y-coordinates for the inner curved elements are calculated as follows:

$$X_{50} = X_1 + R_1 \sin \frac{\theta_1}{4}$$
$$Y_{50} = Y_1 - R_1 \cos \frac{\theta_1}{4} \tag{28}$$

$$\vdots$$

$$X_{54} = X_2 + R_2 \sin \left(\theta_1 + \frac{\theta_2}{3}\right)$$
$$Y_{54} = Y_2 - R_2 \cos \left(\theta_1 + \frac{\theta_2}{3}\right) \tag{29}$$

$$\vdots$$

$$X_{66} = X_5 + R_5 \sin (\theta_1 + \theta_2 + \theta_3 + \theta_4 + \theta_5)$$
$$Y_{66} = Y_5 - R_5 \cos (\theta_1 + \theta_2 + \theta_3 + \theta_4 + \theta_5) \tag{30}$$

For the upper surface elements

$$X_{67} = X_5 + R_5 \sin \sum_{i=1}^{5} \theta_i - \frac{L_1}{2} \cos \theta_u$$
$$Y_{67} = Y_5 - R_5 \cos \sum_{i=1}^{5} \theta_i + \frac{L_1}{2} \sin \theta_u \tag{31}$$

Similarly for the back plate elements

$$X_{69} = X_{68} + L_2 \cos(\theta_6 + \theta_u)$$
$$Y_{69} = Y_{68} - L_2 \sin(\theta_6 + \theta_u) \tag{32}$$

and finally

$$X_{71} = 0$$
$$Y_{71} = \tau \tag{33}$$

Thus, from the simple input as shown in Figure 4 and from the 50 equations written above, the x,y-location of each interior element is computed by the digital computer. These coordinates are then included in the view factor equations and the grey body view factors, as required in the energy equation, are calculated. (Ref 4:57-63 and 5:72-76)

Internal Areas. Defining the internal area of the "i"th element as A_i, the area of element 47, per unit span of the wing, is

$$A_{47} = \frac{2}{3} X_1 \tag{34}$$

Similarly,

$$A_{48} = \frac{X_1}{6} \tag{35}$$

$$A_{49} = \frac{X_1}{6} \tag{36}$$

For the curved areas

$$A_{50} = R_1 \frac{\theta_1}{4} \tag{37}$$

$$\vdots$$

$$A_i = R_i \frac{\theta_i}{n} \tag{38}$$

where R_i is the internal radius for the major segment θ_i and where $n = 3$ or 4, depending upon the subdivision of θ_i.

$$\vdots$$

$$A_{66} = R_5 \frac{\theta_5}{3} \tag{39}$$

For the remaining straight areas

$$A_{67} = \frac{L_1}{2} \tag{40}$$

$$\vdots$$

$$A_{69} = L_2 \tag{41}$$

$$\vdots$$

$$A_{71} = \sqrt{(\bar{X}_{70})^2 + (\bar{Y}_{70} - \tau)^2} \tag{42}$$

With these equations, the internal areas are mathematically described from the simple computer input. Note that the area for element 71 is computed from the calculated values X_{70} and Y_{70} to absorb any cumulative error which might occur in the numerous computations above.

External Areas. Defining the area per unit span of external elements 1 through 24 as ΔS_i, these areas are computed as below:

$$\Delta S_1 = \tau_b \tag{43}$$

$$\Delta S_2 = \frac{2X_1}{3} \tag{44}$$

$$\Delta S_3 = \frac{X_1}{6} \tag{45}$$

$$\Delta S_4 = \frac{X_1}{6} \tag{46}$$

$$\Delta S_5 = (R_1 + \tau)\frac{\theta_1}{4} \tag{47}$$

$$\vdots$$

$$\Delta S_i = (R_i + \tau)\frac{\theta_i}{n} \tag{48}$$

where $(R_i + \tau)$ is the external radius ρ_i for the major segment θ_i and $n = 3$ or 4, depending upon the subdivision of θ_i.

$$\vdots$$

$$\Delta s_{22} = \frac{L_1}{2} \tag{49}$$

$$\Delta s_{24} = \tau_b \tag{50}$$

Again, a set of required variables in the energy balance equation has been completed as a function of the simple input to the computer.

Conductive Length Between Elements. Defining the center length between two adjacent elements as b_{ij}, these values are calculated as below. Starting at the origin and proceeding around the figure counterclockwise, first for the outer two rows of elements, the lengths are

$$b_{2\text{-}25} = 0.4995\ \tau \tag{51}$$

$$b_{2\text{-}3} = \frac{5X_1}{12} \tag{52}$$

$$b_{3\text{-}26} = 0.4995\ \tau \tag{53}$$

$$b_{3\text{-}4} = \frac{X_1}{6} \tag{54}$$

For the curved elements, the conductive length is written as the circular arc length around the periphery, and as the radial distance in the transverse or τ direction. Proceeding from the lower surface to the first curved element

$$b_{4-5} = \frac{X_1}{12} + (R_1 + 0.9995\ \tau)\ \frac{\theta_1}{8} \tag{55}$$

$$b_{5-28} = 0.4995\ \tau \tag{56}$$

$$b_{5-6} = (R_1 + 0.9995\ \tau)\ \frac{\theta_1}{4} \tag{57}$$

.
.
.
.

Between adjacent curved elements of different R_i, the length is

$$b_{8-9} = (R_1 + 0.9995\ \tau)\ \frac{\theta_1}{8} + (R_2 + 0.9995\ \tau)\ \frac{\theta_2}{6} \tag{58}$$

.
.
.
.

For the upper surface

$$b_{22-23} = \frac{L_1}{2} \tag{59}$$

and for the back plate

$$b_{24-69} = \frac{I}{2} + \frac{L_2}{2} \tag{60}$$

and for element 71

$$b_{71-1} = \frac{\sqrt{(X_{70})^2 + (Y_{70} - \tau)^2}}{2} + \frac{I}{2} \tag{61}$$

This procedure is continued for the conductive lengths between all elements. Special mention should be made of the pivot elements 1 and 24. These elements are used to include conduction from the main body into the back plate. This is accomplished by element 1, for example, assuming that the heat is transferred between element 1 and elements 2, 25, and 47 by virtue of the conductivity of the main body. Then the length of element one in this direction is

$$b_{1-2} = b_{1-25} = b_{1-47} = \frac{X_1}{3} + \frac{\tau_b}{2} \tag{62}$$

Heat is conducted between elements one and seventy-one with conductivity k_b of the back plate. Thus b_{71-1} is as given in Eq (61). The choice of directional conductivity for elements one and twenty-four was due to the prevailing conductivity in the direction of heat transfer, i.e., body conductivity in the horizontal direction and back plate conductivity in the vertical direction. Element twenty-four and its adjacent elements are treated in a similar manner.

Conductive Areas Between Elements. Expressions for the adjacent areas per unit span between elements, defined as a_{ij}, were written in a manner similar to the conductive lengths above. A few examples are included below:

$$a_{1-2} = 0.001\ \tau \tag{63}$$

$$a_{1-25} = 0.998\ \tau \tag{64}$$

$$\vdots$$

$$a_{25-26} = 0.998\,\tau \tag{65}$$

$$a_{26-48} = \frac{X_1}{6} \tag{66}$$

For the curved elements

$$a_{4-5} = 0.001\,\tau \tag{67}$$

$$a_{5-28} = (R_1 + 0.999\,\tau)\,\frac{\theta_1}{4} \tag{68}$$

$$a_{5-6} = 0.001\,\tau \tag{69}$$

$$\vdots$$

$$a_{31-53} = (R_1 + 0.001\,\tau)\,\frac{\theta_1}{4} \tag{70}$$

$$a_{31-32} = 0.988\,\tau \tag{71}$$

$$\vdots$$

With the conductive areas between elements completed, approximately 720 relations have been written to describe the mathematical model as a function of the simple computer input. These equations enable the automatic calculation of all required variables in the energy balance equation with the exception of the heating rate for exterior elements. This topic and its computer formulation are discussed below.

Heating Rate Distribution

As presented in section II, Lees' equation for the heating rate distribution over a blunt nosed two dimensional body is

$$\frac{\dot{q}_i}{\dot{q}_o} = \frac{\left(\frac{P_i}{P_o}\right)\left(\frac{V_\delta}{V_\infty}\right)_i}{\left[\frac{2\beta_o}{(R_o+\tau)}\int_o^{S_i}\left(\frac{P}{P_o}\right)\left(\frac{V_\delta}{V_\infty}\right)dS\right]^{\frac{1}{2}}} \qquad (4)$$

when $\dot{q}_i$ is the local heating rate for the "i"th element and $\dot{q}_o$ is the stagnation point heating rate. The equation as presented here does not lend itself readily to the computer program. As with other parts of the basic energy balance equation, it is desirable to reduce the equation to be a function of the standard computer input values. Two major problems are apparent here.

First, the desire for a program to handle arbitrary shapes eliminates the possibility of writing any standard heating rate profile for all configurations. To clarify, the outer elements to which the convective heating applies, will, in general, be located at different points in the flow with changing nose shapes. The heating rate to the "i"th element thus cannot be a fixed value for that element and still maintain flexibility and generality in the program. Second, it is desirable to have a program capable of analyzing the heating cap at different angles of attack and therefore different locations of the stagnation point on the cap. Thus, the constraints of variable geometry, variable element

location and variable stagnation point location complicate the formulation of Eq (4) as a function of the computer input.

Reduction of Equation. From the above listed constraints, the best approach to the reduction of Eq (4) is to express all unknowns in terms of the geometry of each run and therefore in terms of the basic computer input. With reference to Figure 3, the key to the solution lies in using the angle ϕ_i between the tangents to the stagnation point and the center-point of the "i"th element. Figure 3 shows this angle for two example elements, one above the stagnation point and one below. The angle ϕ_i describes the location of the center of the "i"th element from the stagnation point and is the variable through which a solution of the heating rate distribution is possible. ϕ_i is considered always positive.

From Figure 3 and Figure 23, it can be seen that the orientation of the tangent at the stagnation point may be referred to the x,y-axis system by

$$\nu = 90 - \delta' \tag{72}$$

where δ' is a standard program input. Because the stagnation point will always be on the lower half of the body, ν will always be positive and acute.

From modified Newtonian Aerodynamics, the pressure ratio $\frac{P_i}{P_o}$ may be expressed in terms of ϕ_i by (Ref 4:25).

$$\frac{P_i}{P_o} = \cos^2 \phi_i \tag{73}$$

where P_i is the static pressure for element "i" and P_o is the static pressure = total pressure at the stagnation point. Note that at stagnation $\frac{P_i}{P_o} = 1.0$ while at or past 90^o, the line of sight, $\frac{P_i}{P_o} = 0$ as expressed by modified Newtonian theory. With Eq (73), the desired pressure ratio for the "i"th element is obtained as a function of the geometric orientation of that element with respect to the stagnation point.

To obtain the velocity ratio $\left.\frac{V_\delta}{V_\infty}\right|_i$, the energy equation may be written in the inviscid flow field as

$$h_o = h_\delta + \frac{V_\delta^2}{2} = \text{constant} \tag{74}$$

where the subscript δ refers to the conditions at the boundary layer thickness δ and where h_o is the total or stagnation enthalpy. Solving for V_δ^2,

$$V_\delta^2 = 2(h_o - h_\delta) \tag{75}$$

and for the case of constant specific heats,

$$V_\delta^2 = 2\, C_p (T_o - T_\delta) \tag{76}$$

$$V_\delta^2 = 2\, C_p T_o \left(1 - \frac{T_\delta}{T_o}\right) \tag{77}$$

Assuming isentropic conditions exist or that the total pressure is constant, along a streamline (Ref 2:45)

$$V_\delta^2 = 2\, C_p T_o \left[1 - \left(\frac{P_\delta}{P_o}\right)^{\frac{\gamma-1}{\gamma}}\right] \tag{78}$$

Dividing both sides by V_∞^2 gives

$$\frac{V_\delta^2}{V_\infty^2} = \frac{C_p T_o}{\frac{V_\infty^2}{2}} \left[1 - \left(\frac{P_\delta}{P_o} \right)^{\frac{\gamma-1}{\gamma}} \right] \tag{79}$$

or finally

$$\frac{V_\delta^2}{V_\infty^2} \cong \left[1 - \left(\frac{P_\delta}{P_o} \right)^{\frac{\gamma-1}{\gamma}} \right] \tag{80}$$

where $\frac{C_p T_o}{\frac{V_\infty^2}{2}}$ hypersonically approaches unity based on the assumption that h_∞ is small compared to $\frac{V_\infty^2}{2}$. Finally, using Eq (73) for the pressure ratio we get

$$\frac{V_\delta^2}{V_\infty^2} \cong \left[1 - \cos^{2\left(\frac{\gamma-1}{\gamma}\right)} \phi_i \right] \tag{81}$$

Therefore, with equation (81), we now have both the velocity and pressure ratio as a function of the angle ϕ_i.

β_o in the heating rate distribution equation is defined as the non-dimensional stagnation point velocity gradient. Or, in general,

$$\beta_i \triangleq \frac{D}{V_\infty} \frac{\rho_i}{dS} \frac{dV_\delta}{}_i \tag{82}$$

From Eq (81) the derivative of V_δ may be obtained as

$$\left.\frac{dV_\delta}{dS}\right)_i = \frac{V_\infty^2}{2V_\delta} \; 2\left(\frac{\gamma-1}{\gamma}\right) \sin\phi_i \; \cos^{\left(\frac{\gamma-2}{\gamma}\right)} \phi_i \; \left(\frac{d\varphi}{dS}\right)_i \tag{83}$$

Substituting this expression into Eq (82)

$$\beta_i = \frac{\rho_i V_\infty}{V_\delta} \left(\frac{\gamma-1}{\gamma}\right) \cos^{\left(\frac{\gamma-2}{\gamma}\right)} \phi_i \sin\phi_i \left(\frac{d\varphi}{dS}\right)_i \tag{84}$$

For a circular arc of the nose

$$\left(\frac{d\varphi}{dS}\right)_i = \frac{1}{\rho_i} \tag{85}$$

and

$$\beta_i = \left(\frac{V_\delta}{V_\infty}\right)^{-1} \left(\frac{\gamma-1}{\gamma}\right) \cos^{\left(\frac{\gamma-2}{\gamma}\right)} \phi_i \sin\phi_i \tag{86}$$

To evaluate β_i at the stagnation point, $\phi_i = 0$ which results in an indeterminant form.

With Eq (81) for $\frac{V_\infty}{V_\delta}$, β_o may be obtained as

$$\lim_{\phi_i \to 0} \beta_i = \beta_o = \lim_{\phi_i \to 0} \frac{\left(\frac{\gamma-1}{\gamma}\right) \cos^{\left(\frac{\gamma-2}{\gamma}\right)} \phi_i \sin\phi_i}{\sqrt{1 - \cos^{2\left(\frac{\gamma-1}{\gamma}\right)} \phi_i}} \tag{87}$$

and by small angle approximation, $\sin\phi_i \approx \phi_i$, $\cos\phi_i \approx 1.0$ and expressing $\cos\phi_i$ as a series in the denominator,

$$\beta_o = \lim_{\phi_i \to 0} \frac{\left(\frac{\gamma-1}{\gamma}\right) \phi_i}{\sqrt{1 - \left[1 - \frac{\phi_i^2}{2} + \ldots.\right]^{2\left(\frac{\gamma-1}{\gamma}\right)}}} \tag{88}$$

expanding the exponent in the denominator by the binomial series

$$\beta_o = \lim_{\phi_i \to 0} \frac{\left(\frac{\gamma-1}{\gamma}\right) \phi_i}{\sqrt{1 - \left[1 - \left(\frac{\gamma-1}{\gamma}\right) \phi_i^2 + \ldots.\right]}} \tag{89}$$

$$\beta_o = \sqrt{\frac{\gamma-1}{\gamma}} \tag{90}$$

dropping higher order terms.

Using Eqs (90), (81), and (73) in Eq (4), we obtain for the heating rate distribution

$$\frac{\dot{q}_i}{\dot{q}_o} = \frac{\cos^2 \phi_i \sqrt{1 - \cos^2\left(\frac{\gamma-1}{\gamma}\right) \phi_i}}{\left[\frac{2\sqrt{\frac{\gamma-1}{\gamma}}}{\rho_o} \int_o^{S_i} \cos^2 \phi \sqrt{1 - \cos^2\left(\frac{\gamma-1}{\gamma}\right) \phi}\, dS\right]^{\frac{1}{2}}} \tag{91}$$

or in terms β_o

$$\frac{\dot{q}_i}{\dot{q}_o} = \frac{\cos^2 \phi_i \sqrt{1 - \cos^2 2\beta_o^2 \phi_i}}{\left[\frac{2\beta_o}{\rho_o} \int_o^{S_i} \cos^2 \phi \sqrt{1 - \cos^2 2\beta_o^2 \phi}\, dS\right]^{\frac{1}{2}}} \tag{92}$$

and over an arc of radius ρ

$$\frac{\dot{q}_i}{\dot{q}_o} = \frac{\cos^2 \phi_i \sqrt{1 - \cos^{2\beta_o^2} \phi_i}}{\left[\frac{2\beta_o}{\rho_o} \int_o^{\phi_i} \cos^2 \phi \sqrt{1 - \cos^{2\beta_o^2} \phi} \; \rho \, d\phi\right]^{\frac{1}{2}}} \tag{93}$$

From the reduction thus far, the heating rate distribution equation is obtained as a function of the angular location of the "i"th element. Although Eq (93) is a function of ϕ_i, in its present form it is inconvenient and complex. Guided by past work (Ref 4:25) an additional simplification was desired. In particular, the integral of Eq (93) is complex and no simple method of integration presents itself. In an attempt to find a simplification, a plot of the velocity ratio

$$\left.\frac{V_s}{V_\infty}\right|_i = \sqrt{1 - \cos^{2\left(\frac{\gamma-1}{\gamma}\right)} \phi_i} \tag{94}$$

against the variable ϕ_i was made for various values of γ (Figure 22). For higher values of γ, the plot very closely approximates a straight line. In addition, for the dissociated monatomic gas behind the strong shock a γ of 1.66 is the correct value to use. Therefore, the simplification that the velocity ratio $\left.\frac{V_s}{V_\infty}\right|_i$ may be expressed as a straight line function of ϕ_i was adopted, or,

$$\left.\frac{V_s}{V_\infty}\right|_i \cong 0.608 \, \phi_i \quad \text{(radians)} \tag{95}$$

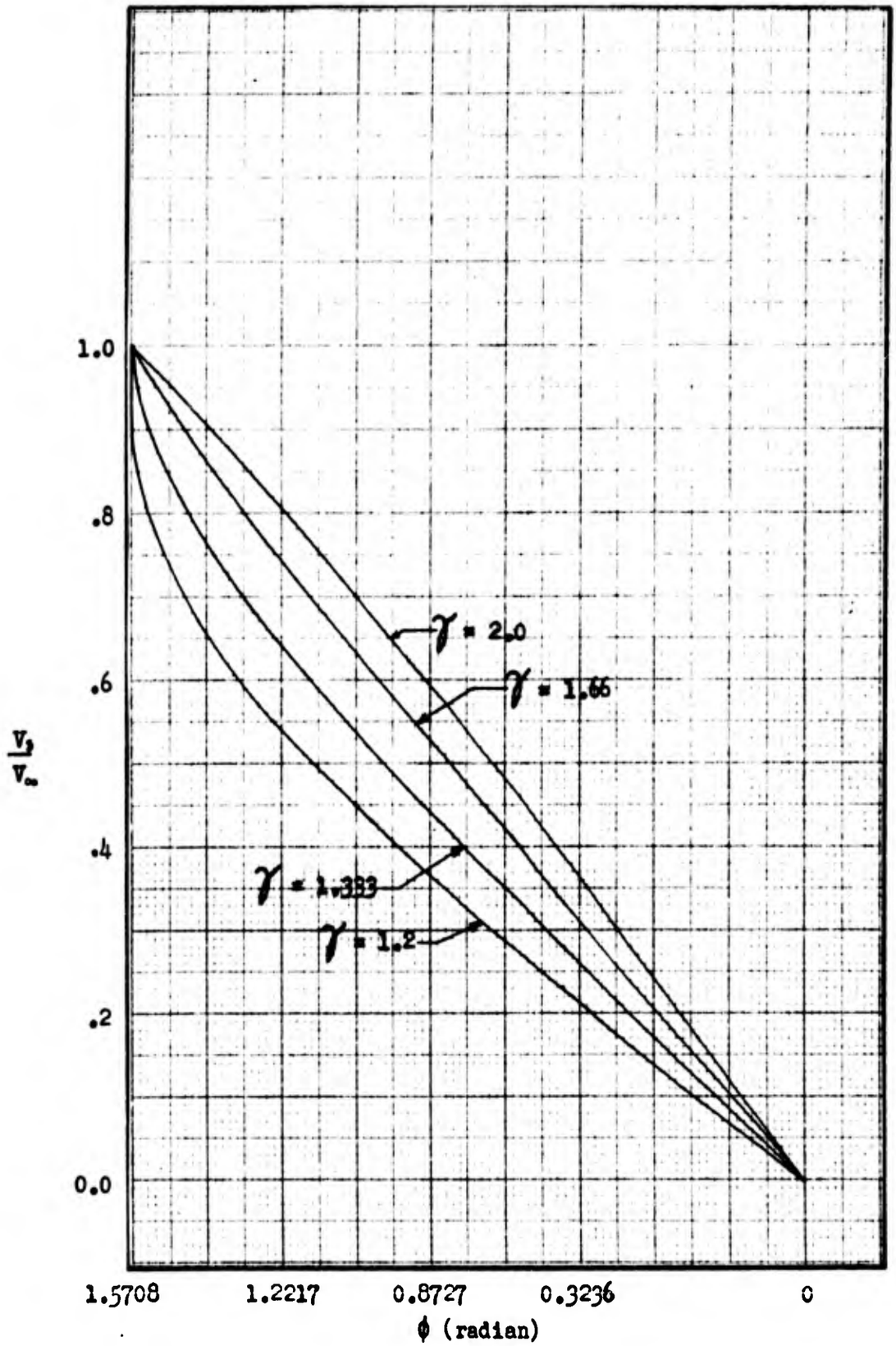

Figure 22

Variation of V_ζ/V_∞ with ϕ for Various Values of γ

where the constant is obtained from Figure 22.

Thus Eq (93) is further simplified to

$$\frac{\dot{q}_i}{\dot{q}_o} = \frac{(0.608\ \phi_i)\ \cos^2 \phi_i}{\left[\frac{2\beta_o}{\rho_o}\int_0^{\phi_i} (0.608\ \phi)\ \cos^2 \phi\ \rho\ d\phi\right]^{\frac{1}{2}}} \tag{96}$$

and collecting constants, define

$$\bar{a} = \frac{D}{\sqrt{\frac{2\beta_o\ (0.608)}{\rho_o}}} \tag{97}$$

and for $\gamma = 1.66$, $\beta_o = 0.613$

$$\bar{a} = \sqrt{\frac{\rho_o\ (0.608)}{2\ (0.613)}} \tag{98}$$

$$\bar{a} = \sqrt{0.496\ \rho_o} \tag{99}$$

and finally

$$\frac{\dot{q}_i}{\dot{q}_o} = \frac{\bar{a}\ \phi_i\ \cos^2 \phi_i}{\left[\int_0^{\phi_i} \phi\ \cos^2 \phi\ \rho\ d\phi\right]^{\frac{1}{2}}} \tag{100}$$

Equation (100) represents the reduced and simplified heating rate equation in terms of the variable ϕ. In its present form, however, two difficulties are still present. The first and most obvious is that the radius ρ inside the integral is a discontinuous step function of the variable ϕ as the integration is performed over the nose. The integration cannot be performed except in steps over which the radius ρ is constant and may thus be taken outside the integral. Second, keeping in mind the ultimate computer adaptation of the solution, the location of the stagnation point, and therefore the location of the lower limit in the integral for element "i", is not fixed with a variable angle of attack as required in an arbitrary program. These points will be further clarified in the next section.

Adaptation to Computer-Curved Elements. To further clarify the problems mentioned above, consider, for example, that the stagnation point, as determined by the angle of attack and element distribution, is on element 9 as shown in Figure 23. If the body configuration, element distribution, and angle of attack are always to be fixed values, the unknown ϕ_i angles at the centerpoint of the "i"th element could be measured. Then Eq (100) could be solved by substitution of these ϕ_i values and by stepwise integration over segments for which ρ is constant. But a solution of this type would not be in keeping with the desired simple input and the capability to handle arbitrary shapes and configurations.

As the first step in solving the present problem, note from Figure 3 that if the angle ϕ'_i which the tangent of the "i"th element makes with

the + x axis is known, that from simple geometry and Eq (72) defining ν,

$$\phi_i = |\phi'_i - \nu| \tag{101}$$

where the absolute value sign is provided to keep ϕ_i always positive. Thus, if the angles ϕ'_i were known for all configurations, or, as a function of the basic input angles θ_i, the required angles ϕ_i for any configuration and all angles of attack would be known by Eq (101). To repeat and clarify, having ν as a function of the input by Eq (72) for all angles of attack and if ϕ'_i were a function of the input major segment angles θ_i, then by Eq (101) we would have the angles ϕ_i as a function of the input for all configuration, angles of attack and for all element distributions.

To obtain the magnitude of the "i"th elements' ϕ'_i, note that the tangent to a circular arc is always normal to the radius of that arc. For the radius ρ_1 to point to the center of element five, ρ_1 was rotated through $\frac{\theta_1}{8}$ degrees and, as a consequence, the tangent to the center point of element five was also rotated $\frac{\theta_1}{8}$ degrees from the x-axis. Thus the orientation of the center of element five with respect to the + x-axis is known by

$$\phi'_5 = \frac{\theta_1}{8} \tag{102}$$

With this value of ϕ'_5 in Eq (101) and the value of ν from Eq (72), ϕ_5 may be determined. As another example

$$\phi'_{18} = \theta_1 + \theta_2 + \theta_3 + \frac{7}{8}\theta_4$$

A similar expression is written for all exterior elements 5 through 21.

With the ϕ_i values now automatically computed as a function of the basic simple input, Eq (100) may be used for any variable configuration or element distribution over the surface of the nose.

To continue with the example of the stagnation point on element 9, assume that for a given configuration and angle of attack, the unknown ϕ_i values have been obtained from the procedure outlined above. To adapt the distribution equation, Eq (100), to computer computation, the equation may be written as

$$\dot{q}_i = \dot{q}_o \frac{N_i}{D_i} \tag{103}$$

where

$$N_i \overset{D}{=} \bar{a}\, \phi_i \cos^2 \phi_i \tag{104}$$

or for the example presented here when element 9 contains the stagnation radius $\rho_o = \rho_2 = R_2 + \tau$,

$$N_i = \sqrt{0.496\, \rho_2}\ \phi_i \cos^2 \phi_i \tag{105}$$

Thus the numerator of the $\dot{q}_i$ equation is readily solved by computer techniques by substituting the appropriate pre-calculated ϕ_i values. The N_i values are then stored for future use.

To evaluate the denominator, note that D_i is defined as

$$D_i \overset{D}{=} \left[\int_0^{\phi_i} \phi \cos^2 \phi \, \rho \, d\phi \right]^{\frac{1}{2}} \tag{106}$$

As stated before, the required integration in D_i may be accomplished by a step-wise integration over $d\phi$ for which ρ is constant, i.e., ρ_1, ρ_2, . . . ρ_5. For example, to evaluate the integral for element 13, D_i would be

$$D_{13} = \rho_2 \int_0^{\phi_{11\frac{1}{2}}} \phi \cos^2 \phi \, d\phi + \rho_3 \int_{\phi_{11\frac{1}{2}}}^{\phi_{13}} \phi \cos^2 \phi \, d\phi \tag{107}$$

where $\phi_{11\frac{1}{2}}$, the angular orientation of the junction of elements 11 and 12, is obtained by Eq (101) the same as the ϕ_i values for element center locations. Here again a simplification is available.

By defining the integral in D_i as I_i,

$$I_i \overset{D}{=} \int_0^{\phi_i} \phi \cos^2 \phi \, d\phi \tag{108}$$

and evaluating this integral with zero as a lower limit,

$$I_i \overset{D}{=} \frac{\phi_i^2}{4} + \frac{\phi_i \sin 2\phi_i}{4} + \frac{\cos 2\phi_i}{8} - \frac{1}{8} \tag{109}$$

The use of zero as a lower limit reduces the complexity of I_i and thus simplifies the working expressions. By the use of the I_i operation notation and with ϕ_i obtained as before, the D_i values are finally obtained as follows with the stagnation point on element 9:

$$D_{10} = (\rho_2 I_{10})^{\frac{1}{2}} \tag{110}$$

$$D_{11} = (\rho_2 I_{11})^{\frac{1}{2}} \tag{111}$$

$$D_{12} = \left[(\rho_2 I_{11\frac{1}{2}}) + \rho_3 \ (I_{12} - I_{11\frac{1}{2}})\right]^{\frac{1}{2}} \tag{112}$$

$$\vdots$$

$$D_{15} = \left[\rho_2 I_{11\frac{1}{2}} + \rho_3 \left(I_{14\frac{1}{2}} - I_{11\frac{1}{2}} \right) + \rho_4 \ (I_{15} - I_{14\frac{1}{2}})\right]^{\frac{1}{2}} \tag{113}$$

$$\vdots$$

$$D_9 = (\rho_2 I_9)^{\frac{1}{2}} \tag{114}$$

$$D_8 = \left[\rho_2 I_{8\frac{1}{2}} + \rho_1 \ (I_8 - I_{8\frac{1}{2}})\right]^{\frac{1}{2}} \tag{115}$$

$$\vdots$$

Thus with these values of D_i computed, the expression for $\dot{q}_i$ at the center of each curved element is obtained by Eq (103).

It should be noted that the system as written here is valid for the stagnation point on any element in the θ_2 segment. This is required by virtue of the solution in terms of the D_i values but is not a great restriction in that θ_2 may be placed to include the stagnation point over a range of effective angles of attack of about 85°, with a slight sacrifice in ideal element distribution.

The procedure described above was adapted to the computer and has been checked by hand calculations for accuracy. Two additional points should be noted. If by chance, the center of either elements 9, 10, or 11 should exactly contain the stagnation point, the expression for $\dot{q}_i$ will be indeterminate by virtue of a zero value for ϕ_i. A stop in the computer program was used to identify $\dot{q}_i$ in this case as the computer input value $\dot{q}_o$ for the stagnation point. Second, for upper elements at or past the line of sight of V_{∞_n} ($\phi_i \geq 90^o$) the heating rate is zero as dictated by modified Newtonian theory. In addition, no provision for a heating rate to elements 22, 23, and 24 is made. The program is written for critical heating flight altitudes, and under such conditions, efficient design would dictate that the upper surface be hidden from the Newtonian flow. In reality, the upper surfaces will receive a small amount of convective heating but this is considered negligible.

Adaptation to Computer-Straight Elements. For $\dot{q}_i$ of the lower straight afterbody elements 1 through 4, a similar routine is established. Recall that these elements are all orientated with respect to the stagnation point tangent at an angle ν. Or

$$\phi_1 = \phi_2 = \phi_3 = \phi_4 = \nu \tag{116}$$

and therefore

$$N_i = \bar{a}\, \nu \cos^2 \nu \tag{117}$$

where

$$i = 1, 2, 3 \text{ and } 4$$

For the denominator D_i, note that the integral is evaluated around the curved nose to point $4\frac{1}{2}$ similar to the curved elements and, at this point, the variable will revert back to the variable dS or

$$I\Big]_{4\frac{1}{2}}^{i} = \left[\int_{o}^{S'} \nu \cos^2 \nu \; dS\right]^{\frac{1}{2}} \tag{118}$$

$$I\Big]_{4\frac{1}{2}}^{i} = \left[\nu \cos^2 \nu \; (S)_{o}^{S'}\right]^{\frac{1}{2}} \tag{119}$$

when the length S' pertains to the linear distance from point $4\frac{1}{2}$ to the center point in question. Therefore,

$$D_4 = \left[\rho_2 I_{8\frac{1}{2}} + \rho_1 (I_\nu - I_{8\frac{1}{2}}) + \nu \cos^2 \nu \frac{X_1}{12}\right]^{\frac{1}{2}} \tag{120}$$

$$\vdots$$

$$D_1 = \left[\rho_2 I_{8\frac{1}{2}} + \rho_1 (I_\nu - I_{8\frac{1}{2}}) + \nu \cos^2 \nu \left(x_1 + \frac{\tau_b}{2}\right)\right]^{\frac{1}{2}} \tag{121}$$

and the $\dot{q}_i$ expressions are completed for the straight lower afterbody elements by Eq (103).

Summary of Heating Equations. To show again, but in more concise form, the equations and the interrelation of variables, the equations are re-printed below as the finalized computer program was written. Items marked * indicate those items which would be altered in the event that a program change is desired which would place the stagnation point on either θ_1 or θ_3.

1. Stagnation tangent to x-axis (introduces variable angle of attack into the heating rate distribution routine)

$$\nu = 90 - \delta' \tag{72}$$

2. ϕ_i location of tangent to center point (or θ_i major segment junction points) of "i"th element with respect to stagnation tangent (combines variable angle of attack and variable element distribution to find the primary heating variable ϕ_i)

Point	ϕ'_i	ϕ_i
$4\frac{1}{2}$	0	ν
5	$\frac{\theta_1}{8}$	$\left\lvert \frac{\theta_1}{8} - \nu \right\rvert$
.	.	.
.	.	.
.	.	.
i	$\sum \theta_i$	$\left\lvert \sum \theta_i - \nu \right\rvert$
.	.	.
.	.	.
.	.	.
$21\frac{1}{2}$	$\theta_1 + \theta_2 + \theta_3 + \theta_4 + \theta_5$	$\left\lvert \theta_{21\frac{1}{2}} - \nu \right\rvert$

3. Integral operator I_i

$$I_i = \left[\frac{\phi_i^2}{4} + \frac{\phi_i \sin 2\phi_i}{4} + \frac{\cos 2\phi_i}{8} - \frac{1}{8} \right] \tag{109}$$

$$I_{4\frac{1}{2}} = I(\nu) \tag{122}$$

$$I_5 = I(\phi_5) \tag{123}$$

$$\vdots$$

$$I_{21} = I(\phi_{21}) \tag{124}$$

where $\phi_i < 90^\circ$ only.

4. $$\bar{a}^* = \sqrt{0.496\ (R_2 + \tau)}^* = \sqrt{0.496\ \rho_2}^* \tag{99}$$

5. $$\dot{q}_i = q_o \frac{N_i}{D_i}$$ (curved elements) where (103)

$$N_i = \bar{a}\ \phi_i \cos^2 \phi_i \qquad \phi_i < 90^\circ \tag{104}$$

$$D_5 = \left[\rho_2 I_{8\frac{1}{2}} + \rho_1 (I_5 - I_{8\frac{1}{2}})\right]^{\frac{1}{2}*} \tag{125}$$

$$\vdots$$

$$D_{21} = \left[\rho_2 I_{11\frac{1}{2}} + \rho_3 (I_{14\frac{1}{2}} - I_{11\frac{1}{2}}) + \rho_4 (I_{18\frac{1}{2}} - I_{14\frac{1}{2}}) + \rho_5 (I_{21} - I_{18\frac{1}{2}})\right]^{\frac{1}{2}*} \tag{126}$$

6. $$\dot{q}_i = \dot{q}_o \frac{N_i}{D_i}$$ (straight elements) where (103)

$$N_i = \bar{a}\ \nu \cos^2 \nu \tag{117}$$

$$D_4 = \left[\rho_2 I_{8\frac{1}{2}} + \rho_1 (I_\nu - I_{8\frac{1}{2}}) + \nu \cos^2 \nu \frac{X_1}{12}\right]^{\frac{1}{2}*} \tag{120}$$

$$D_1 = \left[\rho_2 I_{8\frac{1}{2}} + \rho_1 \left(I_\nu - I_{8\frac{1}{2}} \right) + \nu \cos^2 \nu \left(X_1 + \frac{\tau_b}{2} \right) \right]^{\frac{1}{2}} * \qquad (121)$$

Note again that Eq (72) for the angle ν contains the effective angle of attack of the body. Then the equations in item two, above, in terms of the $\theta_1 \ldots . \theta_5$ inputs and the angle ν, incorporate element location and changing angle of attack. Finally, using the system of integrals in items five and six, the heating rate for any element is obtained for all angles of attack, and for all element distributions, so long as stagnation falls on the θ_2 segment.

Program Check Out

With the complex nature of the computer program, a detailed check of calculated results was mandatory. Many checks were made, as listed below, before results from the program could be accepted. The check out was made on an arbitrary shape, and a simple cylindrical shape with parallel afterbodies to simulate the WADD program. All items listed below were checked, for these shapes, from the initial computer print-outs which listed all calculations of the program. The items checked were:

1. X_i, Y_i for centers $C_1 \ldots . C_5$ and R_i
2. Gray body $A_i \mathcal{F}_{ij}$ symmetry in a 71 x 71 matrix

3. Internal, external and conductive areas

4. Conductive lengths

5. Heating rate distribution by hand calculation for several elements

6. X_i, Y_i location of interior elements

Finally, the most conclusive check was an overall energy balance for the cap. Under steady-state conditions, all energy leaving the cap must equal all energy entering the cap. Using the solution temperatures to express energy leaving; and the heating rate distribution to express energy entering, a balance was made and a percent error calculated. This percent error based on heat added has been about 0.006 to 0.008 but never greater than 0.10. The check represents a valid investigation of the manner in which the mechanisms of conduction and internal cross radiation redistribute the energy in the cap.

With the accuracy and reliability of the program so established, an investigation was made as presented in section IV.

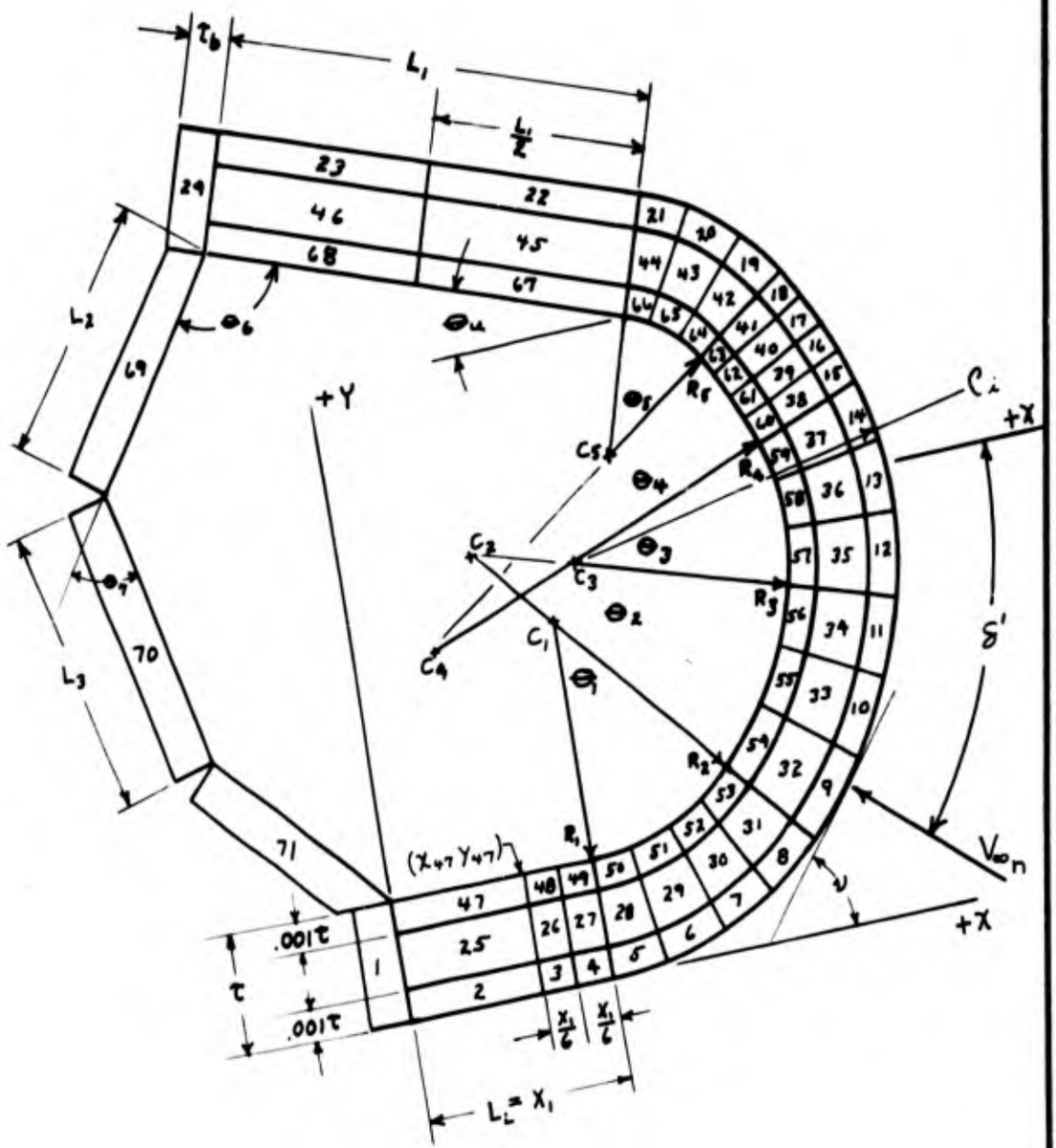

Figure 23

Mathematical Model of Leading Edge Cap

APPENDIX B

EXAMPLE COMPUTER DATA SHEETS

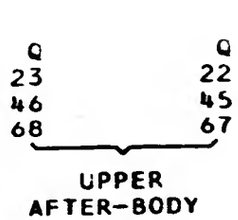

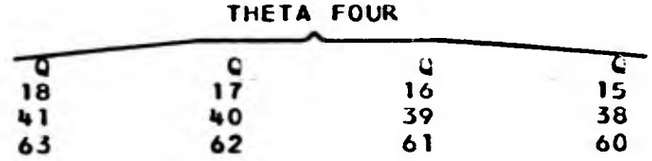

K=CONDUCTIVITY OF BODY
KB=CONDUCTIVITY OF BACK PLATE
QDOT=HEATING RATE PARAMETER $\dot{q}\sqrt{\rho_o}$
TAU=THICKNESS OF BODY
TAUB=THICKNESS OF BACK PLATE

EEXT=EMISSIVITY-EXTERNAL
EINT=EMISSIVITY-INTERNAL
EB=EMISSIVITY-BACK PLATE

DELTAP=EFFECTIVE ANGLE OF ATTACK
THETAU=BODY DIVERGENCE ANGLE
THETA6=BACK PLATE ANGLE
THETA7=BACK PLATE ANGLE

L1=UPPER BODY LENGTH
L2=BACK PLATE LENGTH
L3=BACK PLATE LENGTH
LL=LOWER BODY LENGTH

THETA1
THETA2
THETA3
THETA4
THETA5
} NOSE GEOMETRY

δ'RHO1
RHO2
RHO3
RHO4
RHO5
} NOSE RADII

THETA THREE: 59, 37, 14, Q, 58, 36, 13, Q, 57, 35, 12, Q

* NOTE ==== 1.ALL TEMPERATURES IN DEGREES-F
2.ALL Q IN BTU/(SEC)(SQIN)
3.ALL LENGTHS IN INCHES
4.ALL ANGLES IN DEGREES
5.ELEMENTS 2-23,EXTERIOR(.001 τ THICK)
6.ELEMENTS 47-68,INTERIOR(.001 τTHICK)

24 PIVOT ELEMENT
69
70 } BACK PLATE
71
1 PIVOT ELEMENT
Q

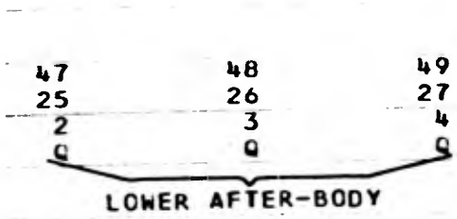

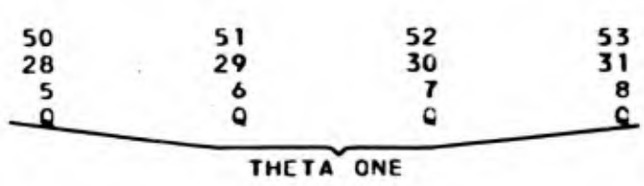

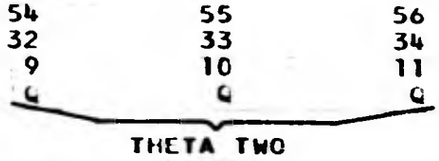

```
 Q  0.          Q  0.
23  902.    22  901.     Q 0.005     Q 0.039     Q 0.094
45  913.    45  913.    21  925.    20 1636.    19 2160.     Q 0.152     Q 0.204     Q 0.256     Q 0.304
67  913.    67  913.    44  929.    43 1635.    42 2159.    18 2493.    17 2719.    16 2902.    15 3051.
                         66  929.    65 1635.    64 2159.    41 2493.    40 2719.    39 2902.    38 3051.
                                                              65 2493.    62 2719.    61 2902.    60 3051.

                                                                                                  59 3187.
24  913.                                                                                          37 3187.
                                                                                                  14 3188.
69 1257.                                                                                       Q 0.354     58 3301.
                                                                                                           36 3301.
70 1927.                                                                                                   13 3302.
71 2599.                                                                                       57 3375.    Q 0.401
 1 2946.                                                                                       35 3375.
 Q 0.263                                                                                       12 3375.
                                                                                               Q 0.433

47 2949.    48 2950.    49 2950.    50 3006.    51 3133.    52 3235.    53 3313.    54 3375.    55 3411.    56 3411.
25 2949.    26 2950.    27 2950.     5 3006.     6 3134.     7 3235.     8 3313.    32 3375.    33 3411.    34 3411.
 2 2942.     3 2942.     4 2943.    Q 0.288     Q 0.334     Q 0.373     Q 0.406     9 3375.    10 3411.    11 3411.
 Q 0.264     Q 0.264     Q 0.264                                                    Q 0.433     Q 0.450     Q 0.450
```

Page 103

```
K= 1.000000E-05                    THETA1= 0.270000E 02
KB= 1.000000E-05                   THETA2= 0.270000E 02
GDOT= 0.694400E 00                 THETA3= 0.270000E 02
TAU= 0.400000E-01                  THETA4= 0.270000E 02
TAUB= 0.150000E-01                 THETA5= 0.270000E 02

DEXT= 0.600000E 00
DINT= 0.
EB= 0.

DELTAP= 0.450000E 02               RHO1= 0.234500E 01
THETAU= 0.450000E 02               RHO2= 0.234500E 01
THETA6= 0.676000E 02               RHO3= 0.234500E 01
THETA7= 0.                         RHO4= 0.234500E 01
                                   RHO5= 0.234500E 01
L1= 1.000000E-03
L2= 0.141600E 01
L3= 0.141600E 01
LL= 1.000000E-03
```

```
 0.          0.
23  769.    22  769.      0.005     0.039     0.094
46  780.    45  780.    21  794.    20 1438.  19 1909.    0.152     0.204     0.256     0.304
68  780.    67  780.    44  797.    43 1437.  42 1908.  18 2210.  17 2414.  16 2579.  15 2713.
                        66  797.    65 1437.  64 1908.  41 2209.  40 2413.  39 2579.  38 2713.
                                                        63 2209.  62 2413.  61 2579.  60 2713.
```



```
K= 1.000000E-05
KB= 1.000000E-05
QDOT= 0.694400E 00
TAU= 0.4000000E-01
TAUB= 0.1500000E-01

EFXT= 0.9000000E 00
EINT= 0.
EB= 0.

DELTAP= 0.4500000E 02
THETAU= 0.4500000E 02
THETA6= 0.6760000E 02
THETA7= 0.

L1= 1.0000000E-03
L2= 0.1416000E 01
L3= 0.1416000E 01
LL= 1.0000000E-03

THETA1= 0.2700000E 02
THETA2= 0.2700000E 02
THETA3= 0.2700000E 02
THETA4= 0.2700000E 02
THETA5= 0.2700000E 02

RHO1= 0.2345000E 01
RHO2= 0.2345000E 01
RHO3= 0.2345000E 01
RHO4= 0.2345000E 01
RHO5= 0.2345000E 01
```

```
 4  780.                                                                  59 2837.
                                                                          37 2837.
 9 1091.                                                                  14 2837.
                                                                           0.354    58 2939.
                                                                                    36 2939.
 0 1696.                                                                            13 2940.
                                                                          57 3006.   0.401
 1 2304.                                                                  35 3006.
                                                                          12 3006.
  1 2618.                                                                  0.433
  0.263
```

```
                                                                          54 3006.  55 3038.  56 3038.
                                                 50 2672.  51 2788.  52 2880.  53 2950.  32 3006.  33 3038.  34 3038.
47 2620.  48 2621.  49 2621.  28 2672.  29 2788.  30 2880.  31 2950.   9 3006.  10 3039.  11 3039.
25 2620.  26 2621.  27 2621.   5 2672.   0.288   7 2880.   8 2950.    0.433   0.450   0.450
  2 2614.   3 2614.   4 2614.   0.288   0.334   0.373   0.406
  0.264     0.264     0.264
```

RUN 6-B

```
 Q 0.          Q 0.
23 1804.      22 1804.      Q 0.005       Q 0.039       Q 0.094
46 1805.      45 1805.      21 1788.      20 1943.      19 2210.      Q 0.152       Q 0.204       Q 0.256       Q 0.304
68 1805.      67 1805.      44 1789.      43 1944.      42 2210.      18 2468.      17 2676.      16 2860.      15 3013.
                            66 1789.      65 1944.      64 2210.      41 2468.      40 2676.      39 2859.      38 3013.
                                                                     63 2468.      62 2676.      61 2859.      60 3013.
```



```
                                  K= 0.833330E-03                    THCTA1= 0.270000E 02
                                  KB= 0.833330E-03                   THETA2= 0.270000E 02
                                  QDOT= 0.694400E 00                 THETA3= 0.270000E 02
                                  TAU= 0.400000E-01                  THETA4= 0.270000E 02
24 1805.                          TAUB= 0.150000E-01                 THETA5= 0.270000E 02          59 3158.
                                                                                                   37 3158.
69 2015.                          EEXT= 0.600000E 00                                              14 3158.
                                  EINT= 0.                                                         Q 0.354      58 3277.
70 2423.                          EB= 0.                                                                        36 3277.
                                                                                                                13 3277.
71 2833.                          DELTAP= 0.450000E 02               RHO1= 0.234500E 01            57 3354.      Q 0.401
                                  THETAU= 0.450000E 02               RHO2= 0.234500E 01            35 3354.
 1 3044.                          THETA6= 0.676000E 02               RHO3= 0.234500E 01            12 3354.
 Q 0.263                          THETA7= 0.                         RHO4= 0.234500E 01             Q 0.433
                                                                     RHO5= 0.234500E 01

                                  L1= 1.000000E-03
                                  L2= 0.141600E 01
                                  L3= 0.141600E 01
                                  LL= 1.000000E-03
```

```
                                                                                                   54 3356.      55 3392.      56 3391.
                                                50 3062.      51 3140.      52 3223.      53 3294.      32 3356.      33 3392.      34 3391.
47 3045.      48 3045.      49 3045.      28 3062.      29 3140.      30 3223.      31 3294.       9 3356.      10 3392.      11 3391.
25 3045.      26 3045.      27 3045.       5 3062.       6 3140.       7 3223.       8 3294.       Q 0.433       Q 0.450       Q 0.450
 2 3044.       3 3044.       4 3044.       Q 0.288       Q 0.334       Q 0.373       Q 0.406
 Q 0.264       Q 0.264       Q 0.264
```

RUN 6-C

```
 Q 0.         Q 0.        Q 0.005     Q 0.039     Q 0.094
23 1562.     22 1562.    21 1548.    20 1696.    19 1946.    Q 0.152     Q 0.264     Q 0.256     Q 0.304
46 1563.     45 1563.    44 1550.    43 1697.    42 1946.   18 2185.    17 2376.    16 2543.    15 2682.
68 1563.     67 1563.    66 1550.    65 1697.    64 1946.   41 2185.    40 2376.    39 2543.    38 2682.
                                                            63 2185.    62 2376.    61 2543.    60 2682.
```

```
                         K= 0.833330E-03                    THETA1= 0.270000E 02
                         KB= 0.833330E-03                   THETA2= 0.270000E 02
                         QDOT= 0.694400E 00                 THETA3= 0.270000E 02
                         TAU= 0.400000E-01                  THETA4= 0.270000E 02
24 1564.                 TAUB= 0.150000E-01                 THETA5= 0.270000E 02        59 2812.
                                                                                        37 2812.
69 1757.                 EEXT= 0.900000E 00                                             14 2813.
                         EINT= 0.                                                        Q 0.354    58 2919.
70 2132.                 EB= 0.                                                                     36 2919.
                                                                                                    13 2920.
71 2509.                 DELTAP= 0.450000E 02               RHO1= 0.234500E 01          57 2988.     Q 0.401
                         THETAU= 0.450000E 02               RHO2= 0.234500E 01          35 2988.
 1 2703.                 THETA6= 0.676000E 02               RHO3= 0.234500E 01          12 2989.
 Q 0.263                 THETA7= 0.                         RHO4= 0.234500E 01           Q 0.433
                                                            RHO5= 0.234500E 01
                         L1= 1.000000E-03
                         L2= 0.141600E 01
                         L3= 0.141600E 01
                         LL= 1.000000E-03
```

```
                                                                        54 2990.    55 3023.    56 3022.
                                     50 2720.    51 2793.    52 2869.    53 2934.    32 2990.    33 3023.    34 3022.
                                     28 2720.    29 2793.    30 2869.    31 2934.     9 2990.    10 3023.    11 3023.
47 2704.     48 2704.    49 2704.     5 2720.     6 2793.     7 2869.     8 2934.     Q 0.433     Q 0.450     Q 0.450
25 2704.     26 2704.    27 2704.     Q 0.288     Q 0.334     Q 0.373     Q 0.406
 2 2704.      3 2704.     4 2704.
 Q 0.264      Q 0.264     Q 0.264
```

RUN 6-D

CASE/ME/L9-8

Q 0.	Q 0.							
23 2562.	22 2562.	Q 0.005	Q 0.039	Q 0.094				
46 2566.	45 2566.	21 2550.	20 2606.	19 2703.	Q 0.152	Q 0.204	Q 0.256	Q 0.304
68 2569.	67 2569.	44 2554.	43 2609.	42 2706.	18 2800.	17 2881.	16 2957.	15 3024.
		66 2557.	65 2612.	64 2708.	41 2801.	40 2882.	39 2957.	38 3023.
					63 2803.	62 2883.	61 2958.	60 3023.

Page 107

K= 0.833330E-03
KB= 0.833330E-03
QDOT= 0.694400E 00
TAU= 0.400000E-01
TAUB= 0.150000E-01

EEXT= 0.600000E 00
EINT= 0.800000E 00
EB= 1.000000E-01

DELTAP= 0.450000E 02
THETAU= 0.450000E 02
THETA6= 0.676000E 02
THETA7= 0.

L1= 1.000000E-03
L2= 0.141600E 01
L3= 0.141600E 01
LL= 1.000000E-03

THETA1= 0.270000E 02
THETA2= 0.270000E 02
THETA3= 0.270000E 02
THETA4= 0.270000E 02
THETA5= 0.270000E 02

RHO1= 0.234500E 01
RHO2= 0.234500E 01
RHO3= 0.234500E 01
RHO4= 0.234500E 01
RHO5= 0.234500E 01

24 2566.							59 3088.	
							37 3089.	
69 2842.							14 3090.	
							Q 0.354	58 3144.
70 3046.								36 3146.
								13 3147.
71 3091.							57 3182.	Q 0.401
							35 3184.	
1 3054.							12 3186.	
Q 0.263							Q 0.433	
				50 3054.	51 3089.	52 3129.	53 3162.	54 3190.	55 3205.	56 3203.
47 3054.	48 3054.	49 3054.		28 3054.	29 3090.	30 3129.	31 3163.	32 3191.	33 3207.	34 3205.
25 3054.	26 3054.	27 3054.		5 3053.	6 3090.	7 3130.	8 3164.	9 3193.	10 3209.	11 3207.
2 3053.	3 3053.	4 3053.		Q 0.288	Q 0.334	Q 0.373	Q 0.406	Q 0.433	Q 0.450	Q 0.450
Q 0.264	Q 0.264	Q 0.264								

```
 0.          0.
23 2188.    22 2187.     0.005      0.039      0.094
46 2191.    45 2191.    21 2178.   20 2239.   19 2346.     0.152      0.204      0.256      0.304
68 2193.    67 2193.    44 2180.   43 2242.   42 2348.   18 2451.   17 2539.   16 2619.   15 2689.
                        66 2182.   65 2245.   64 2350.   41 2452.   40 2539.   39 2619.   38 2689.
                                                         63 2454.   62 2540.   61 2620.   60 2689.

                        K= 0.833330E-03                 THETA1= 0.270000E 02
                        KB= 0.833330E-03                THETA2= 0.270000E 02
                        QDOT= 0.694400E 00              THETA3= 0.270000E 02
                        TAU= 0.400000E-01               THETA4= 0.270000E 02
24 2191.                TAUB= 0.150000E-01              THETA5= 0.270000E 02        59 2757.
                                                                                    37 2757.
                                                                                    14 2758.
69 2440.                EEXT= 0.900000E 00                                           0.354      58 2815.
                        EINT= 0.900000E 00                                                      36 2816.
70 2684.                EB= 0.500000E-01                                                        13 2818.

71 2748.                DELTAP= 0.450000E 02            RHO1= 0.234500E 01          57 2855.    0.401
                        THETAU= 0.450000E 02            RHO2= 0.234500E 01          35 2856.
 1 2720.                THETA6= 0.676000E 02            RHO3= 0.234500E 01          12 2858.
 0 0.263                THETA7= 0.                      RHO4= 0.234500E 01           0.433
                                                        RHO5= 0.234500E 01

                        L1= 1.000000E-03
                        L2= 0.141600E 01
                        L3= 0.141600E 01
                        LL= 1.000000E-03

                                                                                    54 2861.   55 2877.   56 2875.
                                                 50 2720.   51 2758.   52 2798.   53 2833.   32 2863.   33 2879.   34 2877.
47 2720.    46 2720.    49 2720.   28 2720.   29 2758.   30 2799.   31 2834.    9 2865.   10 2881.   11 2879.
25 2720.    26 2720.    27 2720.    5 2720.    6 2758.    7 2800.    8 2835.    0.433      0.450      0.450
 2 2719.     3 2719.     4 2719.    0.288      0.334      0.376      0.408
 0.264       0.264       0.264
```

```
 Q  0.          Q  0.
23  2436.      22  2464.      Q  0.005     Q  0.041     Q  0.100
46  2439.      45  2467.      21  2533.    20  2587.    19  2661.      Q  0.169     Q  0.256     Q  0.292     Q  0.329
68  2442.      67  2471.      44  2537.    43  2590.    42  2663.      18  2743.    17  2820.    16  2886.    15  2934.
                               66  2540.    65  2593.    64  2665.      41  2744.    40  2820.    39  2885.    38  2932.
                                                                       63  2745.    62  2820.    61  2885.    60  2931.
```



```
                    K= 0.833330E-03                    THETA1= 0.300000E 02
                    KB= 0.833330E-03                   THETA2= 0.300000E 02
                    QDOT= 0.694400E 00                 THETA3= 0.180000E 02
                    TAU= 0.400000E-01                  THETA4= 0.320000E 02
24  2459.           TAUB= 0.150000E-01                 THETA5= 0.250000E 02                59  2969.
                                                                                           37  2970.
69  2729.           EEXT= 0.600000E 00                                                     14  2972.
                    EINT= 0.800000E 00                                                      Q  0.348      58  2989.
70  2902.           EB= 1.000000E-01                                                                     36  2991.
                                                                                                         13  2992.
71  2958.           DELTAP= 0.450000E 02               RHO1= 0.200000E 01                 57  2990.      Q  0.359
                    THETAU= 0.450000E 02               RHO2= 0.400000E 01                 35  2992.
 1  2972.           THETA6= 0.676000E 02               RHO3= 0.200000E 01                 12  2993.
 Q  0.266           THETA7= 0.                         RHO4= 0.100000E 01                  Q  0.347
                                                       RHO5= 0.100000E 01
                    L1= 0.107500E 01
                    L2= 0.141600E 01
                    L3= 0.141600E 01
                    LL= 1.000000E-03
```

```
                                          50  2973.    51  3003.    52  3024.    53  3023.    54  3008.    55  3006.    56  2988.
47  2972.      48  2972.      49  2972.   28  2974.    29  3004.    30  3025.    31  3024.    32  3009.    33  3008.    34  2989.
25  2972.      26  2972.      27  2972.    5  2974.     6  3005.     7  3026.     8  3026.     9  3010.    10  3009.    11  2990.
 2  2972.       3  2972.       4  2972.    Q  0.292    Q  0.333    Q  0.357    Q  0.350    Q  0.338    Q  0.347    Q  0.338
 Q  0.267      Q  0.267      Q  0.267
```

Q 0.	Q 0.	Q 0.005	Q 0.041	0.100	Q 0.169	Q 0.236	Q 0.292	Q 0.329
23 2075.	22 2109.	21 2188.	20 2247.	19 2326.	18 2413.	17 2495.	16 2564.	15 2614.
46 2078.	45 2112.	44 2191.	43 2250.	42 2328.	41 2414.	40 2494.	39 2563.	38 2613.
68 2080.	67 2115.	66 2194.	65 2252.	64 2330.	63 2415.	62 2495.	61 2562.	60 2612.

```
24 2096.
69 2339.
70 2558.
71 2638.
 1 2655.
 Q 0.266
```

```
K= 0.833330E-03
K3= 0.833330E-03
WDOT= 0.694400E 00
TAU= 0.400000E-01
TAUB= 0.150000E-01

EEXT= 0.900000E 00
EINT= 0.900000E 00
EB= 0.500000E-01

DELTAP= 0.450000E 02
THETAU= 0.450000E 02
THETA6= 0.676000E 02
THETA7= 0.

L1= 0.107500E 01
L2= 0.141600E 01
L3= 0.141600E 01
LL= 1.000000E-03
```

```
THETA1= 0.300000E 02
THETA2= 0.300000E 02
THETA3= 0.180000E 02
THETA4= 0.320000E 02
THETA5= 0.250000E 02

RHO1= 0.200000E 01
RHO2= 0.400000E 01
RHO3= 0.200000E 01
RHO4= 0.100000E 01
RHO5= 0.100000E 01
```

```
59 2651.
37 2653.
14 2654.
 Q 0.348

57 2675.
35 2676.
12 2678.
 Q 0.347

58 2673.
36 2674.
13 2676.
 Q 0.359
```

RUN 6-H

47 2654.	48 2654.	49 2654.	50 2656.	51 2687.	52 2708.	53 2708.	54 2692.	55 2691.	56 2672.
25 2655.	26 2655.	27 2655.	28 2657.	29 2687.	30 2709.	31 2709.	32 2693.	33 2692.	34 2674.
2 2654.	3 2654.	4 2654.	5 2657.	6 2688.	7 2710.	8 2710.	9 2694.	10 2694.	11 2675.
Q 0.267	Q 0.267	Q 0.267	Q 0.292	Q 0.333	Q 0.357	Q 0.350	Q 0.338	Q 0.347	Q 0.338

APPENDIX C

FORTRAN COMPUTER PROGRAM

```
      WRITEOUTPUTTAPE3,552,(I,TEST(I),I=1,22)
CHEAT TRANSFER DIST.
      DIMENSION T(71),TN(71),XP(26),YP(26),AP(25),SP(24),PSI(24),
     1A(71,71),B(71,71),F(25,25),C(25,25),Q(24),H(24),SUM(25),ANT(24),
     2AK(24),BP(24),X(5),Y(5),R(5),RHO(5),THETA(5),TR(4),RM(4),
     3AB(71,72),ABB(25,50),TEST(22)
      EQUIVALENCE(AB,ABB)
    1 READINPUTTAPE2,201,NC,THETAU,DELTAP,ULT,UL2,UL3,ULL,THETA6,THETA7,
     1CD,CDB,TAU,YAUB,EINT,EXT,SB,CDOY,X,Y,RHO,THETA,TR,TG
  201 FORMAT(I1/(5E13.7))
      DO75I=1,71
   75 T(I)=TG
      DO2I=1,71
      DO2J=1,71
    2 A(I,J)=0
      THETAU=THETAU*.0174532925
      THETA6=THETA6*.0174532925
      THETA7=THETA7*.0174532925
      DELTAP=DELTAP*.0174532925
      IF(NC)9,3,9
    3 R(1)=Y(1)-TAU
      DO5I=2,5
      TEMP=SQRTF((X(I)-X(I-1))**2+(Y(I)-Y(I-1))**2)
      IF(TR(I-1))5,4,5
    4 TEMP=-TEMP
    5 R(I)=R(I-1)+TEMP
      DO6I=1,5
    6 RHO(I)=R(I)+TAU
      THETA(1)=ATANF(ABSF(X(2)-X(1))/ABSF(Y(2)-Y(1)))
      DO7I=2,5
    7 RM(I)=(Y(I)-Y(I-1))/(X(I)-X(I-1))
      DO8I=2,4
    8 THETA(I)=ATANF((RM(I+1)-RM(I))/(1.+RM(I)*RM(I+1)))
      THETA(5)=3.141592653-(THETA(1)+THETA(2)+THETA(3)+THETA(4))-THETAU
      GOTO12
    9 DO10I=1,5
      R(I)=RHO(I)-TAU
   10 THETA(I)=THETA(I)*.0174532925
      X(1)=ULL
      Y(1)=R(1)+TAU
      X(2)=ULL-(R(2)-R(1))*SINF(THETA(1))
      Y(2)=R(1)+TAU+(R(2)-R(1))*COSF(THETA(1))
      TEMP=THETA(1)
      DO11I=3,5
      TEMP=TEMP+THETA(I-1)
      X(I)=X(I-1)-(R(I)-R(I-1))*SINF(TEMP)
   11 Y(I)=Y(I-1)+(R(I)-R(I-1))*COSF(TEMP)
   12 XP(1)=0
      XP(2)=2.*X(1)/3.
```

```
      XP(3)=5.*X(1)/6.
      XP(4)=X(1)
      DO 13 I=1,4
   13 YP(I)=TAU
      TEMP=0
      DO 14 I=5,8
      TEMP=TEMP+THETA(1)/4.
      XP(I)=X(1)+R(1)*SINF(TEMP)
   14 YP(I)=Y(1)-R(1)*COSF(TEMP)
      TEMP=THETA(1)
      DO 15 I=9,11
      TEMP=TEMP+THETA(2)/3.
      XP(I)=X(2)+R(2)*SINF(TEMP)
   15 YP(I)=Y(2)-R(2)*COSF(TEMP)
      TEMP=THETA(1)+THETA(2)
      DO 16 I=12,14
      TEMP=TEMP+THETA(3)/3.
      XP(I)=X(3)+R(3)*SINF(TEMP)
   16 YP(I)=Y(3)-R(3)*COSF(TEMP)
      TEMP=THETA(1)+THETA(2)+THETA(3)
      DO 17 I=15,18
      TEMP=TEMP+THETA(4)/4.
      XP(I)=X(4)+R(4)*SINF(TEMP)
   17 YP(I)=Y(4)-R(4)*COSF(TEMP)
      TEMP=THETA(1)+THETA(2)+THETA(3)+THETA(4)
      DO 18 I=19,21
      TEMP=TEMP+THETA(5)/3.
      XP(I)=X(5)+R(5)*SINF(TEMP)
   18 YP(I)=Y(5)-R(5)*COSF(TEMP)
      TEMP=UL1*COSF(THETAL)
      XP(22)=XP(21)-TEMP/2.
      XP(23)=XP(21)-TEMP
      TEMP=UL1*SINF(THETAL)
      YP(22)=YP(21)+TEMP/2.
      YP(23)=YP(21)+TEMP
      XP(24)=XP(23)+UL2*COSF(THETA6+THETAL)
      YP(24)=YP(23)-UL2*SINF(THETA6+THETAL)
      XP(25)=XP(24)+UL3*COSF(THETA6+THETAL-THETA7)
      YP(25)=YP(24)-UL3*SINF(THETA6+THETAL-THETA7)
      XP(26)=0
      YP(26)=TAU
      AP(1)=2.*X(1)/3.
      AP(2)=X(1)/6.
      AP(3)=AP(2)
      DO 19 I=4,7
   19 AP(I)=R(1)*THETA(1)/4.
      DO 20 I=8,10
   20 AP(I)=R(2)*THETA(2)/3.
      DO 21 I=11,13
```

```
21    AP(I)=R(3)*THETA(3)/3.
      DO22I=14,17
22    AP(I)=R(4)*THETA(4)/4.
      DO23I=18,20
23    AP(I)=R(5)*THETA(5)/3.
      AP(21)=LL1/2.
      AP(22)=AP(21)
      AP(23)=LL2
      AP(24)=LL3
      AP(25)=SQRTF(XP(25)**2+(YP(25)-TAU)**2)
      SP(1)=TAUB
      SP(2)=AP(1)
      SP(3)=AP(2)
      SP(4)=SP(3)
      DO24I=5,8
24    SP(I)=(R(1)+TAU)*THETA(1)/4.
      DO25I=9,11
25    SP(I)=(R(2)+TAU)*THETA(2)/3.
      DO26I=12,14
26    SP(I)=(R(3)+TAU)*THETA(3)/3.
      DO27I=15,18
27    SP(I)=(R(4)+TAU)*THETA(4)/4.
      DO28I=19,21
28    SP(I)=(R(5)+TAU)*THETA(5)/3.
      SP(22)=LL1/2.
      SP(23)=SP(22)
      SP(24)=TAUB
      A(1,2)=X(1)/3.+TAUB/2.
      A(1,25)=A(1,2)
      A(1,47)=A(1,2)
      A(1,71)=(AP(25)+TAU)/2.
      A(2,3)=5.*X(1)/12.
      A(2,25)=.4995*TAU
      A(3,4)=X(1)/6.
      A(3,26)=A(2,25)
      TEMP=(R(1)+.9995*TAU)*THETA(1)/4.
      A(4,5)=.5*(X(1)/6.+TEMP)
      A(4,27)=A(2,25)
      A(5,6)=TEMP
      A(5,28)=A(2,25)
      A(6,7)=TEMP
      A(6,29)=A(2,25)
      A(7,8)=TEMP
      A(7,30)=A(2,25)
      TEMP1=(R(2)+.9995*TAU)*THETA(2)/3.
      A(8,9)=.5*(TEMP+TEMP1)
      A(8,31)=A(2,25)
      A(9,10)=TEMP1
      A(9,32)=A(2,25)
```

```
      TEMP=(R(3)+.9995*TAU)*THETA(3)/3.
      A(11,12)=.5*(TEMP1+TEMP)
      A(11,34)=A(2,25)
      A(12,13)=TEMP
      A(12,35)=A(2,25)
      A(13,14)=TEMP
      A(13,36)=A(2,25)
      TEMP1=(R(4)+.9995*TAU)*THETA(4)/4.
      A(14,15)=.5*(TEMP+TEMP1)
      A(14,37)=A(2,25)
      A(15,16)=TEMP1
      A(15,38)=A(2,25)
      A(16,17)=TEMP1
      A(16,39)=A(2,25)
      A(17,18)=TEMP1
      A(17,40)=A(2,25)
      TEMP=(R(5)+.9995*TAU)*THETA(5)/3.
      A(18,19)=.5*(TEMP1+TEMP)
      A(18,41)=A(2,25)
      A(19,20)=TEMP
      A(19,42)=A(2,25)
      A(20,21)=TEMP
      A(20,43)=A(2,25)
      A(21,22)=.5*(TEMP+UL1/2.)
      A(21,44)=A(2,25)
      A(22,23)=UL1/2.
      A(22,45)=A(2,25)
      A(23,24)=.5*(A(22,23)+TAUB)
      A(23,46)=A(2,25)
      A(24,46)=A(23,24)
      A(24,68)=A(23,24)
      A(24,69)=.5*(TAU+UL2)
      A(25,26)=A(2,3)
      A(25,47)=A(2,25)
      A(26,27)=A(3,4)
      A(26,48)=A(2,25)
      TEMP=(R(1)+TAU/2.)*THETA(1)/4.
      A(27,28)=.5*(A(26,27)+TEMP)
      A(27,49)=A(2,25)
      A(28,29)=TEMP
      A(28,50)=A(2,25)
      A(29,30)=TEMP
      A(29,51)=A(2,25)
      A(30,31)=TEMP
      A(30,52)=A(2,25)
      TEMP1=(R(2)+TAU/2.)*THETA(2)/3.
      A(31,32)=.5*(TEMP+TEMP1)
      A(31,53)=A(2,25)
      A(32,33)=TEMP1
```

```
A(32,54)=A(2,25)
A(33,34)=TEMP1
A(33,55)=A(2,25)
TEMP=(R(3)+TAU/2.)*THETA(3)/3.
A(34,35)=.5*(TEMP1+TEMP)
A(34,56)=A(2,25)
A(35,36)=TEMP
A(35,57)=A(2,25)
A(36,37)=TEMP
A(36,58)=A(2,25)
TEMP1=(R(4)+TAU/2.)*THETA(4)/4.
A(37,38)=.5*(TEMP+TEMP1)
A(37,59)=A(2,25)
A(38,39)=TEMP1
A(38,60)=A(2,25)
A(39,40)=TEMP1
A(39,61)=A(2,25)
A(40,41)=TEMP1
A(40,62)=A(2,25)
TEMP=(R(5)+TAU/2.)*THETA(5)/3.
A(41,42)=.5*(TEMP1+TEMP)
A(41,63)=A(2,25)
A(42,43)=TEMP
A(42,64)=A(2,25)
A(43,44)=TEMP
A(43,65)=A(2,25)
A(44,45)=.5*(TEMP+A(22,23))
A(44,66)=A(2,25)
A(45,46)=A(22,23)
A(45,67)=A(2,25)
A(46,68)=A(2,25)
A(47,48)=A(25,26)
A(48,49)=A(26,27)
TEMP=(R(1)+.0005*TAU)*THETA(1)/4.
A(49,50)=.5*(A(48,49)+TEMP)
A(50,51)=TEMP
A(51,52)=TEMP
A(52,53)=TEMP
TEMP1=(R(2)+.0005*TAU)*THETA(2)/3.
A(53,54)=.5*(TEMP+TEMP1)
A(54,55)=TEMP1
A(55,56)=TEMP1
TEMP=(R(3)+.0005*TAU)*THETA(3)/3.
A(56,57)=.5*(TEMP1+TEMP)
A(57,58)=TEMP
A(58,59)=TEMP
TEMP1=(R(4)+.0005*TAU)*THETA(4)/4.
A(59,60)=.5*(TEMP+TEMP1)
A(60,61)=TEMP1
```

```
A(61,62)=TEMP1
A(62,63)=TEMP1
TEMP=(R(5)+.0005*TAU)*THETA(5)/3.
A(63,64)=.5*(TEMP1+TEMP)
A(64,65)=TEMP
A(65,66)=TEMP
A(66,67)=.5*(TEMP+A(45,46))
A(67,68)=A(45,46)
A(69,70)=.5*(UL2+UL3)
A(70,71)=.5*(AP(25)+UL3)
B(1,2)=.001*TAU
B(1,25)=.998*TAU
B(1,47)=B(1,2)
B(1,71)=TAU8
B(2,3)=B(1,2)
B(2,25)=2.*X(1)/3.
B(3,4)=B(1,2)
B(3,26)=X(1)/6.
B(4,5)=B(1,2)
B(4,27)=B(3,26)
B(5,6)=B(1,2)
B(5,28)=(R(1)+.999*TAU)*THETA(1)/4.
B(6,7)=B(1,2)
B(6,29)=B(5,28)
B(7,8)=B(1,2)
B(7,30)=B(5,28)
B(8,9)=B(1,2)
B(8,31)=B(5,28)
B(9,10)=B(1,2)
B(9,32)=(R(2)+.999*TAU)*THETA(2)/3.
B(10,11)=B(1,2)
B(10,33)=B(9,32)
B(11,12)=B(1,2)
B(11,34)=B(9,32)
B(12,13)=B(1,2)
B(12,35)=(R(3)+.999*TAU)*THETA(3)/3.
B(13,14)=B(1,2)
B(13,36)=B(12,35)
B(14,15)=B(1,2)
B(14,37)=B(12,35)
B(15,16)=B(1,2)
B(15,38)=(R(4)+.999*TAU)*THETA(4)/4.
B(16,17)=B(1,2)
B(16,39)=B(15,38)
B(17,18)=B(1,2)
B(17,40)=B(15,38)
B(18,19)=B(1,2)
B(18,41)=B(15,38)
B(19,20)=B(1,2)
```

```
B(19,42)=(R(5)+.999*TAU)*THETA(5)/3.
B(20,21)=B(1,2)
B(20,43)=B(19,42)
B(21,22)=B(1,2)
B(21,44)=B(19,42)
B(22,23)=B(1,2)
B(22,45)=UL1/2.
B(23,24)=B(1,2)
B(23,46)=B(22,45)
B(24,46)=B(1,25)
B(24,68)=B(1,2)
B(24,69)=TAUB
B(25,26)=B(1,25)
B(25,47)=B(2,25)
B(26,27)=B(1,25)
B(26,48)=B(4,27)
B(27,28)=B(1,25)
B(27,49)=B(4,27)
B(28,29)=B(1,25)
B(28,50)=(R(1)+.001*TAU)*THETA(1)/4.
B(29,30)=B(1,25)
B(29,51)=B(28,50)
B(30,31)=B(1,25)
B(30,52)=B(28,50)
B(31,32)=B(1,25)
B(31,53)=B(28,50)
B(32,33)=B(1,25)
B(32,54)=(R(2)+.001*TAU)*THETA(2)/3.
B(33,34)=B(1,25)
B(33,55)=B(32,54)
B(34,35)=B(1,25)
B(34,56)=B(32,54)
B(35,36)=B(1,25)
B(35,57)=(R(3)+.001*TAU)*THETA(3)/3.
B(36,37)=B(1,25)
B(36,58)=B(35,57)
B(37,38)=B(1,25)
B(37,59)=B(35,57)
B(38,39)=B(1,25)
B(38,60)=(R(4)+.001*TAU)*THETA(4)/4.
B(39,40)=B(1,25)
B(39,61)=B(38,60)
B(40,41)=B(1,25)
B(40,62)=B(38,60)
B(41,42)=B(1,25)
B(41,63)=B(38,60)
B(42,43)=B(1,25)
B(42,64)=(R(5)+.001*TAU)*THETA(5)/3.
B(43,44)=B(1,25)
```

```
      B(43,65)=B(42,64)
      B(44,45)=B(1,25)
      B(44,66)=B(42,64)
      B(45,46)=B(1,25)
      B(45,67)=B(23,46)
      B(46,68)=B(23,46)
      DO29I=47,67
      J=I+1
29    B(I,J)=B(1,2)
      B(69,70)=B(24,69)
      B(70,71)=B(24,69)
      DO31I=1,71
      DO31J=1,71
      IF(A(I,J))30,31,30
30    A(I,J)=CD*B(I,J)/A(I,J)
31    CONTINUE
      A(1,71)=A(1,71)*CDB/CD
      A(24,69)=A(24,69)*CDB/CD
      A(69,70)=A(69,70)*CDB/CD
      A(70,71)=A(70,71)*CDB/CD
      DO32I=1,71
      DO32J=1,71
32    A(J,I)=A(I,J)
      DO34I=1,71
      TEMP=0
      DO33J=1,71
33    TEMP=TEMP+A(I,J)
34    A(I,I)=-TEMP
      DO37I=1,25
      DO37J=1,25
      IF(I-J)35,36,35
35    F(I,J)=.5*ABSF(SQRTF((XP(I+1)-XP(J+1))**2+(YP(I+1)-YP(J+1))**2)
     1-SQRTF((XP(I+1)-XP(J))**2+(YP(I+1)-YP(J))**2)-SQRTF((XP(I)-XP(J+1)
     2)**2+(YP(I)-YP(J+1))**2)+SQRTF((XP(I)-XP(J))**2+(YP(I)-YP(J))**2))
      GOTO37
36    F(I,I)=0
37    CONTINUE
      DO39I=1,25
      DO38J=1,25
38    C(I,J)=F(I,J)
39    C(I,1)=-AP(I)/(1.-EINT)
      DO40I=23,25
40    C(I,I)=-AP(I)/(1.-EB)
      DO42I=1,25
      DO41J=1,22
41    F(I,J)=-F(I,J)*EINT
      DO42J=23,25
42    F(I,J)=-F(I,J)*EB
      DO420I=1,25
```

```
      DO 419 J=1,25
  419 ABB(I,J)=C(I,J)
      DO 420 J=26,50
  420 ABB(I,J)=F(I,J-25)
      CALL MATS(ABB,C,25,25)
      DO 43 I=1,22
      DO 43 J=1,25
   43 F(I,J)=C(I,J)*AP(I)*EINT/(1.-EINT)
      DO 44 I=23,25
      DO 44 J=1,25
   44 F(I,J)=C(I,J)*AP(I)*EB/(1.-EB)
      GAMMA=1.570796326-DELTAP
      SA=SQRTF(.496*RHO(2))
      PSI(1)=GAMMA
      PSI(2)=ABSF(THETA(1)/8.-GAMMA)
      PSI(3)=ABSF(3.*THETA(1)/8.-GAMMA)
      PSI(4)=ABSF(5.*THETA(1)/8.-GAMMA)
      PSI(5)=ABSF(7.*THETA(1)/8.-GAMMA)
      PSI(6)=ABSF(THETA(1)-GAMMA)
      PSI(7)=ABSF(THETA(1)+THETA(2)/6.-GAMMA)
      PSI(8)=ABSF(THETA(1)+THETA(2)/2.-GAMMA)
      PSI(9)=ABSF(THETA(1)+5.*THETA(2)/6.-GAMMA)
      PSI(10)=ABSF(THETA(1)+THETA(2)-GAMMA)
      TEMP=THETA(1)+THETA(2)
      PSI(11)=ABSF(TEMP+THETA(3)/6.-GAMMA)
      PSI(12)=ABSF(TEMP+THETA(3)/2.-GAMMA)
      PSI(13)=ABSF(TEMP+5.*THETA(3)/6.-GAMMA)
      TEMP=TEMP+THETA(3)
      PSI(14)=ABSF(TEMP-GAMMA)
      PSI(15)=ABSF(TEMP+THETA(4)/8.-GAMMA)
      PSI(16)=ABSF(TEMP+3.*THETA(4)/8.-GAMMA)
      PSI(17)=ABSF(TEMP+5.*THETA(4)/8.-GAMMA)
      PSI(18)=ABSF(TEMP+7.*THETA(4)/8.-GAMMA)
      TEMP=TEMP+THETA(4)
      PSI(19)=ABSF(TEMP-GAMMA)
      PSI(20)=ABSF(TEMP+THETA(5)/6.-GAMMA)
      PSI(21)=ABSF(TEMP+THETA(5)/2.-GAMMA)
      PSI(22)=ABSF(TEMP+5.*THETA(5)/6.-GAMMA)
      PSI(23)=ABSF(TEMP+THETA(5)-GAMMA)
      DO 45 I=1,23
   45 ANT(I)=.25*(PSI(I)**2+PSI(I)*SINF(2.*PSI(I))+
     1.5*COSF(2.*PSI(I))-.5)
      SQR=SQRTF(RHO(2))
      TEMP=GAMMA*(COSF(GAMMA))**2
      TEMP1=RHO(2)*ANT(6)+RHO(1)*(ANT(1)-ANT(6))
      Q(1)=(SA*TEMP/SQRTF(TEMP1+TEMP*(X(1)+TAUB/2.)))*QDOT/SQR
      Q(2)=(SA*TEMP/SQRTF(TEMP1+TEMP*2.*X(1)/3.))*QDOT/SQR
      Q(3)=(SA*TEMP/SQRTF(TEMP1+TEMP*X(1)/4.))*QDOT/SQR
      Q(4)=(SA*TEMP/SQRTF(TEMP1+TEMP*X(1)/12.))*QDOT/SQR
```

```
      DO 46 I=5,8
   46 Q(I)=(SA*PSI(I-3)*COSF(PSI(I-3))**2/(SQRTF(RHO(2)*ANT(6)+RHO(1)*
     1(ANT(I-3)-ANT(6))))*QDOT/SQR
      DO 49 I=9,11
      IF(PSI(I-2)-10.**(-5))47,47,48
   47 Q(I)=QDOT/SQR
      GOTO 49
   48 Q(I)=(SA*PSI(I-2)*COSF(PSI(I-2))**2/(SQRTF(RHO(2)*ANT(I-2))))
     1*QDOT/SQR
   49 CONTINUE
      DO 50 I=12,14
   50 Q(I)=(SA*PSI(I-1)*COSF(PSI(I-1))**2/(SQRTF(RHO(2)*ANT(10)+RHO(3)
     1*(ANT(I-1)-ANT(10))))*QDOT/SQR
      TEMP=RHO(2)*ANT(10)+RHO(3)*(ANT(14)-ANT(10))
      DO 53 I=15,18
      IF(PSI(I)-1.57079632)51,52,52
   51 Q(I)=(SA*PSI(I)*COSF(PSI(I))**2/(SQRTF(TEMP+RHO(4)*(ANT(I)-ANT(14)
     1))))*QDOT/SQR
      GOTO 53
   52 Q(I)=0
   53 CONTINUE
      TEMP=TEMP+RHO(4)*(ANT(19)-ANT(14))
      DO 56 I=19,21
      IF(PSI(I+1)-1.57079632)54,55,55
   54 Q(I)=(SA*PSI(I+1)*COSF(PSI(I+1))**2/(SQRTF(TEMP+RHO(5)*(ANT(I+1)
     1-ANT(19))))))*QDOT/SQR
      GOTO 56
   55 Q(I)=0
   56 CONTINUE
      DO 57 I=22,24
   57 Q(I)=0
      DO 58 I=1,24
   58 H(I)=-(EXT*.00854+Q(I))*SP(I)
      DO 60 I=1,25
      TEMP=0
      DO 59 J=1,25
   59 TEMP=TEMP+F(I,J)
   60 SUM(I)=TEMP
  500 DO 61 I=1,71
      DO 61 J=1,71
   61 B(I,J)=A(I,J)
      DO 62 I=1,24
      BP(I)=-4.*T(I)**3*SP(I)*EXT*3.3402*10.**(-15)
   62 AK(I)=-3.*T(I)**4*SP(I)*EXT*3.3402*10.**(-15)
      DO 63 I=1,25
      DO 63 J=1,25
   63 C(I,J)=4.*3.3402*10.**(-15)*T(J+46)**3*F(I,J)
      DO 64 I=1,25
   64 C(I,I)=C(I,I)-T(I+46)**3*4.*3.3402*10.**(-15)*SUM(I)
```

```
      DO64I=1,25
64    C(I,I)=C(I,I)-T(I+46)**3*4.*3.3402*10.**(-15)*SUM(I)
      DO640I=1,24
640   B(I,I)=B(I,I)+BP(I)
      DO65I=47,71
      DO65J=47,71
65    B(I,J)=B(I,J)+C(I-46,J-46)
      DO66I=1,24
66    TN(I)=H(I)+AK(I)
      DO67I=25,46
67    TN(I)=0
      DO69I=1,25
      TEMP=0
      DO68J=1,25
68    TEMP=TEMP+F(I,J)*T(J+46)**4*3.*3.3402*10.**(-15)
      K=I+46
69    TN(K)=TEMP-3.*3.3402*10.**(-15)*T(K)**4*SUM(I)
      DO690I=1,71
      DO689J=1,71
689   AB(I,J)=B(I,J)
690   AB(I,72)=TN(I)
      CALL MAATS(AB,TN,71,1)
      DO70I=1,71
      IF(ABSF(T(I)-TN(I))-3.)70,70,72
70    CONTINUE
      DO85I=1,71
 85   T(I)=TN(I)
      DELTAP=DELTAP/.0174532925
      THETAU=THETAU/.0174532925
      THETA6=THETA6/.0174532925
      THETA7=THETA7/.0174532925
      DO80I=1,5
80    THETA(I)=THETA(I)/.0174532925
      TEMP=0.
      DO81I=1,24
81    TEMP=TEMP+SP(I)*(Q(I)-EXT*T(I)**4*3.3402*10.**(-15)+EXT*.000854)
      CK1=TEMP
      TEMP=0.
      DO82I=1,24
82    TEMP=TEMP+SP(I)*(Q(I)+EXT*.000854)
      CK2=TEMP
      TEMP=0.
      DO83I=1,24
83    TEMP=TEMP+SP(I)*3.3402*10.**(-15)*EXT*T(I)**4
      CK3=TEMP
      CK4=(CK1/CK2)*100.
      TEST(1)=A(25,2)*(T(25)-T(2))+A(25,1)*(T(25)-T(1))+A(25,26)*
     1(T(25)-T(26))+A(25,47)*(T(25)-T(47))
      TEST(22)=A(46,23)*(T(46)-T(23))+A(46,45)*(T(46)-T(45))+A(46,24)*
```

```
      K=I+24
94    TEST(I)=A(K,I+1)*(T(K)-T(I+1))+A(K,K-1)*(T(K)-T(K-1))+
     1A(K,K+1)*(T(K)-T(K+1))+A(K,K+22)*(T(K)-T(K+22))
      DO71I=1,71
71    T(I)=TN(I)-459.688
      WRITEOUTPUTTAPE3,599,Q(23),Q(22)
      WRITEOUTPUTTAPE3,600,T(23),T(22),Q(21),Q(20),Q(19)
      WRITEOUTPUTTAPE3,601,T(46),T(45),T(21),T(20),T(19),
     1Q(18),Q(17),Q(16),Q(15)
      WRITEOUTPUTTAPE3,602,T(68),T(67),T(44),T(43),T(42),T(18),T(17),
     1T(16),T(15)
      WRITEOUTPUTTAPE3,603,T(66),T(65),T(64),T(41),T(40),T(39),T(38)
      WRITEOUTPUTTAPE3,604,T(63),T(62),T(61),T(60)
      WRITEOUTPUTTAPE3,605,CD,THETA(1)
      WRITEOUTPUTTAPE3,606,CDB,THETA(2)
      WRITEOUTPUTTAPE3,607,CDOT,THETA(3)
      WRITEOUTPUTTAPE3,608,TAU,THETA(4)
      WRITEOUTPUTTAPE3,609,T(24),TAUB,THETA(5),T(59)
      WRITEOUTPUTTAPE3,610,T(37)
      WRITEOUTPUTTAPE3,611,T(69),EXT,T(14)
      WRITEOUTPUTTAPE3,612,EINT,Q(14),T(58)
      WRITEOUTPUTTAPE3,613,T(70),EB,T(36)
      WRITEOUTPUTTAPE3,614,T(13)
      WRITEOUTPUTTAPE3,615,T(71),DELTAP,RHO(1),T(57),Q(13)
      WRITEOUTPUTTAPE3,616,THETAU,RHO(2),T(35)
      WRITEOUTPUTTAPE3,617,T(1),THETA6,RHO(3),T(12)
      WRITEOUTPUTTAPE3,618,Q(1),THETA7,RHO(4),Q(12)
      WRITEOUTPUTTAPE3,619,RHO(5)
      WRITEOUTPUTTAPE3,620,UL1,UL2,UL3,LLL
      WRITEOUTPUTTAPE3,621,T(54),T(55),T(56)
      WRITEOUTPUTTAPE3,622,T(50),T(51),T(52),T(53),T(32),T(33),T(34)
      WRITEOUTPUTTAPE3,623,T(47),T(48),T(49),T(28),T(29),T(30),T(31),
     1T(9),T(10),T(11)
      WRITEOUTPUTTAPE3,624,T(25),T(26),T(27),T(5),T(6),T(7),T(8),
     1Q(9),Q(10),Q(11)
      WRITEOUTPUTTAPE3,625,T(2),T(3),T(4),Q(5),Q(6),Q(7),Q(8)
      WRITEOUTPUTTAPE3,626,Q(2),Q(3),Q(4)
      WRITEOUTPUTTAPE3,650
      WRITEOUTPUTTAPE3,651,CK2,CK3,CK1,CK4
      WRITEOUTPUTTAPE3,652,(I,TEST(I),I=1,22)
599   FORMAT(1H1///////4H  Q F5.3,6H     Q F5.3)
600   FORMAT(4H 23 F5.0,6H   22 F5.0,3(6H     Q F5.3))
601   FORMAT(1X,3H46 F5.0,6H   45 F5.0,6H   21 F5.0,6H   20 F5.0,
     16H   19 F5.0,4(6H     Q F5.3))
602   FORMAT(1X,3H68 F5.0,6H   67 F5.0,6H   44 F5.0,6H   43 F5.0,
     16H   42 F5.0,6H   18 F5.0,6H   17 F5.0,6H   16 F5.0,6H   15 F5.0)
603   FORMAT(23X,3H66 F5.0,6H   65 F5.0,6H   64 F5.0,6H   41 F5.0,
     16H   40 F5.0,6H   39 F5.0,6H   38 F5.0)
604   FORMAT(1 X,3H63 F5.0,6H   62 F5.0,6H   61 F5.0,6H   60 F5.0)
```

```
605  FORMAT(//////23X,2HK=E13.6,18X,7HTHETA1=E13.6)
606  FORMAT(23X,3HKB=E13.6,17X,7HTHETA2=E13.6)
607  FORMAT(23X,5HQDOT=E13.6,15X,7HTHETA3=E13.6)
608  FORMAT(23X,4HTAU=E13.6,16X,7HTHETA4=E13.6)
609  FORMAT(4H 24 F5.0,14X,5HTAUB=E13.6,15X,7HTHETA5=E13.6,13X,
    13H59 F5.0)
610  FORMAT(69X,3H37 F5.0)
611  FORMAT(4H 69 F5.0,14X,5HEEXT=E13.6,48X,3H14 F5.0)
612  FORMAT(23X,5HEINT=E13.6,49X,2HQ F5.3,6H   58 F5.0)
613  FORMAT(4H 70 F5.0,14X,3HEB=E13.6,61X,3H36 F5.0)
614  FORMAT(100X,3H13 F5.0)
615  FORMAT(4H 71 F5.0,14X,7HDELTAP=E13.6,13X,5HRHO1=E13.6,15X,
    13H57 F5.0,6H    Q F5.3)
616  FORMAT(23X,7HTHETAU=E13.6,13X,5HRHO2=E13.6,15X,3H35 F5.0)
617  FORMAT(4H  1 F5.0,14X,7HTHETA6=E13.6,13X,5HRHO3=E13.6,15X,
    13H12 F5.0)
618  FORMAT(4H  Q F5.3,14X,7HTHETA7=E13.6,13X,5HRHO4=E13.6,16X,
    12HQ F5.3)
619  FORMAT(56X,5HRHO5=E13.6)
620  FORMAT(23X,3HL1=E13.6/23X,3HL2=E13.6/23X,3HL3=E13.6/
    123X,3HLL=E13.6/////)
621  FORMAT(78X,3H54 F5.0,6H   55 F5.0,6H   56 F5.0)
622  FORMAT(34X,3H50 F5.0,6H   51 F5.0,6H   52 F5.0,6H   53 F5.0,
    16H   32 F5.0,6H   33 F5.0,6H   34 F5.0)
623  FORMAT(4H 47 F5.0,6H   48 F5.0,6H   49 F5.0,6H   28 F5.0,
    16H   29 F5.0,6H   30 F5.0,6H   31 F5.0,6H    9 F5.0,
    26H   10 F5.0,6H   11 F5.0)
624  FORMAT(4H 25 F5.0,6H   26 F5.0,6H   27 F5.0,6H    5 F5.0,
    16H    6 F5.0,6H    7 F5.0,6H    8 F5.0,3(6H    Q F5.3))
625  FORMAT(4H  2 F5.0,6H    3 F5.0,6H    4 F5.0,4(6H    Q F5.3))
626  FORMAT(4H  Q F5.3,6H    Q F5.3,6H    Q F5.3)
650  FORMAT(1H1///////50X,18HERROR CALCULATIONS)
651  FORMAT(///1CH  HEAT IN=E13.6,4X,9HHEAT OUT=E13.6,3X,
    112H DIFFERENCE=E13.6,4X,22HPERCENT ERROR HEAT IN=E13.6///)
652  FORMAT(4(1CX,I2,E15.6))
     GOTO1
72   DO73I=1,71
73   T(I)=TN(I)
     GOTO500
     END
     SUBROUTINE MAATS(CC,X,NR,M)
     DIMENSION CC(71,72),A(71,72),X(71,1)
100  FORMAT (12X,39HMATRIX INVERSION SMALL DIAGONAL ELEMENT)
     N=NR
     MM=N+M
     DO11I=1,N
     DO1J=1,MM
 1   A(I,J)=CC(I,J)
     DO15I=2,N
```

```
      DO151=2,N
70    II=I-1
7     DO15J=1,II
8     IF(A(I,J))9,15,9
9     IF(ABSF(A(J,J))-ABSF(A(I,J)))11,10,10
10    R=A(I,J)/A(J,J)
      GOTO130
11    R=A(J,J)/A(I,J)
      DO12K=1,MM
      B=A(J,K)
      A(J,K)=A(I,K)
12    A(I,K)=B
130   JJ=J+1
13    DO14K=JJ,MM
14    A(I,K)=A(I,K)-R*A(J,K)
15    CONTINUE
      IF(ABSF(A(N,N))-1.E-20)16,16,17
16    WRITE OUTPUT TAPE 3,100
      CALL EXIT
17    DO 28 J =1,M
      KK=N+J
      X(N,J)=A(N,KK)/A(N,N)
      DO28I=2,N
      JJ=N-I+1
      B=0.
      II=N-I+2
      DO25K=II,N
25    B=B+A(JJ,K)*X(K,J)
      IF(ABSF(A(JJ,JJ))-1.0E-20)16,16,28
28    X(JJ,J)=(A(JJ,KK)-B)/A(JJ,JJ)
      RETURN
       END
      SUBROUTINE MATSIC,X,NR,M)
      DIMENSION C(25,50),A(25,50),X(25,25)
100   FORMAT (12X,39HMATRIX INVERSION SMALL DIAGONAL ELEMENT)
      N=NR
      MM=N+M
      DO1I=1,N
      DO1J=1,MM
 1    A(I,J)=C(I,J)
      DO151=2,N
70    II=I-1
7     DO15J=1,II
8     IF(A(I,J))9,15,9
9     IF(ABSF(A(J,J))-ABSF(A(I,J)))11,10,10
10    R=A(I,J)/A(J,J)
      GOTO130
11    R=A(J,J)/A(I,J)
      DO12K=1,MM
```

```
      B=A(J,K)
      A(J,K)=A(I,K)
   12 A(I,K)=B
  130 JJ=J+1
   13 DO14K=JJ,MM
   14 A(I,K)=A(I,K)-R*A(J,K)
   15 CONTINUE
      IF(ABSF(A(N,N))-1.E-12)16,16,17
   16 WRITE OUTPUT TAPE 3,100
      CALL EXIT
   17 DO 28 J =1,M
      KK=N+J
      X(N,J)=A(N,KK)/A(N,N)
      DO28I=2,N
      JJ=N-I+1
      B=0.
      II=N-I+2
      DO25K=II,N
   25 B=B+A(JJ,K)*X(K,J)
      IF(ABSF(A(JJ,JJ))-1.0E-12)16,16,28
   28 X(JJ,J)=(A(JJ,KK)-B)/A(JJ,JJ)
      RETURN
       END
```

VITA

Richard [redacted] Russell was born on [redacted] in the Aeronautical Engineering Department. Upon graduation from Parks, with a degree of Bachelor of Science in Aeronautics, he was employed by the McDonnell Aircraft Corporation of St. Louis in the wing structural design group. Captain Russell entered the Air Force Pilot Training School in August of 1954. After graduation, he was assigned to the Strategic Air Command as a bomber pilot for two years followed by operations work for the next three years. In addition to his design experience at McDonnell Aircraft Corporation, he was employed by St. Louis Machine Company, while in college, doing work on design and certification of cross-wind landing gears. He is a member of Pi Mu Epsilon and Tau Beta Pi honor fraternities, and a member of the Institute of Aerospace Sciences. He entered graduate aeronautical engineering school of the Air University Institute of Technology in February 1960.

Permanent address: [redacted]

This thesis was typed by Mr. Merrill G. Corkum

UNCLASSIFIED